Design, Simulation and Experimental Investigation of High Temperature Solid-state Sensible Heat Storage Systems

A thesis submitted in partial fulfilment of the requirements for the degree

of

DOCTOR OF PHILOSOPHY

Submitted by

K. VIGNESHWARAN

(Roll No. 146151002)

CENTRE FOR ENERGY

INDIAN INSTITUTE OF TECHNOLOGY, GUWAHATI

GUWAHATI-781039, ASSAM, INDIA

NOVEMBER 2019

Thesis is dedicated to

my family, friends and colleagues

for their unconditional love, support and encouragement

“யாதும் ஊரே யாவரும் கேளிர்”

-புறநானூறு, கணியன் பூங்குன்றன் (கி.மு. 600 – 100).

"हम सभी जगहों से संबंधित हैं, सभी लोग हमारे परिजन हैं"

-पुरानानुरु, कनियन पुंगुंद्रन (600 – 100 ई.पू.).

"To us all towns are one, all people our kin"

- Purananuru, Kaniyan Pungundran (600 - 100 B.C.)

Indian Institute of Technology Guwahati

Centre for Energy

Guwahati-781039, Assam, India

STATEMENT

This is to certify that I have carried out the research work in this thesis entitled **"Design, Simulation and Experimental Investigation of High Temperature Solid-state Sensible Heat Storage Systems"**, at the Centre for Energy, Indian Institute of Technology Guwahati, under the supervision of **Prof. P. Muthukumar** and **Dr. S. Senthilmurugan**. The results documented in this thesis are achieved by me and have not been submitted to any other University or Institute for the award of any degree or diploma.

In keeping with the general practice of reporting scientific observation, due acknowledgement has been made wherever the work described is based on the findings of other investigations.

(K. Vigneshwaran)

Roll. No.: 146151002

Centre for Energy

Indian Institute of Technology Guwahati

Guwahati-781039, Assam, India

October 2019

Indian Institute of Technology Guwahati

Centre for Energy

Guwahati-781039, Assam, India

CERTIFICATE

This is to certify that the work contained in this thesis entitled **"Design, Simulation and Experimental Investigation of High Temperature Solid-state Sensible Heat Storage Systems"**, being submitted by **Mr. K. Vigneshwaran** (Roll. No. 146151002) for the award of Ph.D. degree, is a record of bona fide research carried out by him at the Centre for Energy, Indian Institute of Technology Guwahati, under our guidance and supervision. The work embodied in this thesis has not been submitted to any other University or Institute for the award of any other degree or diploma.

(Prof. P. Muthukumar)

Professor

Department of Mechanical Engineering

Indian Institute of Technology Guwahati

Guwahati-781039, Assam, India

October 2019

(Dr. S. Senthilmurugan)

Associate Professor

Department of Chemical Engineering

Indian Institute of Technology Guwahati

Guwahati-781039, Assam, India

October 2019

Acknowledgements

"காலத்தி னாற்செய்த நன்றி சிறிதெனினும்
ஞாலத்தின் மாணப் பெரிது."

- திருக்குறள் எண்: 102, திருவள்ளுவர் (கி.மு. 600- கி.பி .100).

"अति संकट के समय पर, किया गया उपकार
भू से अधिक महान है, यद्यपि अल्पाकार"

-तिरुक्कुरळ संख्या:102, तिरुवल्लुवर (600 ई.पू. – 100 ई.).

"A timely benefit, -though thing of little worth,
The gift itself, -in excellence transcends the earth"

- Sacred Couplets No:102, Tiruvalluvar (600 B.C. - 100 A.D.)

First and foremost, I would like to express the most profound thanks to Prof. P. Muthukumar and Dr. S. Senthilmurugan for the opportunity, support, guidance and patience that they have given me to pursue research in this exciting field. Their guidance and help have been of high value throughout the whole PhD program. During my research, both the supervisors have provided me with the most precious ideas and resources that played a vital role in completing the thesis successfully. I enjoyed every moment working under their supervision and learnt many things from them, which will be an asset for my future research.

I want to thank my doctoral committee members, Prof. Subhash Chandra Mishra (Late), Prof. G. Pugazhenthi, Dr. Chandramohan Somayaji, Dr. Pankaj Kalita, and Dr. R. Anandalakshmi, for their encouragement, help, and insightful comments. I also thank Prof. Vijay S. Moholkar, Head of Centre for Energy for providing all the facilities needed

for my research work. I take this opportunity to thank all the faculty and staff members of the institute for their valuable suggestions and cooperation during this PhD program.

I especially thank our institute staffs, Mr. Dilip Chetri, Mr. Mrinal Sarma, Mr. Nip Borah and Mr. Jogan Nath for their help during fabrication and operation of the experimental setup. I also thank the administration of the IIT Guwahati for making my stay comfortable and secure.

I want to express my sincere gratefulness to all the Taxpayers of the Government of India.

I want to express my appreciation to the Ministry of Human Resource Development, Government of India, for their constant Ph.D. Scholarship support through IIT Guwahati. The research in this thesis is funded by the Department of Science and Technology (DST), Government of India, for their financial support (Project No: DST/TMD/SERI/D12(C)). Their support is gratefully acknowledged. Additionally, I want to thank the Department of Science and Technology (DST), Government of India for their financial support through international travel grant (Grant No: ITS/2019/003370) for presenting the part of our research outcome in 11th International Conference on Applied Energy at Mälardalen University, Västerås, Sweden. Also, I thank Student's Affairs, IIT Guwahati for their student travel assistance fund to attend the above-said conference. I will also be grateful to all the committee members of Stockholm Tamil Sangam for making my stay comfortable in Sweden.

I wanted to express my personal gratitude to my colleagues at Prof. Muthukumar's researcher group and Dr. S. Senthilmurugan researcher group, Centre for Energy, Centre for Nanotechnology, Department of Mechanical, Civil, Chemistry and Chemical

Engineering, for the wonderful time spent together and not only the workplace but also our life in IIT Guwahati. I also want to express special gratitude to Mr. Gurpreet Singh Sodhi, Mr. R Nithin Narmada and Dr. Chilaka Ravichandra Rao for their inputs in the project. Lab mates and friends are a source of enjoyment and fulfilment, and I enjoyed their comradeship.

The occasion to express gratefulness to one's family on text does not present itself often, and I genuinely appreciate their eternal love. Finally, yet importantly, I want to thank my parents (Hav. Major (Tech.) P. Kondalraj and K. Amsaveni) and sisters, for all their help and encouragement, especially for believing in me and supported me in times of adversity. I also thank the rest of my family and friends outside IIT Guwahati.

Sincerely,

K. VIGNESHWARAN

November 2019

Abstract

Energy is one of the essential components needed for economic growth and improvement in the living standard of humanity. In 2017, the global energy demand had increased by 2.1% as compared to the average increase of 0.9% from the last half-decade. Unfortunately, the conventional fuels in reserves are running out of supply while the world energy consumption is increasing rapidly. The full-fledged usage of fossil fuels has intensified global warming and its consequences. Therefore, the rapid upsurge of energy demand has forced the researchers to find cost-effective energy resources, which originate from renewable energy. The research in renewable technologies has given significant attention to alternative energy sources, which are environmentally friendly and economically competitive to sustain future demands worldwide. At present, 17% of the energy generated from renewable resources are contributing to the global energy demand.

Among the accessible renewable energy sources in the world, solar energy is one of the best energy resources in many continents. Large-scale power generation from solar energy has been gaining attraction in recent times, which has helped in solving environmental issues and decreased the dependency on fossil fuels. In this aspect, compared to photovoltaic technology, solar thermal technology might provide a better solution because of the global heat energy requirements and cost-effective thermal storage. The major challenge of solar energy is the lack of its continuous availability and intermittent nature. Therefore, the energy storage system is a critical component to de-couple power production from solar radiation. With the development of efficient and cost-effective energy storage solutions, solar power has the potential to become an alternative to fossil fuels. Out of all energy storage technologies, storing the heat is one of the easiest and most economical option especially compared to battery-based energy storage.

Utilizing solar energy through Concentrated Solar Power (CSP) for power generation is a promising option via Thermal Energy Storage (TES). Among the three types of TES, Sensible Heat Storage (SHS) system is a promising technological solution to store and deliver high-quality heat for multiple thermal cycles in an economical way. In this way, it is possible for the TES to meet minimum baseload requirements even in the absence of required solar

radiation. Conversely, the main disadvantage of TES is high capital cost. Therefore, the crucial part is to develop a TES system with higher energy density using low-cost material.

The work on the thesis is focused on high-temperature thermal energy storage, mainly the design, development and performance investigation of solid SHS. A high-temperature test facility has been built to study the performance characteristics of the TES modules. In the initial phase of research, the study focused on detailed experimental and numerical investigations on a cast steel based sensible heat thermal energy storage system using air as a heat transfer fluid. A dedicated test facility has been designed and developed for studying the performance of the storage system operating in the temperature range of 393 K to 573 K. Three-dimensional (3-D) and one-dimensional (1-D) models are developed for predicting the heat transfer characteristics of the storage system. The developed storage prototype has a shell and tube configuration having 19 passages in the tube side for heat transfer fluid flow. The performance of the storage system during the charging and discharging processes is analysed by varying the operating temperature range and flow velocity of air. The heat transfer characteristics of the system in terms of axial and radial temperature variations are recorded and analysed. Both the experimental and 3-D simulation results show a significant temperature variation in the axial direction than radial direction. The charging and discharging rates are found to be faster at a higher flow velocity of air. The predictions from both 3-D and 1-D models are consistent with the experimental data. The validated 1-D model can be used for real-time monitoring, control, optimisation and integration with various storage applications.

In the next phase of research, the work presents the concept of developing a cost-effective Concrete based Thermal Energy Storage (CTES) system by performing extensive experimental studies and numerical simulations. A stand-alone experimental facility to study the performance of high-temperature thermal energy storage system, which operates up to 773 K using air as the heat transfer fluid, has been developed. The CTES module is made of shell and tube configuration, where the concrete is filled in the shell side, and 22 air passages are provided on the tube side. The inlet air temperature and velocity are the decision parameters used for analyzing the thermal behaviour of the CTES module. From the spatial variations of temperature, it is observed that the heat transfer rate is uniform and faster along all radial planes, whereas, the heat transfer rate drops gradually along the length of the CTES module due to drop in Heat Transfer Fluid (HTF) temperature. The parametric investigation

conducted shows that the charging and discharging times were reduced by approximately 48% and 29%, respectively, with a change in inlet temperature of 40 K and at a fixed air velocity of 2 m/s. A 3-D model for the CTES module developed using the finite element method has been validated with experimental results. The temperature contours plotted from 3-D simulation describe the spatial variation of CTES temperature at different inlet air temperatures. Further, a 1-D dynamic model has been developed, which is fast and accurate with a maximum error of ±4.9 K with reference to real-time experiments and provides a substantial scope of integrating the CTES with industrial applications.

In the final phase of research, a comprehensive coupling strategy is developed to evaluate the performance of a multi-module SHS system using the 1-D dynamic model. The validated 1-D model developed in our previous studies is adopted to scale-up the heat storage capacity for large scale application. The SHS modules used in this study are made of materials such as cast steel, cast iron and concrete with the design similar to shell and tube configuration. Air is used as the heat transfer fluid at a velocity of 15.2 m/s. Six Cases are framed to evaluate the charging (493-573 K) and discharging (373-573 K) behaviour of SHS module coupling strategies in different series and/or parallel arrangements. The performance of the charging and the discharging processes for all the Cases are estimated and compared for forward flow and reverse flow patterns and reverse module arrangements. The cost of the net energy discharged (USD/kW-h) from each arrangement is evaluated. The result shows that the performance of Case 6 (three parallel channels, with two different SHS modules in each channel) is better in terms of heat transfer rate, however, the cost of net energy discharged in Case 6 is 62.26 USD/kW-h, which is very expensive. The Case 3 (six concrete in the series arrangement) can store and discharge more amount of heat with slow heat transfer rate, and the cost of net energy discharged in this Case is 1.18 USD/kW-h. The developed flowsheet models are highly beneficial for studying the performance of the different storage module arrangements along with large scale applications.

The outcomes from the studies highlight that cast steel and concrete TES storage modules are the cost-effective and viable high-temperature storage option for multiple thermal cycles with excellent durability.

NOMENCLATURE

A	:	Area [m^2]
C_p	:	Specific heat [J/kg-K]
D	:	Diameter of the storage module [m]
d	:	Diameter [m]
h_i	:	Heat transfer coefficient [W/m^2-K]
k	:	Thermal conductivity [W/m-K]
L	:	Length [m]
M	:	Molecular weight of air [kg/mol]
m	:	Mass [kg]
N_p *or* n	:	Number of HTF passages
Nu	:	Nusselt number
P	:	Pressure [N/m^2]
Pr	:	Prandtl number
Q	:	Energy [J]
$\dot{Q}$	:	Volumetric flow rate [m^3/s]
q	:	Heat transfer rate [W/m^2]
R	:	Universal gas constant [N m/mol-K]
Re	:	Reynolds number
T	:	Temperature [K]
t	:	Time [s]
U_o	:	Overall heat transfer coefficient [W/m^2-K]
v	:	Velocity of air [m/s]
V	:	Volume [m^3]

Subscript

air	:	air/HTF
avg	:	average
c	:	concrete
ch	:	channel

e	:	element
f	:	fluid
i	:	inner
in	:	inlet
ini	:	initial
Mod	:	module
o	:	outer
out	:	outlet
s	:	solid
Sur	:	surface
p	:	HTF passage/tube
pcd,i	:	inner pitch circle
pcd,o	:	outer pitch circle
tube	:	HTF passage (tube)

Greek symbols

ρ	:	density [kg/m^3]
μ	:	viscosity [N s/m^2]

Acronym

CSP	:	Concentrated solar power
EXP	:	Experiment value
HTF	:	Heat transfer fluid
SHS	:	Sensible heat storage
SIM	:	Simulation value
TES	:	Thermal energy storage
1-D	:	One dimensional
3-D	:	Three dimensional

TABLE OF CONTENTS

LIST OF FIGURES

LIST OF TABLES

CHAPTER 1
INTRODUCTION

In recent years, more research activities have been focused on clean energy sources. The growth of population and energy demand per capita are increasing at an alarming rate. Therefore, alternative sources of energy which are not based on fossil fuels are getting prime importance. The major concern is to control the effect of climate change with sustainable energy solutions. The Paris Climate Agreement states that the emission of CO_2 has to be reduced to zero by 2060 so as to prevent the rise in global average ambient temperature beyond 2 K (Clémençon, 2016). Hence, significant updates are required in the energy sector and the thesis work presented here is a tiny landmark in this energy revolution.

1.1 The scenario of energy and renewable energy

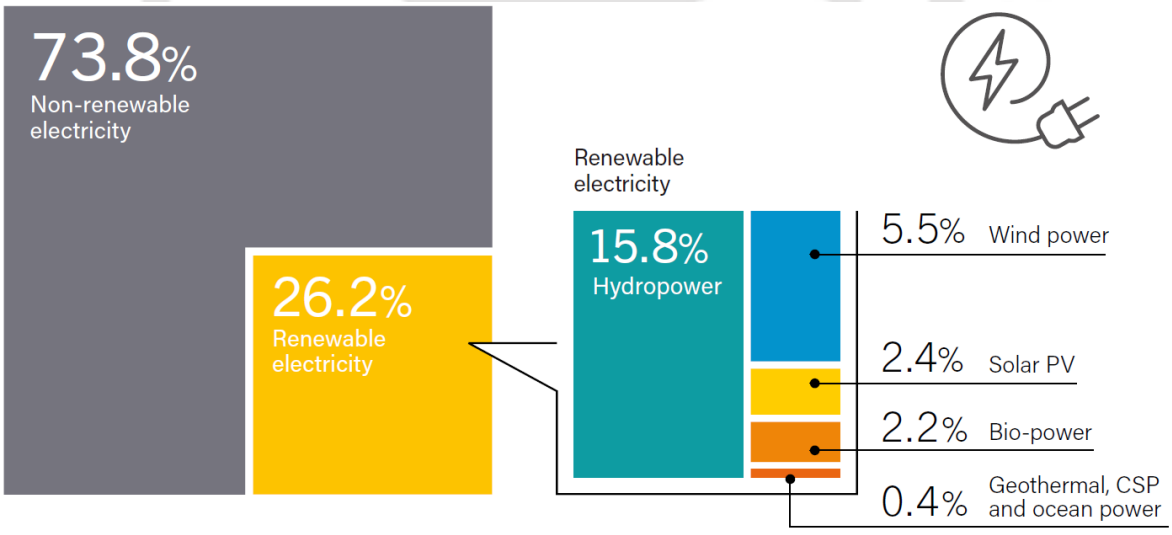

Figure 1-1. Total electrical energy production in 2018 and an estimated renewable energy share (Renewables 2019 Global Status Report, 2019).

Energy is one of the essential components needed for the economic growth and improvement in living standards of mankind (U.S. Energy Information Administration, 2018). Since 1000 B.C, fossil fuels are used as a source of energy. However, during the industrial revolution in

the middle of the 1700s and the 1800s, fossil fuels such as natural gas, coal and oil have provided the main contribution to all human energy needs. This scenario has continued, and in recent years, incessant usage of fossil fuel has created a huge impact on the environment through global warming, climate change and melting of polar ice (Alister Doyle, 2019). The continuous shrinkage of fossil fuel reserves, the increasing global inhabitants and the rapid upsurge of energy demand have forced the scientists to find an alternative source of energy.

In 2018, the global demand for energy had expanded by 2.3% as compared to the average increase of 0.9% from the last half-decade (Renewables 2019 Global Status Report, 2019). Seventy percent of this energy demand is due to heating and cooling requirements raised in countries like the United States, China and India. Such high energy demand countries are adopting various technologies based on renewable sources for clean energy production. Renewable energy technologies are going to play a crucial part in addressing the global energy requirement. A recent report states that 26.2% of global electricity production in 2018 has been contributed by the renewable energy sector (refer to Figure 1-1). Simultaneously, India is rapidly advancing towards meeting 40% of its total energy consumption from the renewable energy sector before 2030. The target includes the completion of projects such as 100 GW from solar energy, 60 GW from the wind energy, 10 GW from the bio-energy resources and 5 GW from the hydropower generation by 2022 ("Year End Review 2018 - MNRE," 2018). At the end of 2018, the country's total renewable energy contribution was 21.12% out of its total production, and which is due to 20% growth in the renewable energy sector during last five years ("Year End Review 2018 - MNRE," 2018). India's major renewable resource contribution is from the wind energy, and recently, the world's largest solar photovoltaic projects with the capacities of 2000 MW, 1000 MW and 648 MW have been installed to achieve this renewable energy target (MNRE-Government of India, 2019). Such an increasing trend of renewable energy contribution has reduced air pollution (Panwar et al., 2011). Despite having a sufficient amount of renewable energy sources and the required technology for energy generation, the government agencies are unable to build standalone renewable energy-based grids. The issue is mainly due to the lack of cost-effective energy storage technology and the energy distribution infrastructure for transporting renewable energy from production to demand site. Among renewable energy sources, solar energy is unique due to its characteristics such as being a clean source, preventing damage to the ecology, fighting against climate change as well as being a small and decentralised energy source. Finally, the important drive for solar energy is "the sun will never stop rising for the

next morning". Therefore, such resources are highly beneficial to the country that has zero contribution from fossil fuels.

1.2 Role of solar power

Solar energy can satisfy the entire energy requirement of the earth if it is successfully utilised (Kalogirou, 2009). The amount of sunlight continuously reaches the earth's ground surface is ~1.05 x 10^5 TW and the estimated global energy requirement for 2050 is 25-30 TW (Goswami, 2015). Even though a sufficient amount of solar energy is available, energy storage technology is required to provide continuous energy supply during off-sunshine hours.

The utilisation of solar energy is mainly categorised into two technologies namely, solar photovoltaic (PV) system and solar thermal system (Psomopoulos, 2013). In the PV system, solar energy is directly converted into electrical energy for utilisation. Although solar PV technology is growing in popularity, it requires an enormous amount of space as compared to solar thermal infrastructures. Further, the performance of the PV panel reduces significantly with respect to an increase in ambient temperature and solar irradiance (Razak et al., 2016). In the years to come, disposal and recycling of PV panels will be a significant concern as well. E-wastes from PV panels are diffusing highly carcinogenic heavy metals like lead, cadmium, etc. to the environment (Brown et al., 2018).

In the solar thermal system, radiation from the sun is converted into thermal energy and utilised for different applications such as power generation, process heating, drying, etc. Therefore, the inherent advantage of concentrated solar power (CSP) over other sources is that it can naturally supply heat energy directly. The solar thermal system consists of a collector, which is designed to convert solar radiation into thermal energy. Based on the temperature ranges of application, the collectors are classified as non-concentrated collector and CSP collector. Non-concentrating solar thermal collectors, the plate that absorbs the radiation acts as the collector to generate heat at a comparatively lower temperature. However, numerous mirrors/heliostats are used in CSP collectors to reflect the solar radiation at a single focus point which has a capability to generate high-quality heat (Fernández et al., 2019). The current positive trend towards the incorporation of Thermal Energy Storage (TES) systems in CSP technologies will help to achieve the goal of reducing CO_2 emissions by

decreasing fossil fuel-based energy generation. This will further bring down global fossil fuel consumption from 79.7% to zero (Renewables 2019 Global Status Report, 2019).

The applicability of TES for CSP is one of the added advantages for CSP plants in comparison to the PV system. Globally, the favourable locations for the installation of CSP systems are the regions of Middle East, Northwestern and Southern India, Australia, Northwestern China, North Africa, Southwestern United States, Peru, Chile and Mexico (National Renewable Energy Laboratory, 2019).

1.2.1 Solar thermal energy technologies

The solar thermal technology is chosen based on the environmental condition of the plant location and the process application (Tian and Zhao, 2013). The following solar thermal collector technologies have been proven effective for both process heat and power generation applications: (i) parabolic trough collector, (ii) linear Fresnel collector, (iii) parabolic dish collector and (iv) heliostat field collector. Figure 1-2 illustrates the different types of CSP collectors and their operation. The operating temperature ranges of each collector technology are detailed in Table. 1-1.

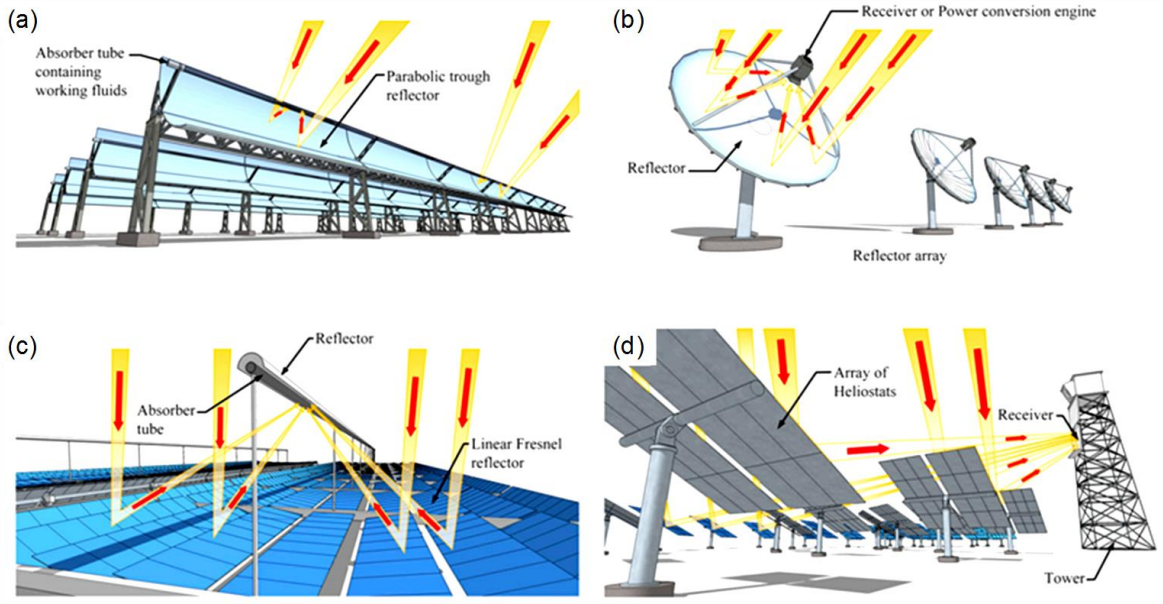

Figure 1-2. Different types of CSP collector technology adopted from the literature (Chamsa-ard et al., 2017). (a) parabolic trough collector, (b) parabolic dish collector, (c) linear Fresnel collector and (d) heliostat field collector or solar power tower.

1.2.1.1 Parabolic trough collector

Parabolic trough collector is made up of curved mirror array, which is used for reflecting the solar radiation towards the receiver tube. The shape of the parabola is such that the receiver is positioned at its focal point, as illustrated in Figure 1-2(a). In general, the collector structure will have an approximate length of 100 m and 5 - 6 m in width. The receiver tube is made of the evacuated glass tube for better performance. These collectors can generate temperature up to 673 K (Llorente García et al., 2011).

1.2.1.2 Parabolic dish collector

In parabolic dish collector, a receiver drum is situated at the focal point of the collector which is of a dish type structure, as shown in Figure 1-2(b). Such collectors can generate temperature up to 1773 K.

1.2.1.3 Linear Fresnel collector

In contrast to the parabolic trough collector, the linear Fresnel collector is made up of multiple rows of flat mirror strips that are used for reflecting the solar radiation towards the downward-facing receiver tube. The main advantage of this collector is that the mirrors used in it are comparatively less expensive than the ones used in the parabolic trough collectors. Due to ground mounting of these structures, as shown in Figure 1-2(c), the infrastructural requirements of this collector is low (Kalogirou, 2004). These collectors can generate up to 573 K and direct steam generation is also possible (Buscemi et al., 2018).

1.2.1.4 Heliostat field collector

Heliostat field collector consists of numerous mirror arrays to reflect the solar radiation towards the receiver drum, as shown in Figure 1-2(d). Receiver drum or steam generator is placed at the top of a centrally mounted tower to generate thermal energy (Romero et al., 2002). The key benefit of this system is that minimum heat exchangers are employed due to direct steam generation, which helps to minimise the transport requirements of thermal energy. It is possible to generate a temperature up to 1273 K using this technology.

1.2.2 Solar tracking system

The solar tracking systems are classified as single-axis tracking (east to west direction) and double axis tracking (all four directions). The single-axis tracking system will increase the

energy extraction by 20-25%, whereas in the double-axis tracking system, it will increase by 40-45% (Aeron, 2019). The tracking systems are engaged to maintain the solar collectors perpendicular to the sun's rays. This perpendicular position of collectors helps in increasing the amount of energy extracted by absorbing maximum solar radiation (Sukhatme SP, 2008).

1.2.3 Challenges of CSP technology

CSP technology is expected to provide higher efficiency than the PV system. However, the development of CSP technology has slowed down due to the multiple technical challenges faced during their implementations. (i) Water is one of the crucial components in CSP for the purpose of wet cooling towers and cleaning the collectors. The availability of water in such high solar radiation (dry) locations is a highly challenging aspect. Approximately 0 to 3.5 m^3/MWh of water is required for operating the current CSP plants (Bracken et al., 2015). (ii) The selection of a suitable Heat Transfer Fluid (HTF) is one of the crucial aspects, which is being chosen based on receiver type, design parameter, power generation unit, storage technology, the life cycle of the HTF and capital cost. Most commonly used HTFs for CSP application which have been reported in the literature are as follows: molten salt, thermal oil, water and air, however, supercritical CO_2 is getting a great attention lately. Among them, molten salt is preferred for high-temperature applications. However, due to the freezing of molten salt at lower temperatures and its corrosive nature, the operation of CSP with molten salt requires special attention (Guillot et al., 2012). Thermal oil is favourable for operating under 523 K, but it is highly unsafe to use beyond this temperature. Water is one of the most commonly used HTF for low-temperature application considering a cost-effective solution. Engaging water/steam as the only heat transfer fluid for power production will decrease the levelized cost of energy by 11% as compared to the oil-based HTFs (Feldhoff et al., 2010). The main drawback of water is its unavailability and the significant corrosion rate observed beyond 573 K when utilised with carbon steels (Van rooyen et al., 1969). Air is one of the cost-effective HTF as it is freely available in the atmosphere. However, it is rarely employed due to its poor thermal conductivity. (iii) The selection of energy storage material and its sizing is a challenging task to achieve cost-effective thermal energy storage (TES) system for CSP. Degradation and heat transfer characteristics of storage material are the important factors to be considered while developing the TES system. By addressing the above-mentioned bottlenecks, CSP community may be able to operate impeccable CSP plant.

1.3 Energy storage technology

Energy Storage (ES) system is one of the important elements in the standalone renewable power generation sector so as to bridge the gap between demand and supply. Development of cost-effective ES technology can lead to an increase in the renewable energy-based power capacity while reducing the contribution from conventional power sources, such that the pollution caused due to the CO_2 emissions can be minimised (Elliott, 2013). The successful demonstration of energy storage technology may be possible by making them cost-effective and reliable for the CSP plant. The benefits of ES are (Dincer and Rosen, 2011) (Kalaiselvam and Parameshwaran, 2014):

- reduced cost of generated power
- energy security
- reduction of environmental pollution
- reduced initial and maintenance cost.

ES can be generally categorised into chemical, mechanical, biological, thermal and magnetic energy storage. Based on the energy storage time, the ES can be classified into short-term and long-term storage (Li et al., 2013). The current thesis work is mainly emphasised on thermal energy storage. In TES, the energy is stored in the form of sensible or latent or thermochemical heat using different storage materials. Section 1.4 will be briefing more about thermal energy storage technology.

1.4 Status of Thermal Energy Storage (TES) technology

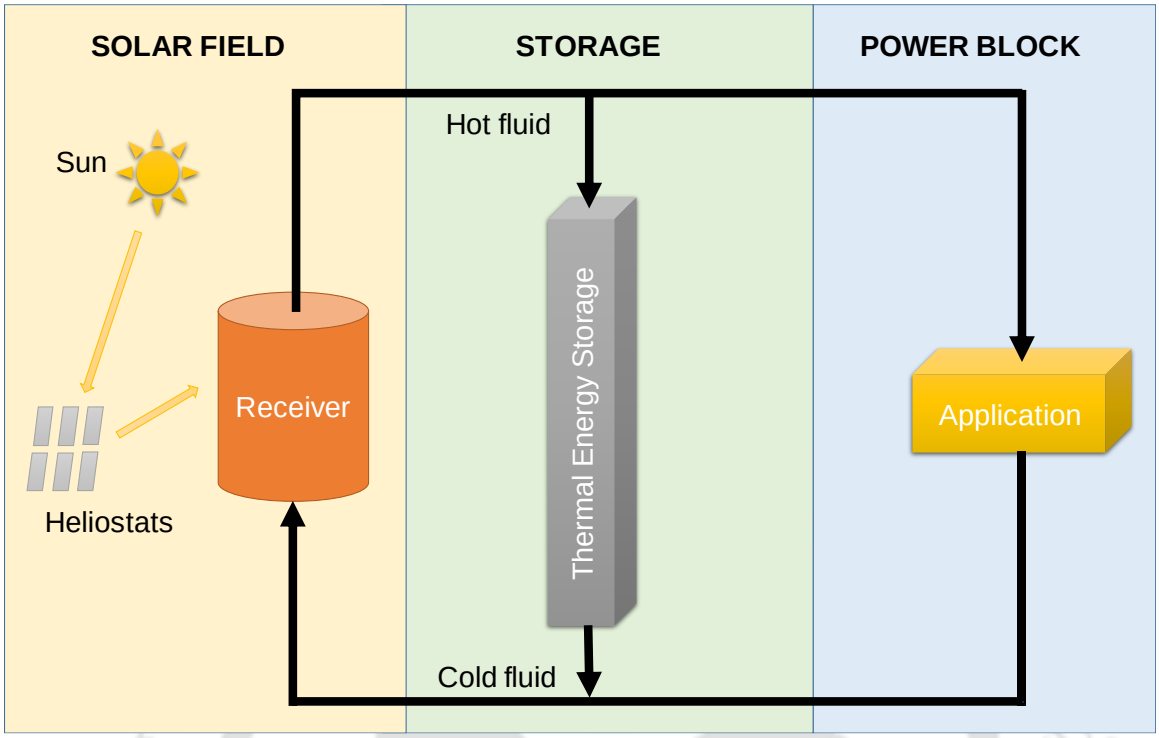

Figure 1-3. A schematic view of integrating CSP and TES technology.

Energy requirement for power production units will be varying with respect to the time and seasonal constraints of the industrial, commercial and domestic sectors. TES systems will help to match the demand and supply synergistically considering the availability of all the energy sources. While integrating the TES with CSP plants, the following characteristics have to be considered such as high discharge efficiency, suitable temperature condition, low cost, low heat loss during storage, convenient availability of material and harmless to the environment (Zalba et al., 2003). Figure 1-3 shows the prospect of integrating TES with CSP technology. The heat energy is the primary driving force for CSP power plants, and without this continuous supply, the power generation unit cannot function 24/7 period, which leads to underutilization of the assets. Generally, the TES systems are also called as the regenerative heat exchanger, which can store and release the heat during charging and discharging processes. Therefore, the integration of TES with CSP will help to bring down the levelized cost of electricity with an increase in capacity factor and efficiency.

Table. 1-1 Various solar thermal energy collectors and the feasibility of their integration with TES (Pelay et al., 2017).

Technology	Operating temperature (K)	Feasibility of TES integration	Merits	De-merits
Parabolic trough collector	393–673	Feasible	- Low cost of installation. - The experimental response is high.	- The comparatively large requirement of space. - Low operating temperature resulting in low efficiency.
Linear Fresnel collector	323–573	Feasible	- Low cost of installation.	- Low operating temperature resulting in low efficiency.
Central Receiver Tower	573–1273	Highly feasible	- High operating temperature resulting in high efficiency.	- The comparatively large requirement of space. - High capital cost.
Parabolic dish collector	393–1773	Not feasible	- Comparatively less space requirement. - High operating temperature resulting in high efficiency.	- High capital cost. - The experimental response is low.

1.4.1 Thermal energy storage concepts and benefits

Globally, different concepts of thermal energy systems are adopted based on the requirements of end application and the availability of infrastructures. In general, active and passive storage

concepts are the common techniques followed to store the thermal energy, which are irrespective of the storage material and the heat exchanger design.

1.4.1.1 Active storage system

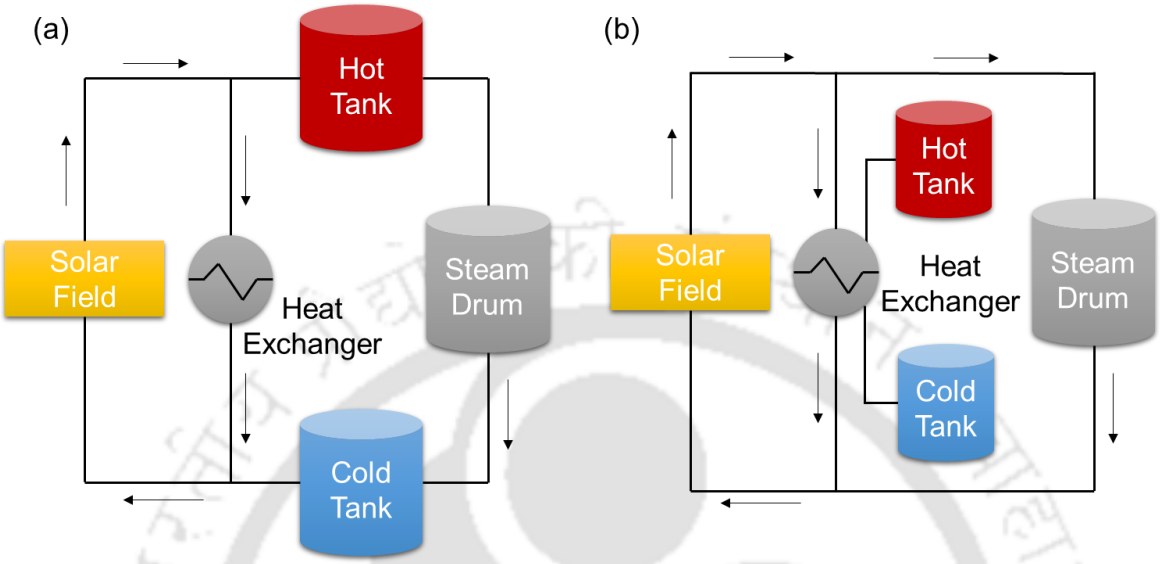

Figure 1-4. A schematic view of the active storage system (a) direct, (b) indirect. Conceptions are adopted from the literature (Gil et al., 2010).

The active storage system is based on the theory of forced convective heat transfer by HTF to the TES material. The active storage system is subdivided as direct and indirect storage system. The direct storage system is one of the most challenging systems to implement in the real-time because the HTF also acts as the storage material. There is a necessity to find an HTF, which itself should have a good capacity to store the heat (Herrmann et al., 2004).

In an indirect storage system, a separate energy storage material will be used to store the heat energy and heat exchangers will be used to transfer the heat between HTF and storage material during charging and discharging processes (Zaversky et al., 2014). Figure 1-4 illustrates the different concepts of the active storage system reported in the literature. The direct storage systems are more complex than indirect storage due to the requirement of multiple tanks for storing HTF (Gil et al., 2010).

1.4.1.2 Passive storage system

In this concept, HTF is pumped to pass through the storage material for storing and releasing the heat during charging and discharging processes, respectively. In contrast to the active

storage system, the storage material in the passive concept is made of the solid medium (as shown in Figure 1-3). A detailed description of the storage materials is being discussed below.

These storage concepts are well-recognised for their different key roles in load management of thermally driven systems (Mehling and Cabeza, 2008; Ö Paksoy, 2007):

- The reliability of the thermal system is improved with TES as a standby option and coupled in a hybrid system with other energy sources.
- The total power generation capacity is improved while shifting from the off-peak period to high-demand period.
- Load shifting from high-tariff time to low-tariff time will decrease the energy cost.

1.4.2 Forms of thermal energy storage systems

The selection criteria of storage methods are purely depending on the net energy stored per unit volume, space, operating temperature range, and the capital investment on infrastructures and technology. There is a possibility to store the thermal energy using the sensible heat of a liquid/solid medium, the latent heat during the phase change of material and through a chemical reaction. Therefore, such useful energy will be stored and used subsequently.

The primary classification of TES methods:

- Sensible Heat Storage (SHS)
- Latent heat storage
- Thermochemical heat storage.

1.4.2.1 Sensible heat storage

In SHS, thermal energy is stored by heating solid or liquid material. The amount of thermal energy stored is related to the heat capacity, change in temperature and quantity of the storage material (Medrano et al., 2010a). The total energy stored and released is given by Eq. (1.1),

$$Q = mC_p \Delta T \tag{1.1}$$

During energy storage and discharging process, the SHS materials do not undergo any phase transformation, as shown in Figure 1-5. Although liquid materials such as molten salts have excellent heat storage properties, they are not completely successful in a commercial aspect,

and this is mainly due to the inherent technical challenges such as high freezing point of liquid salt, corrosive nature and requirement of large volume tanks. Based on different temperature conditions, a wide variety of SHS materials are examined for the heat storage purpose. The conventionally used materials are molten salts, solidly packed beds, refractory materials, industrial wastes, pebbles, water, hydrocarbon oils and liquid metals (Fernandez et al., 2010). The intrinsic characteristics of these materials facilitate energy exchange between the SHS material and suitable HTFs which results in a cost-effective solution. However, one of the technical bottlenecks of SHS is that it cannot provide consistent HTF outlet temperature during the discharge process.

1.4.2.2 Latent heat storage

In latent heat storage, thermal energy is stored/discharged during the phase change of the energy storage material at the nearly same temperature, as shown in Figure 1-5. Generally, the storage of heat is possible during the change in phase from solid to liquid, liquid to vapour and solid to solid. Although the energy density in liquid to vapour transition is very high, it is not practically employed due to the rapid change in volume (Cárdenas and León, 2013).

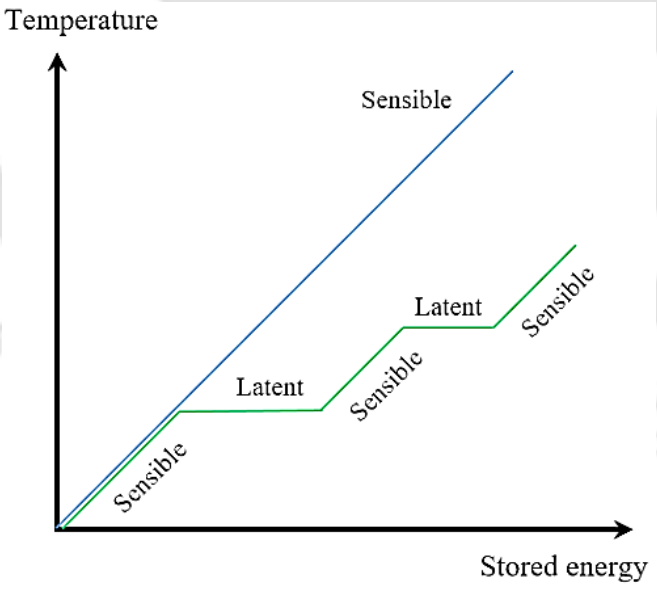

Figure 1-5. Variation of energy with respect to temperature in Sensible and Latent heat storage (Louis Tse, 2016).

The main advantages of using the latent heat storage system are: (i) less volume occupancy per net energy stored and (ii) constant HTF outlet temperature during the discharge process. The major drawbacks of using this technology are poor thermal conductivity (do Couto Aktay

et al., 2008), the highly corrosive nature of salts and its tendency to increase the operation cost of the storage unit. The total energy stored and released is given by Eq.(1.2),

$$Q = m\left(C_p \Delta T + L_f \theta\right) \tag{1.2}$$

1.4.2.3 Thermochemical energy storage

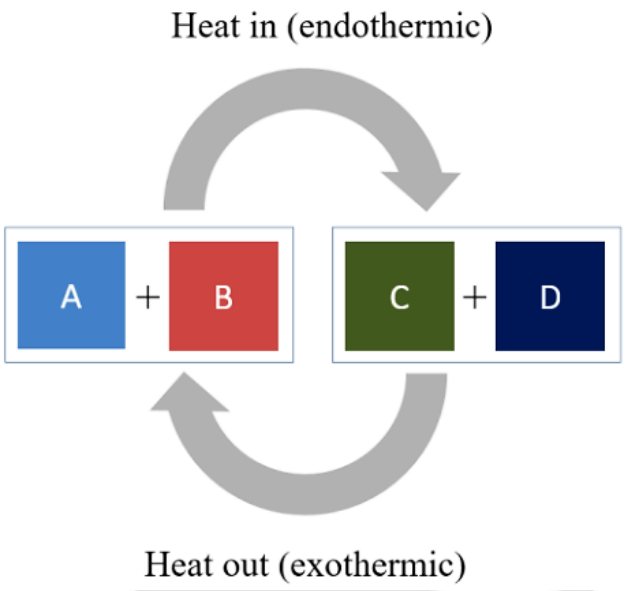

Figure 1-6. Heat storage and release process in Thermochemical energy storage (Louis Tse, 2016).

In thermochemical energy storage, energy is stored and released respectively during reversible endothermic and exothermic chemical reactions, as shown in Figure 1-6. Such chemical reactions will tend to break and reform the molecular bonds during reversible reactions. The total energy stored and released is given by Eq. (1.3),

$$Q = m\Delta h_e \alpha \tag{1.3}$$

where, m, Δh_e and α represents mass, endothermic heat reaction and conversion-fraction reacted, respectively.

The main advantage of this storage technology is its high energy density. However, thermochemical energy storage is yet to be sufficiently established for real-time commercial applications (Pardo et al., 2014). Comparatively, the primary advantage of the SHS system

over the other storage mechanisms is its high durability and wider operating temperature range of the material. The life of solid SHS material is five times more than the latent heat materials and ten times more than the thermochemical storage materials (Nazir et al., 2019). Generally, SHS materials are easily available and economically viable. Unlike the other storage materials, SHS materials are not corrosive to the infrastructures. On the other hand, due to practical challenges in implementation, thermochemical and latent heat storage mechanisms are not much commercialised in the high-temperature thermal energy storage system. However, each mechanism has its own unique merits and demerits.

1.4.3 Potentials and barriers of TES

Thermal energy storage is a perfect alternative energy source to match the demand and supply, such that it can decrease the price of the peak power and global warming by replacing fossil fuel sources. If the thermal energy storage is extensively incorporated with CSP plant and waste heat recovery, it is estimated that approximately 1.4 million GWh of energy per year could be saved from heating and cooling loads in the buildings and the industries. Such implementation will help to avoid 400 million tons of CO_2 emission/year in Europe alone (Hauer, 2013). However, during the real-time implementation, TES is facing more number of challenges such as high capital cost, poor ES material life cycle and corrosion phenomenon.

1.5 Motivation of the thesis work

Solid sensible heat storage systems are highly durable and cost-effective for high-temperature thermal energy storage and discharge process. The overall performance of the high-temperature solid SHS system is highly depended on the optimised design of the heat storage module and selection of storage material based on the final end-user requirement. Since the experimental studies are expensive, there is an apparent need to analyse the heat transfer behaviour of the SHS system using three-dimensional computational study, which also helps to predict the charging and discharging performance of the SHS system. Its practical implementation requires the developed numerical model of the SHS module to be validated through a wide range of high-temperature experimental study as well. In addition, the development of a simplified model for the SHS system is required to understand the overall system performance which can be used to facilitate the practical applicability of the system in various scenarios. In the current thesis work, the performance and aftermaths of the multi-

tube solid SHS system are studied for the high-temperature range with different cost-effective heat storage material.

1.6 Thesis Structure

The thesis is organized into five chapters. A brief description of each chapter's content is detailed below:

Chapter-1 starts with the scenario of energy and renewable energy utilization pattern in India as well as the world. A brief introduction is provided for the various storage concepts of TES systems and their challenges. The importance of using the sensible heat storage system among available TES technology and the subsequent motivation of the present thesis work has been elaborated.

In Chapter-2, the detailed literature survey is presented in the following aspects:

- Exploring the possibilities of employing different SHS materials for high-temperature storage.
- Reviewing the performance enhancement of different SHS materials in real-time.
- Describing the design aspects of the thermal energy storage system.
- Studies on various HTFs employed in TES systems with their merits and demerits.
- Studies on mathematical and numerical models developed for predicting the performance of the TES modules.
- Exploring the integration of different applications employed using the SHS systems.

Chapter-3 presents the experimental and numerical investigations carried out on a cast steel based sensible heat thermal energy storage system using air as a heat transfer fluid. Details of the 3-D model using the COMSOL Multiphysics and 1-D dynamic model using the Dymola software, developed for predicting the performance of cast steel module are presented.

Chapter-4 presents the experimental studies and numerical simulations carried out on concrete based thermal energy storage system with air as HTF. The extensive experimental investigation on multi-tube module for storing the high-temperature heat is discussed. Details of the 3-D model and 1-D dynamic model for predicting the performance of concrete thermal energy storage system during the charging and discharging process are presented.

Chapter- 5 describes an approach to estimate the performance of the high-temperature multi-module arrangements of SHS systems. The dynamic modeling approach discussed in Chapter 3 and Chapter 4 is used to develop the different SHS modules in series/parallel arrangements. The charging and discharging performance of various module arrangements is evaluated and discussed. The net energy discharge unit cost of different SHS module arrangements are calculated and presented.

In chapter-6, important conclusions obtained from experimental and numerical investigations are presented. Scope for future work and recommendations are also presented in this chapter.

1.7 Summary

The introduction section starts with the recent global and Indian scenario of energy and renewable energy. It is extended with the explanation of different concentrated solar thermal power receiver technologies. Further, the classification of energy storage technologies and their respective usages are detailed. Various merits and demerits of the different thermal energy storage technologies with their brief concepts are explained. Design configurations of the different SHS modules are described as well. To sum up, the motivation and structure of the thesis are clearly enlightened in the order.

CHAPTER 2
STATE OF THE ART

2.1 Foreword

United Nations requested the world community to fight against rising global warming and other climate change issues. The solar thermal energy is found to be the best alternative energy source against conventional fossil fuel-based power plants, and that will help us to reduce the greenhouse effect. The intermittent nature of solar energy availability requires the effective TES system to balance both supply and demand during peak hours. Therefore, researchers are focused on developing an innovative low-cost TES system for the solar thermal power application, and a considerable amount of research works has been reported. However, there is always a need to develop a compact, highly durable and cost-effective solid-phase SHS system. Selecting a cheaper SHS material with better thermal properties is an essential factor to achieve low-cost storage technology. Development of a versatile numerical model is highly essential to study the design aspects. The experimental validation of a thermal energy storage model is an important aspect before integrating them with the actual application. Therefore, in this chapter, a detailed literature survey on the potential cost-effective SHS materials, different aspects of the heat transfer fluids, various approaches for numerical modelling of the SHS system, and the practical applicability of solid phase SHS system are presented.

2.2 Sensible Heat Storage (SHS) materials

The components of SHS system such as storage medium and container should be compatible with the HTF in terms of chemical and structural stability, non-flammability and non-toxicity while handling. Any material which is chemically stable, does not degrade rapidly and possesses the same thermal properties over multiple charging and discharging heat cycles are suitable for the SHS applications. Several studies have mainly focused on the development of energy storage material with desired characteristics for the 24/7 operation of the CSP plants.

2.2.1 Liquid SHS materials

The key benefit of liquid SHS material over the solid SHS material is that they can act as both energy storage medium and HTF, and such a system is called an active energy storage system (see Figure 1-4). It also minimizes the number of heat exchanger required between solar and power loop. In liquid SHS, the material undergoes a change in temperature and density during the process of heating and cooling. Therefore, the resultant buoyancy effect creates a thermal gradient within the fluid which separates itself as the hot fluid layer on top and the cold fluid layer on the bottom (Gil et al., 2010).

Water is one of the suitable liquid for thermal energy storage media for industries and domestic applications in the range of 298 K to 363 K (Hasnain, 1998). It is toxic-free, low cost, and has high specific heat capacity. The size of storage tanks may vary from a few hundred litres to a few million litres with respect to the storage capacity. For smaller SHS system, storage tanks are usually made of steel, concrete wall, aluminium, and fiberglass. For a high capacity system, the solar ponds and underground thermal energy storage concept are used for storing the heat along with gravels. Both concepts reduce the infrastructure cost required for energy storage and allow them to store the heat in a cost-effective way (Kousksou et al., 2014). However, the water-based energy storage systems have drawbacks like corrosive nature, high vapour pressure, and high heat loss due to diffusion of steam.

Thermal oil is explored as a thermal energy storage medium that can work for medium temperature (~623 K) because the vapour pressure of thermal oil is lower than the water. The heat capacity of thermal oil is higher than the water. Therefore, thermal oils can be used as both the thermal energy storage material and the HTF in solar thermal applications. As compared to water, thermal oil has very negligible corrosion effect with stainless steel. This

oil does not freeze at atmospheric temperature (~293 to 318 K), and that allows for robust startup and shutdown features for energy storage system without freeze protection system. However, the main drawback of using thermal oil is that it is expensive and has a shorter life span due to thermal degradation.

The molten salt mixtures are mostly used in the high-temperature application (~873 K) such as CSP plants. The specific heat capacity of molten salts such as carbonate salts and fluoride salts are high (approx. 1.5 to 1.9 kJ/kg-K) (Ding et al., 2018). Therefore, the molten salt can store more heat in less volume. Different varieties of molten salts are explored for thermal energy storage application such as chloride, carbonate and fluoride salts with various mass ratio mixtures. Mohan et al. tested the performance of molten chloride salt mixtures as SHS material (Mohan et al., 2018). The low-cost chloride salt mixtures are found to have excellent thermal stability and better thermal properties than the nitrate salt mixtures (Villada et al., 2018). However, molten chloride salt mixtures are hygroscopic and highly corrosive with stainless steel (SS310 and SS316) tank materials. The possibility of reducing the corrosion by molten salt was explored by using the electrolysis (salt purification) process, especially at high temperature (Ding et al., 2019). Due to this salt purification, the rate of corrosion had reduced by 93% after removing the impurity $MgOH^+$ from the molten chloride salt mixtures.

Liquid metals are widely used as HTF in a nuclear reactor and it is explored as a thermal energy storage medium in the solar thermal application. The operating temperature of the liquid metals is lower than the molten salt mixtures. The advantages for the liquid metals are their low viscosity, high thermal conductivity and a wide operating temperature range. The main drawbacks of the liquid metals are their high cost and low specific heat capacity in comparison with molten salts (Alva et al., 2017).

Andreu-Cabedo et al. (2014) had measured the specific heat capacity of eutectic salt mixtures by adding silica nanoparticles at a different weight ratio (0.5, 1, 1.5 and 2%). The specific heat of 1% weight ratio mixture was found to be 25% higher than the eutectic salt mixtures, and such an increase in heat capacity had reduced the cost of TES material.

Herrmann et al. (2004) had studied the techno-economic feasibility of 2-tank molten salt storage system for solar thermal application. The estimated cost of the molten salt system was found to be in the range of 30-40 USD/kWh_{th}. Also, they proposed that by increasing the storage capacity for 12 h, the levelized electricity cost could be reduced by 10%.

Kearney et al. (2003) had analysed the possibility of using the molten salt as HTF and storage material in the parabolic trough collectors based CSP plants. The result has concluded that parabolic trough collectors with a molten salt system can provide low levelized electricity cost (14.2%) than the plant operated with synthetic oil consisting of a eutectic mixture of biphenyl/diphenyl oxide. Also, Kearney et al. (2004) had analysed the engineering aspects for the operation and maintenance of the CSP plants such as freeze protection of molten salts, CSP loop maintenance, selection of materials for piping and fitting materials, and CSP's pre-heat method.

2.2.2 Solid SHS materials

The solid SHS system is suitable for both low and high-temperature applications, and they are highly durable and low cost in comparison to molten salt or liquid metal-based SHS system. They also possess advantages like zero evaporation loss, operation in ambient pressure and can operate without freeze protection system. In solid SHS system, the storage material is in a static condition, and it can be called the passive energy storage system. The temperature of the solid SHS medium varies during the charging and discharging process. Due to this phenomenon, the HTF temperature also varies during the discharge process which leads to variable energy output from the SHS system.

Lugolole et al. (2019) has compared the energy dissipation performance of sunflower oil-based liquid SHS system and granite pebble based solid SHS system. The size of the granite pebble and the HTF velocity are considered as the design variable. The experimental result has concluded that the energy rate, exergy rate and discharging time were the function of the HTF flow rate and granite pebble size. The performance of the granite pebble based solid SHS system was found to be a better performance than the sunflower oil-based liquid SHS system.

Jemmal et al. (2017) had studied the prospects of packed bed flint and quartzite rock as an SHS material. The result from the characterization of these rocks had concluded that the quartzite rock can fulfil the necessity of TES material. In addition, during the cyclic thermal operation, degradation of the rock was observed due to the presence of silanol in the quartzite rocks. This could be avoided by removing the silanol from quartzite rocks using heat treatment.

Girardi et al. (2017) had fabricated and tested two types of concrete based SHS systems such as: (i) concrete with recycled aggregates and (ii) concrete with polyamide fibres, steel fibres and metallic powders or shavings. The later one was found to be 300% more durable than the ordinary concrete. After the heat treatment of the SHS module at 573 K for 4 h, they found that the morphology of the second type material was closely packed with minimal cracks. Further, due to the thermal treatment, the thermal conductivity of the second type of material was reduced from 2.74 W/m-K to 2.13 W/m-K.

Xu et al. (2017) had tested the degradation and thermal expansion characteristics of a low-cost SHS material (sand saturated with thermal conductive fluid) and compared it with concrete based SHS system. The performance of their SHS material was found to be better than concrete or sand-based SHS system. Further, they suggested that the stability of the thermal conductive fluid should be studied for an extended period to conclude the stability of sand saturated with thermal conductive fluid SHS system.

Grirate et al. (2016) had tested the thermal behaviour of different types of rock such as marble, basalt, cipolin, hornfels, granite and quartzite as an SHS material. The properties of the selected SHS materials were tested in the temperature range of 523-623 K with direct contact to the synthetic oil (HTF). The performance of cipolin and quartzite were found to be better than the other materials.

Jemmal et al. (2016) had characterized and tested the potential of gneiss rock as a storage material for the packed bed TES system. The gneiss rock had been subjected to temperature up to 1273 K. The thermal properties of the rock sample were measured using the thermo-gravimetric and differential thermal analyzer; also, crystalline phases and chemical composition of the rock were recognised using the X-ray diffraction and X-ray fluorescence methods, respectively. The result has proved that the selected TES material was exhibiting excellent thermal properties up to 823 K

Schlipf et al. (2015) tested the feasibility of using silica sand (0.2 mm grain size) and quartz gravel (1-2 mm diameter) as the thermal energy storage material. The storage and discharge potential of these materials were found to be superior up to 823 K. The small size of sand had resulted in high heat storage capacity with fast charging and discharging potential.

Klein et al. (2013) had experimented to analyse the performance of the high-temperature packed bed loaded with Denstone ceramic pebbles material for the solar gas turbine cycles.

The experiments were conducted in the temperature range of 623 - 1173 K. The temperatures of the HTF and storage materials were recorded across the packed bed, and the same was used for the validation of a numerical model for the heat transfer analysis.

Zanganeh et al. (2012) had developed and tested the rock-based packed bed SHS system using air as the HTF, with the storage capacity of 6.5 MWh_{th}. A dynamic numerical model was developed to solve the unsteady state heat transfer equations and the same had been validated with the experimental conditions. The developed model was further scaled up for the electricity production of 26 MW_e with two storage system of capacity 7.2 GWh_{th} each. During the steady cyclic behaviour of the plant, 95% of overall thermal efficiency had been achieved in the storage system.

Hänchen et al. (2011) had developed and tested the magnesium silicate rock-based packed bed SHS system using the air as HTF at a maximum operating temperature of 793 K. Using the crushed rock with small particle size resulted with highest overall efficiency (90% at the optimal condition) of the storage. Since the size of the rock was small and the void space was less in-between the rocks, the heat loss was minimized despite the poor thermal conductivity. The main advantage of rock is that they are readily available, very cheap, non-flammable and non-toxic. However, the disadvantages are high-pressure drop and high HTF flow rate requirements.

Brosseau et al. (2005) had performed a life cycle study to demonstrate the stability of filler based SHS material like quartzite rock and silica in the molten nitrate salt (HTF) environment. The filler loaded molten salt SHS system was able to provide a stable performance without degradation.

Fricker (1991) had tested the performance of high temperature (673 K) heat storage system based on a natural rock as storage material and air as the HTF. The rocks were arranged in a pebble bed structure inside the steel container. The problem due to the ratcheting had been addressed by decreasing the container height with respect to diameter. Further to achieve optimized pressure drop and heat transfer rate, the diameter of the container was recommended to be maintained between 16 - 20 m.

Beasley et al. (1985) had studied the transient behaviour of the rock-based SHS system while being charged by a solar air heating system. The dynamic temperature profile across the SHS system during discharge at no airflow condition showed that net heat was transferred from

high-temperature section to low-temperature section due to internal heat diffusion and natural convective mixing of air within the packing. The heat losses from the SHS module boundary to the environment had resulted in a 30% reduction in energy availability. Therefore, while designing the SHS module, the effect of the above-mentioned phenomenon has to be taken care to minimize energy loss.

Although there were multiple choices for storing the heat in a solid medium, there was a parallel development in exploring concrete which is exhibiting high specific heat capacity, low cost, high thermal conductivity, easy adaptability, high durability, no thermal expansion coefficient, wide operating temperature ranges and environment-friendly. Due to its better stability, it does not require a storage tank for SHS material, and hence it acts as a passive heat storage system. Considering the advantages of concrete as SHS material, recently, Hoivik et al. (2019) have demonstrated the performance of two concrete based thermal energy storage systems of capacity 500 kWh_{th}. The material used for TES has been mass-produced from a unique concrete mixture called HEATCRETE® vp1. The performance of concrete SHS system was analysed at the temperature of 653 K for 20 months, comprising of 279 charging and discharging cycles. The result showed that there was no cracking or spalling on the TES material. The mechanical and thermal properties of the sample before and after the test has shown that the properties were stable.

Felizardo et al. (2019) have tested the thermal performance and stability of the concrete structure with and without the refractory coatings (alumina mortar and zircon paint), and allowed them to be in contact with the mixture of molten salts for 1500 h. The concrete structure was tested by varying the temperature from 563 - 773 K. The result showed that the thermal conductivity of the concrete with the refractory coating has increased without affecting the heat capacity. The molten salt was able to penetrate with sand alone concrete, but it was not able to diffuse in the case of refractory coated concrete.

The SHS system can not provide constant energy output in comparison with latent heat based storage system. Therefore, the integration of both systems may enable benefits like high heat storage density, constant temperature output during discharge, and at a low cost. To achieve the same, Miliozzi et al. (2019) have studied the performance of concrete SHS system by adding 2% of phase change material (PCM) by weight. The PCM embedded concrete material was found to have increased heat capacity and thermal conductivity than the stand-alone

concrete. The volume and cost of the PCM embedded concrete material were reduced by 10% compared to the stand-alone concrete based TES system.

Many studies have reported that the expansion of concrete material might lead to a gap between HTF tubes and SHS material, which would result in reduced heat transfer and storage capacity (Khoury, 2000; Li et al., 2004; Sivakumar and Santhanam, 2007; Skinner et al., 2014). To overcome this issue, Skinner et al. had introduced heat curing fibered paste (HCFP) and polytetrafluoroethylene (PTFE) layer in between the SHS material and HTF tubes. The stability of the concrete SHS system was tested using molten salt as the HTF by varying temperature from 673 – 773 K. The HCFP layer had reduced the crack formation but not to the expected level, and PTFE had improved the heat transfer in-between the HTF and concrete material (Skinner et al., 2014).

In another approach, Ozger et al. (2013) had mixed the nylon fibre inside the concrete TES material to test thermal and mechanical properties by comparing it with the ordinary concrete. The respective thermal conductivity and specific heat capacity for the fibre reinforced concrete was 1.16 W/m-K and 0.63 J/kg-K, whereas for the ordinary concrete was 1.02 W/m-K and 0.81 J/kg-K. After introducing the nylon fibres with the TES material, the thermal stability had increased until 773 K. After 433 K, the nylon fibres melted and filled the gaps generated due to spalling and this avoided the formation of cracks by bearing the thermal strains

Similarly, Skinner et al. (2011) had tested the ability of the polytetrafluoroethylene (PTFE) and a heat-curing, fibered paste to reduce the cracks between HTF tube and concrete using nitrate salt as the HTF. The SHS unit was operated in the temperature range from 723 K to 773 K. The long-term performance analysis of SHS module concluded that both interfacing materials were able to reduce the number of cracks in the SHS module.

John et al. (2011) had tested concrete based thermal energy storage material using a cement mixture consisting of steel fibres, calcium aluminate, and polypropylene. The study comprised of testing the TES sample material by varying the temperature from ambient to 773 K. The result has concluded that after ten heating and cooling cycles, the material could retain 75% of the compressive strength without any cracks.

Khare et al. (2013) had proposed a methodology to identify the best suitable SHS material for the high-temperature TES. The proposed method used the cost of SHS material, mechanical

and thermal properties as an input parameter to select the best material for high-temperature application. The SHS materials such as alumina, silicon carbide, high-temperature concrete, graphite, cast iron and steel were found to be highly suitable for high-temperature application. The performance of SHS material was benchmarked based on the cost of thermal energy storage, i.e. $US/kWh. The proposed methodology concluded that the high alumina concrete and magnesia were found to be cost-effective material with better thermal properties

John et al. (2013) had prepared SHS material by manipulating concrete mixture proportions and its unit cost of storage varied from $ 30/ kWh_{th} to $ 0.88/ kWh_{th}. The stability of concrete mixtures was tested under different operating conditions as follows: (i) The concrete sample was kept in a molten salt bath at 858 K for 500 h; (ii) after 500 h, the sample was exposed to 30 cycles of charging and discharging process (between 573 - 873 K). The test result concluded that the concrete made out of ordinary portland cement and fly ash was found to be inexpensive SHS material with high specific heat and thermal conductivity.

John et al. (2010) had tested the durability of the concrete TES material with respect to the heating rate. The testing material had been moulded with the water and cement ratio of 0.15 to 0.3 at 180 MPa of compressive strength. The casted material was exposed to the heat in the rate of 9, 7, 5 and 3 K/min. The test samples were prepared with and without the mixing of polypropylene fibres. Beyond 773 K, at the heating rate of 7 K/min, the concrete mixture without the polypropylene fibres had lost the stability and spalling was observed. However, at all the heating rates, the concrete mixture with polypropylene fibres was able to withstand up to 873 K without any spalling.

Guo et al. (2010) had developed a new mixture of concrete material for high-temperature TES application in CSP plants. They added graphite material for improving the thermal conductivity while basalt and bauxite rocks were added as an aggregate to enhance the specific heat capacity of the TES material. The new concrete mixture was found to have improved thermal conductivity of 2.34 W/m-K, which is higher than the conventional concrete (1.4 W/m-K) material used in TES. On the other hand, the mechanical strength of the new concrete mixture had decreased due to the addition of graphite.

Laing et al. (2006) had compared the performance of cast-able ceramic and high-temperature concrete as SHS material at 663 K for storing 350 kW of energy. Due to the low cost, high mechanical strength and ease of handling, concrete was preferred than the ceramic. However,

the ceramic material was having 35% more thermal conductivity and 20% more heat capacity when compared to concrete. After 60 thermal cycles of charging and discharging operation, both materials were found to be stable, and no degradation in heat transfer was observed. After successful testing in lab scale, both the materials were used in a commercial application.

2.3 Heat transfer fluid

The HTF is a crucial component for storing and transferring of energy within the TES system. The efficiency and stability of the CSP plants are also based on the selection of most suitable heat transfer fluids and its compatibility with the SHS material. There are some parameters which should be considered while selecting the HTF such as low viscosity, cost-effectiveness, high thermal conductivity, low corrosion with infrastructure, thermal stability without the degradation for a longer duration, low vapour pressure, high boiling point and low melting point (Cordaro et al., 2011; Pacio and Wetzel, 2013). The HTF can be majorly classified based on the nature of the material. The materials are thermal oils, molten salts, water/steam, liquid metal and air/other gases (Pacio and Wetzel, 2013; Tian and Zhao, 2013). Some of the HTFs have the potential to act as the thermal energy storage material as well in the active type storage system which were previously detailed in Section 2.2.1.

Air as HTF fluid is not studied extensively in the CSP plants. At present, Ait-Baha CSP pilot plant (Good et al., 2014) and Jülich solar tower (Zunft et al., 2011) are using air as the HTF. Though the thermal properties of air such as thermal conductivity and specific heat are more inferior than other commercially available HTFs, the air has its advantages such as free availability, high corrosion-resistance (Guillot et al., 2012) and higher operating temperature range of up to 1373 K. It is suitable to be used for a wide variety of thermal applications. Additionally, the air has excellent flowing characteristics at higher temperature due to low dynamic viscosity (approx. 3×10^{-5} Pa s at 773 K) (Liu et al., 2014). Apart from the air, supercritical CO_2 and helium are being used as HTF in nuclear power and CSP plants. The cost of these gases is found to be affordable for the continuous operation of power plants. Although helium gas can be used for high-temperature applications similar to air (Xu et al., 2010), the specific heat capacity and heat transfer efficiency are observed to be below than that of air. Results from National Renewable Energy Laboratory's research have highlighted the possibility of using supercritical CO_2 for very high-temperature CSP application (Neises and Turchi, 2014).

2.4 Design of the thermal energy storage module

The optimal sizing of thermal storage will minimize the energy storage time and maximize storage capacity per unit volume of the module. The sizing of the module includes the design of HTF passages and the capacity of the module. Four types of thermal storage modules are studied in the literature, and their potentials and limitations are summarised below:

- Water tank storage system: Water is one of the most available and cheapest material commonly used in the SHS system (Basecq et al., 2013). Storing of heat via hot aquatic containers are a well-known technology. In this type, water is directly allowed to pass through the solar collector, and once it attains the required storage temperature, it is directly stored in a well-insulated container and can be used for various applications.
- Seasonal bore well storage: In this type, the energy can be stored whenever it is available and used whenever it is needed. Vertical pipes containing HTFs will be used for transferring the heat from ground level to underground level where the heat is stored inside the soil, gravel and clay around the different borehole provisions (Lanahan and Tabares-Velasco, 2017). The countries which have poor access to solar energy are adopting this technology for the extended usage during long winters (Gao et al., 2015).
- Packed bed storage system: In this system, rocks or pebbles are the storage material packed inside the container. The hot/cold HTF is pumped through porous SHS material for charging and discharging operations (Singh et al., 2010).
- Shell and tube heat storage system: In this configuration, the solid or liquid SHS materials are filled in the shell side, and tube side is used as HTF passages. HTFs like thermal oil, air and molten salts are commonly used for the effective heat transfer operation.

From the literature mentioned above, it can be concluded that most engineering systems employed structural pipelines in the plants which were cylindrical in shapes. Therefore, implementing the cylindrical structured shell and tube heat storage system provides the advantage of even distribution of heat in radial planes with the minimal heat loss to the surroundings (Kuravi et al., 2013).

2.5 Modelling of the SHS system

The optimal design of a thermal energy storage system is an influential part of achieving low energy cost. Mathematical models are being developed to study the optimization of the design configuration of the TES system. To identify the different modelling methodologies and their application, a more detailed literature analysis on modelling of energy storage systems is presented in this section. In recent times, Singh et al. (2019) have developed a 1-D model based on the Schumann model (refers to the transient convective heat transfer between the fluid and solid medium (Schumann, 1929)). The dynamic models were developed to simulate the fluid and solid phases of the conical shaped packed-bed TES with a volume of 1,75,000 m^3. Various design parameters such as the thickness of the insulation, rock diameter, energy storage-discharge rate and shape of the storage module were analysed to estimate the overall performance of the storage system. During the discharging process, the minimum loss of 1% of the energy stored was achieved when parameters such as 3 cm of average rock diameter, 0.6 m of insulation thickness and 553 kg/s of energy storage and discharge rate were considered. Also, the resultant energy and exergy efficiencies were above 98%.

Doretti et al. (2019) have developed the 1-D model for two different concrete mixtures based on the lumped capacitance method. Mineral oil was used as the HTF for charging and discharging of the concrete TES. They suggested that the developed model is a useful tool for estimating the overall performance of any SHS system with less computational time as compared to the conventional three-dimensional model. Besides, they also proposed a methodology for the estimation of the thermal efficiency of the storage module. The result has concluded that the mass flux of the HTF was proportional to the efficiency of the storage module.

Mahmood et al. (2018) have developed 1-D and 2-D dynamic models, where the storage characteristics of honeycomb ceramic module TES system were validated with the help of an experimental study. It was concluded that the computational time and cost could be reduced by solving the system using 1-D dynamic model while comparing it with the commercially available 3-D modelling software's.

Buscemi et al. (2018) had studied the feasibility of integrating the linear Fresnel collector and concrete thermal energy storage. For this, they had developed a TRANSYS model to simulate the performance of the overall system with the objective of optimizing the design parameters

such as storage volume, insulation thickness and the number of collectors. Based on the developed model they proposed that, for the available direct normal irradiance (~39% of average annual efficiency), it is possible to supply 40% of yearly baseload using power generated from the solar collector and SHS system. They also determined that the payback period could be eight years.

Bataineh and Gharaibeh (2018) had developed a 3-D model to study the performance of the storage module. The material used for studying the storage module was Basalt rocks, concrete bed and the Dead Sea salt. The temperature range of the heat storage was from 523 K to 673 K and the estimated capacity of the system was 136.7 MW. The performance of the SHS system was studied with the variation in the number of HTF tubes, diameter of charging tubes, number of fins, and storage volume. It took approximately three hours for charging of all three storage modules and the incorporation of fins played a significant role in charging. The results concluded that the Dead Sea salt and Basalt rocks performed superior when compared to other solid SHS materials.

Montañés et al. (2018) had developed a dynamic model using the Modelica language. Several models were integrated to study the complete functioning of the solar power plant. The models included in the study were that of Sun, parabolic trough collector, thermal energy storage tank of molten salts, power block and influence of climatic condition. The integrated models were beneficial for analysing the storage concepts, design configurations and plant operation strategies. Regarding the TES model, the developed model was able to predict on par with the literature.

Singh and Sørensen (2017) had studied the performance of concrete thermal energy storage system using the 3-D model. The model was employed to analyse the heat transfer from the fluid flow to the storage module considering with and without fins. The addition of fins on the heat transfer tube had decreased the charging time by 11%. The same effect was reflected in the energy and exergy efficiency variation as well.

Jian et al. (2015a), (2015b) had derived an analytical solution to predict the performance of the SHS system by assuming the lumped capacitance concept. They derived the effective heat transfer coefficient equation for the lumped capacitance concept by including transient terms in the fluid energy equation. The dynamic lumped capacitance model was compared against analytical results and was validated with experimental data. They used water as the heat

transfer fluid and concrete as the storage material. The model-based SHS storage design procedure was also presented. Later, the validated model was used for the optimization of SHS system by minimizing energy storage cost, wherein the design parameters such as diameter ratio, storage length, average velocity in the tubes and the number of heat transfer tubes were calculated. The optimized results indicated that the optimal storage cost increased as the required HTF outlet temperature was increased. This finding is important because operating cost is a very large part of the total storage system cost when large storage capacity systems are considered.

Strasser and Selvam (2014) had suggested the usage of concrete structural modules in the thermocline based storage systems to tackle the issues faced due to thermal ratcheting and material settlement. They developed a model to analyse the performance of the packed bed thermocline storage system and the concrete based thermocline storage system. The result concluded that the packed bed systems were 8.5% more efficient than the concrete based thermocline storage system. However, ratcheting due to the thermal stress was a significant concern in the packed bed system. Therefore, structured concrete based thermocline storage system was found to be most suitable for long-term operation of the power plant. To overcome the problem due to the thermal stress and expansion of the storage material, Zanganeh et al. (2012) had demonstrated a new concept tank in the shape of an inverted frustum. Such novel tanks are helpful to move the thermal expansion of material in the upward direction.

Wu et al. (2014) had developed a transient model using the lumped capacitance method to analyse the discharging performance of four different configurations of concrete based thermocline TES system. The configurations were (a) packed-bed structure, (b) rod-bundle structure, (c) parallel-plate structure and (d) channel-embedded structure. The performance parameters analysed were structure size and HTF fluid inlet velocity. The discharging efficiency of the packed-bed structure was best which was followed by the rod-bundle configuration and then the parallel-plate configuration. The performance of channel-embedded configuration was poor among them all. The velocity of the HTF significantly influenced the discharging efficiency of all the storage configurations except that of packed-bed structure.

Zavattoni et al. (2014) had developed a transient 3-D model to analyse the performance of the rock-bed based TES system. They continuously studied the performance over time for 15 charging and discharging cycles. The developed model was having a good agreement with

the experimental result of 6.5 MWh_{th} prototype system. The study was also used for analysing round the clock efficiency for charging, discharging and overall cycle, and they were reported to be 96%, 95% and 92%, respectively.

Cascetta et al. (2014) had studied the dynamic behaviour of the packed bed TES system made up of spherical alumina particles considering different HTFs (air, oil and molten salt). The model was based on the 1-D modified Schumann model. Analysing the distribution of temperature inside the storage system and thermocline formation during the continuous charging and discharging cycle were the key objectives of the study. Usage of oil and molten salt had exhibited good performance after continuous cycles. However, in the case of air, the energy storage capacity had reduced after the few charging and discharging cycles. The result also suggested that using air as HTF has benefits of operating with wide operating temperature range and availability without environmental impact.

Prasad and Muthukumar (2013) had developed a finite element based 3-D model for analysing the performance of concrete TES system of 10 MJ energy capacity in the working temperature range of 523 K–673 K. The heat transfer fluid used in the study was Therminol 55, which was allowed to pass through the tubes embedded inside the concrete material. They analysed the concrete TES system considering a different number of fin configurations on the HTF tubes. The result showed that the charging time had reduced by 41.41% (charging time = 1187 s) and 35.48% (charging time=1307 s) for the six and four fin configurations, respectively.

Bindra et al. (2013) had analysed the dynamic behaviour of the packed bed thermal energy storage based on the alumina particles of 3 mm size. The heat transfer inside wall and diffusion effects in between the particles were considered during the modelling. The model was able to predict the performance of the packed bed system considering the axial dispersion, ambient heat losses and energy storage density of the storage material. In results, low exergy efficiency was observed due to the higher axial dispersion and higher ambient heat losses.

B. Xu et al. (2012) had developed the 1-D dynamic model based on the lumped capacitance method to predict the heat transfer coefficient between fluid and solid materials. The developed model was mainly used to predict the heat storage for four different configurations such as solid TES with a flat plate; a cylinder with HTF flowing around it; a tube with HTF flowing inside it; and spherical particles. Increase in the HTF flow rate was not having much

influence in the thermocline development and discharging efficiency. This study has given a framework for finding the optimized design parameters, operational strategies and thermocline behaviour.

C. Xu et al. (2012) had developed a 2-D model to predict the behaviour of the discharging process in the pack-bed thermocline system. Molten salt was used as the HTF material. The developed model was used to evaluate the interstitial heat transfer coefficient, and the effect of the thermal conductivity of solid fillers. During the discharging process, the TES tank was observed with the expansion of the thermocline region in an upward direction. Based on the correlations in the developed model, the study had also concluded that increasing the thermal conductivity of solid filler material from 0 to 400 W/m-K or decreasing the interstitial heat transfer coefficient by $1/100^{th}$ would increase the thickness of the thermocline region. Varying these two parameters would help to reduce the time taken for discharging and lower the discharging efficiency from 89.9% to 81.7%. Therefore, the study recommended not to prefer high thermal conductive materials for packed-bed molten-salt thermocline thermal storage system primarily considering the cost.

Bai and Xu (2011) had carried out the thermal analysis of two-stage TES system through the numerical simulation. The material used in the first stage for storing the high temperature was concrete, and steam accumulator was used in the second stage for storing the low-temperature heat. From results, the drop in temperature from the outlets of the steam accumulator and concrete TES were observed throughout the discharging process. The temperature distribution was observed to be uniform while increasing the thermal conductivity of the concrete. The concept of this study would be helpful in considering the cascaded application of heat energy storage.

Van Lew et al. (2011) had developed the model to simulate the packed bed TES system performance. The model was developed by reducing the governing equations into dimensionless forms and with good versatility for describing the initial and boundary conditions. Therefore, the results obtained from this model were a powerful and highly accurate solution in a short computational time. The work also details about the methodology of designing and operating strategies of the thermocline heat storage system. The results obtained were having close agreements with the experimental results from the literature Pacheco et al. (2002).

Selvam and Castro (2010) had developed a 3-D model to study the charging and discharging performance of the concrete based TES with different fin configuration in the HTF tubes. The different fin configurations in HTF tubes were an attachment of rods, plates and disks. The result concluded that adding four disks at the equal interval was able to reduce the charging time by 37%. Comparatively, the addition of two plates to the HTF tube had reduced the charging time by 58.6%, while eight rods configuration had reduced the charging time by 19.4% only. Increasing the fin sizes and shapes may increase the rate of heat transfer, but it decreases the amount of energy stored for the same size of the storage module.

Mawire et al. (2009) had developed a simplified 1-D model in terms of the vertical axis for the pebble bed TES system with thermal oil as HTF. The model was used to evaluate the performance of three different storage materials such as stainless steel, alumina and fused silica glass. The results indicated that the amount of energy stored was high in terms of stainless steel while the thermal stratification was high in silica glass. The material which possesses high value in terms of total exergy to total energy ratio was said to be the good thermal performance material. Therefore, alumina was exhibiting high thermal performance with high storage and discharged rate as compared to the fused silica. The results of the developed model were having a good agreement with experimental results by Mawire and McPherson (2009).

Laing et al. (2008) had numerically investigated the performance of the concrete based TES with three different heat exchanger configurations in the temperature range between 623 K and 663 K. Synthetic oil was used as the HTF. Different heat exchanger configurations were adopted to make TES system such as tubeless, encapsulated and tube register designs. The heat exchanger with straight parallel tube and without any added shapes or structures was observed to improve the heat transfer.

Tamme et al. (2004) had developed a numerical model based on the Modelica language to analyse the performance of cast-able ceramic and concrete storage material with synthetic oil as HTF. The rectangular storage unit was of 23 m in length with 36 simple HTF tubes. The storage temperature was in the range of 623 K to 663 K. The developed model was highly useful to study the influence and importance of design parameters in the storage system. The results obtained from the simulation showed that the role of storage material properties was not significant. The study further suggested that the economics of the storage system can be improved by developing optimized operation strategies.

Tamme et al. (2003) had studied the effect of tube arrangement in the solid SHS system through numerical simulations. The result concludes that if the distance between each HTF channel exceeds 0.08 m, the amount of energy stored would be reduced even with no heat loss to surrounding. Such low energy capacity was due to more radial temperature difference at the end of the charging process.

Ismail and Stuginsky Jr (1999) had developed and investigated four different numerical models with varying assumptions to analyse the computational effort required for solving the packed bed storage system. The different models were Schumann's model, a continuous solid phase model (storage material was assumed to behave as a continuous solid medium), a model with the thermal gradient in the solid particles, and a single-phase model (instantaneous temperatures of the solid and fluid phases were equal). The result showed that the time and effort required to solve the model with a thermal gradient inside the packed solid material was twenty times more than the Schumann's model. Schumann's model is one of the popular model employed in the study of solid thermal energy storage. It should also be noted that the effect of packed solid material size was high in case of the model with the thermal gradient in solid particles.

Eames and Norton (1998) had developed a 3-D model based on the finite volume method to investigate the effect of the tank geometry on the thermal stratification. The results of the developed model were validated with the experiments performed. The parameters used to study the thermal behaviour inside the water tank were initial storage stratification profiles, inlet velocity and temperature of the water. The study on storage tank performance also considered the positions of the inlet and the outlet ports of the water with different temperature and velocity. The result showed that a single inlet port with a different temperature at inlet port resulted in poor charging performance. The improved performance of the storage tank could be attained by having a range of ports at a different height while the fluid inlet of the tank was at the height at which the resident storage tank fluid temperature was nearly same as that of the inlet temperature of the water.

Aly and El-Sharkawy (1990) had developed the 1-D model to estimate the performance of packed bed TES concerning the thermal properties of the storage material. The developed model had concluded that the increase in specific heat capacity or density of the storage material would increase the rate and amount of energy stored. Also, the increase in thermal conductivity would reduce the charging time.

Sragovich (1989) had evaluated the performance of the high-temperature sensible heat storage system in transient conditions. The configuration of the TES system was tubular. The selected material for storage was magnesia and heat transfer fluid as air. The results were concluding that sudden drop in outlet temperature was observed during a shift in the flow from laminar to transitional. He also reported that the increase in convective heat transfer was observed while decreasing the HTF tube diameter. This has resulted in an increase in outlet temperature from the TES system. The evaluation was helpful to understand the TES system operation.

Riaz (1977) had developed an analytical model to predict the dynamic performance of the rock-bed TES system. They developed two models based on the Schumann two-phase model and the single-phase model. In the Schumann two-phase model, the axial conduction of heat was ignored while the single-phase model was considering simple convection and conduction from the air to rock at the same temperature. The results of both the models were similar and helped to estimate the long-term performance of the TES system without complex simulations.

2.6 Established applications of SHS

The success of the SHS system depends upon the selection of appropriate energy storage material and application. The storage temperature range is decided based on the end-use of the thermal energy. In this section, various energy storage applications of the SHS system reported in the literature are detailed. Gibb et al. (2018) had conducted a detailed review of integrating TES with real-time applications operating between low and high temperatures. Many researchers have studied the application of SHS system for the following applications: steam generation for power (Martins et al., 2015), chemical process (Geyer et al., 1987), desalination (Gude, 2015), cooking (Okello et al., 2016), and district and water heating (Gudmundsson et al., 2018). These applications were integrated with either solid or liquid-based energy storage mediums. The solid mediums used were concrete, rock and cast iron, whereas, in the liquid medium, synthetic oils and molten salts are most commonly used.

Solar heating/cooling application: In many large communities, there is always a demand for peak power just before the business hours. Once the peak power load is balanced, the load requirement decreases. Mostly, the requirements are thermal management of hot water generation, cooking, space heating and melting the snow on roads and runways during the

winters (Epting et al., 2018). The project namely "Drake Landing Solar Community" had made a massive impact on energy saving with the proficient utilisation of available natural resources in borehole seasonal storage for heating applications (Mesquita et al., 2017). In similar projects, the cold stored during winter can be used in various buildings during summer for the replacement of conventional chillers. Such cooling application had facilitated Çukurova University Balcali Hospital in Turkey to save 10,000 MW annually (Paksoy et al., 2000).

Power production: CSP is one of the attractive energy conversion technologies for power production. However, to overcome the intermittent character of solar power, an efficient and cost-effective TES technology has to be integrated. Due to the high durability, high operating temperature range, stress-free erection, high experimental feedback and low cost, the SHS is mostly preferred for integration with CSP plants.

Cooking application: Solar thermal energy-based cooking is having immense scope in the domestic sector. Solar steam generation projects such as the one at Brahmakumaris, India (CSH India, 2001) have been found to be cost-effective while addressing the cooking needs of small communities and districts which reduces tons of natural gas consumption every year.

Solar Drying: The quality of the several agriculture products deteriorates due to poor storage provisions and poor preservation methods. The practice of drying food for its conservation is very common. One of the ancient technique to preserve the food is drying by solar energy. Continuous drying of agriculture and food products requires TES based solar dryer during the off-Sun period. In general, the best suitable temperature for drying the agriculture product is 313-333 K. Lingayat et al. (2020) and Kant et al. (2016) have carried out a detailed review about the importance of SHS in solar dryer. The most commonly used SHS materials in solar drying application are Earth materials.

Waste heat recovery: Industries such as paper and pulp mills, die casting, steelworks, industrial waste incineration, etc. are generating excess heat beyond their requirement. Such industries can save a considerable amount of energy and reduce CO_2 emissions by recovering waste heat. This waste heat can be recovered using the compact and adequately sized SHS module. The recovered heat could be utilised to cope up with the heat loads in different applications in the industry during high peak power demand (Miró et al., 2016).

2.7 Literature closure

The following conclusions are made from the above-discussed works of literature:

- Several researchers have studied the possibility of using different solid and liquid sensible heat storage materials. They have analysed the potential of the material through various characterisation process. However, most of the identified materials are neither cost-effective nor highly durable for operation in the high-temperature heat storage.
- The previously reported literature on solid TES was mainly focused on the improvement of material properties (Diago et al., 2018; Xu et al., 2017), studying the degradation of material properties at high temperature (Hoivik et al., 2019; John et al., 2011; Skinner et al., 2014) and exploration of new materials (Lin et al., 2019; Lopez Ferber et al., 2019; Mohan et al., 2018). Very few research works have concentrated towards the design, modeling and experimentation of multi-tube SHS system for high-temperature application (Buscemi et al., 2018) and very few efforts have been made to improve the heat transfer in a concrete based energy storage system (Girardi et al., 2017).
- Many researchers have reported the SHS system based on the simple configuration. But there is a lack of study on the shell and multi-tubes configuration design of the high-temperature sensible heat storage system.
- The capital investment on the thermal energy storage materials and HTF is the primary stake for the high-temperature SHS system. The majority of the high-temperature CSP projects in operation use molten salts and thermal oils as HTF. The major issues concerned with these HTFs are their high capital cost, thermal degradation, incompatibility with heat exchanger materials due to their highly corrosive nature, and the requirement of additional infrastructures like freeze protection system in case of molten salts.
- There is a lack of profound experimental investigations on TES systems with the cost-effective SHS materials having high thermal conductivity and high durability for high-temperature energy storage using ambient air as heat transfer fluid.
- It is also observed from the literature survey that no investigator has developed a dynamic model for predicting the real-time performance of the solid TES system by

considering the actual variation in inlet temperature and velocity of HTF encountered during experiments.

By considering the above-mentioned research gaps from the literature review, the motivation of this thesis is to expand the research in the area of thermal energy storage and to specifically contribute towards the understanding of the developed system of this study. To accomplish this, the specific goals for this work are as follows:

- Design and fabrication of experimental setup of High-temperature TES system with air heater.
- Design and development of high-temperature sensible heat storage modules that are made up of cast steel and concrete.
- Develop 3-D numerical model to predict the performance of the high-temperature under various operating conditions.
- Test the heat storage performances of the developed storage module at different operating conditions during charging and discharging processes.
- To develop a dynamic model for simulating the performances of the SHS prototypes with real-time experimental conditions.
- To study the performance of multiple-module SHS systems in different series/parallel arrangements using the 1-D dynamic model and to estimate the cost of the net energy discharged.

2.8 Summary

In this chapter, the detailed literature survey is presented covering the following aspects:

- Explored the possibilities of employing different solid and liquid SHS materials for high-temperature storage.
- Literature published on performance enhancement of different SHS materials in real-time.
- Design aspects of the thermal energy storage system.
- Various studies regarding the different HTFs employed in TES systems with their merits and demerits.
- Various studies on mathematical and numerical models developed for predicting the performance of the TES modules.

- Exploring the different applications employed using the SHS systems.

Finally, the research gaps from reported literature have been identified and based on this, the principle objectives of this dissertation have been framed.

CHAPTER 3
STUDIES ON CAST STEEL BASED SHS SYSTEM[1]

3.1 Foreword

The work presented in this chapter is focused on the design and development of a multi-passage high-temperature SHS system with an SHS-HTF combination having a higher heat transfer rate at lower system cost. Cast steel and atmospheric air are chosen as the SHS material and HTF, respectively. The use of air highlights its potential as HTF for high-temperature application, which further reduces the overall cost of the system. The experiments are designed based on the inlet process conditions for studying the thermal behaviour of the SHS module and the HTF fluid. To observe the intrinsic spatial behaviour during energy transfer between the SHS material and the air, a 3-D model based on the finite volume method is developed. This model helps in studying the charging and discharging characteristics of the SHS system. In addition, a simplified 1-D dynamic model is developed to study the performance of the SHS module and also to explore the possibility of analysing system behaviour in a relatively shorter time as compared to the 3-D model. Numerical predictions from the developed 3-D and 1-D models are validated with the experiment results. Based on the results obtained, various applications of the SHS system are explored.

[1]Content in this chapter has been published as the following research article:

- Vigneshwaran, K., Sodhi, G.S., Muthukumar, P., Guha, A. and Senthilmurugan, S., 2019. Experimental and numerical investigations on high temperature cast steel based sensible heat storage system. *Applied Energy*, *251*, p.113322.

3.2 Description of Experimental Setup and Procedure

3.2.1 Experimental Setup

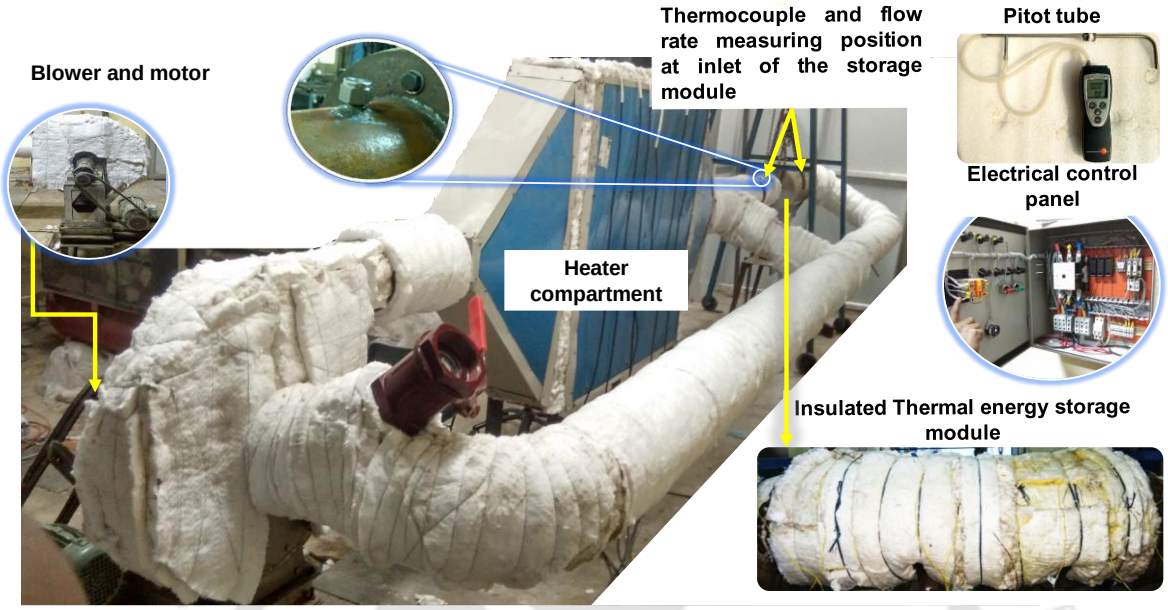

Figure 3-1. Schematic of the fully insulated experimental setup of cast steel based TES system with important components.

In order to analyse the performance of the TES system in the real-time, an experimental setup has been designed and fabricated at the Indian Institute of Technology Guwahati. The TES system has been designed to have maximum flexibility in the criterion like topology, orientation, the quantity of storage material and placement of temperature sensors for testing various TES prototypes. The schematic representation given in Figure 3-1 illustrates the experimental setup of the TES system. The TES system comprised of several major components like control panel, air blower, nichrome element heaters, Pitot tube, data acquisition system and thermal energy storage module. Air is chosen as HTF for energy interaction with the storage medium. The details of the major components used in the experimental setup are briefed in Appendix-A.

3.2.2 The thermal energy storage module

The horizontal cut-section view of the SHS module is shown in Figure 3-2(a). Cast steel used as the storage material in the present study has a high volumetric heat capacity and thermal conductivity. Even though, the initial cost of the cast steel is comparatively higher than other solid-state storage materials such as cast iron, concrete and magnesia bricks (Gil et al., 2010),

cast steel is selected as the storage material due to its favourable thermal properties and no deformation over time. The dimensions of the storage module are given in Table. 3-1. Nineteen holes (HTF passages/tubes) of diameter 12.7 mm each are drilled throughout the length of the storage module. Nine K-Type thermocouples are used for measuring the temperature of the SHS module at different axial and radial locations (illustrated in Figure 3-2 (a) and (b) and described in Table. 3-2). The total volume of the storage module is divided into three sections namely: 'Section- A', 'Section- B' and 'Section- C'. Additionally, the air inlet and outlet temperatures of the SHS module are also measured and recorded.

Table. 3-1 Geometric configuration of SHS module.

SHS medium	Length, L (mm)	Diameter, D (mm)	n	N_P	$D_{pcd,i}$ (mm)	$D_{pcd,o}$ (mm)	d_{tube} (mm)
Cast-Steel	740	267	19	1, 6 and 12	110	220	12.7

Table. 3-2 Thermocouple positions in the SHS module.

Thermocouple nomenclature	Axial length position from module inlet section of HTF (mm)	Radial distance from module outer periphery (mm)
A_25/A_50/A_75	22/370/718	25/50/75
B_25/B_50/B_75	22/370/718	25/50/75
C_25/C_50/C_75	22/370/718	25/50/75

Table. 3-3 SHS material properties (Pilkington Solar International GmbH, 2000).

Material	k_s (W/mK)	C_{ps} (J/kgK)	ρ_s(kg/m^3)
Cast steel	40	600	7800

The number of HTF passages are decided based on previous studies on SHS design optimization conducted by the author's research team (Prasad and Muthukumar, 2013). It was observed that though the charging time got reduced by adding more number of tubes, there was a definite threshold after which the charging time does not reduce with further increase

in the number of HTF passages. So, SHS module with 19 tubes embedded in concrete as the storage medium was selected for performance evaluation. In the current study, SHS material has been replaced by cast steel (1.0% C) having a higher thermal conductivity and hence, lesser charging and discharging times are expected than the concrete module. The properties of cast steel are presented in Table. 3-3. The arrangement of HTF tubes in the current SHS module is presented in Figure 3-2(c).

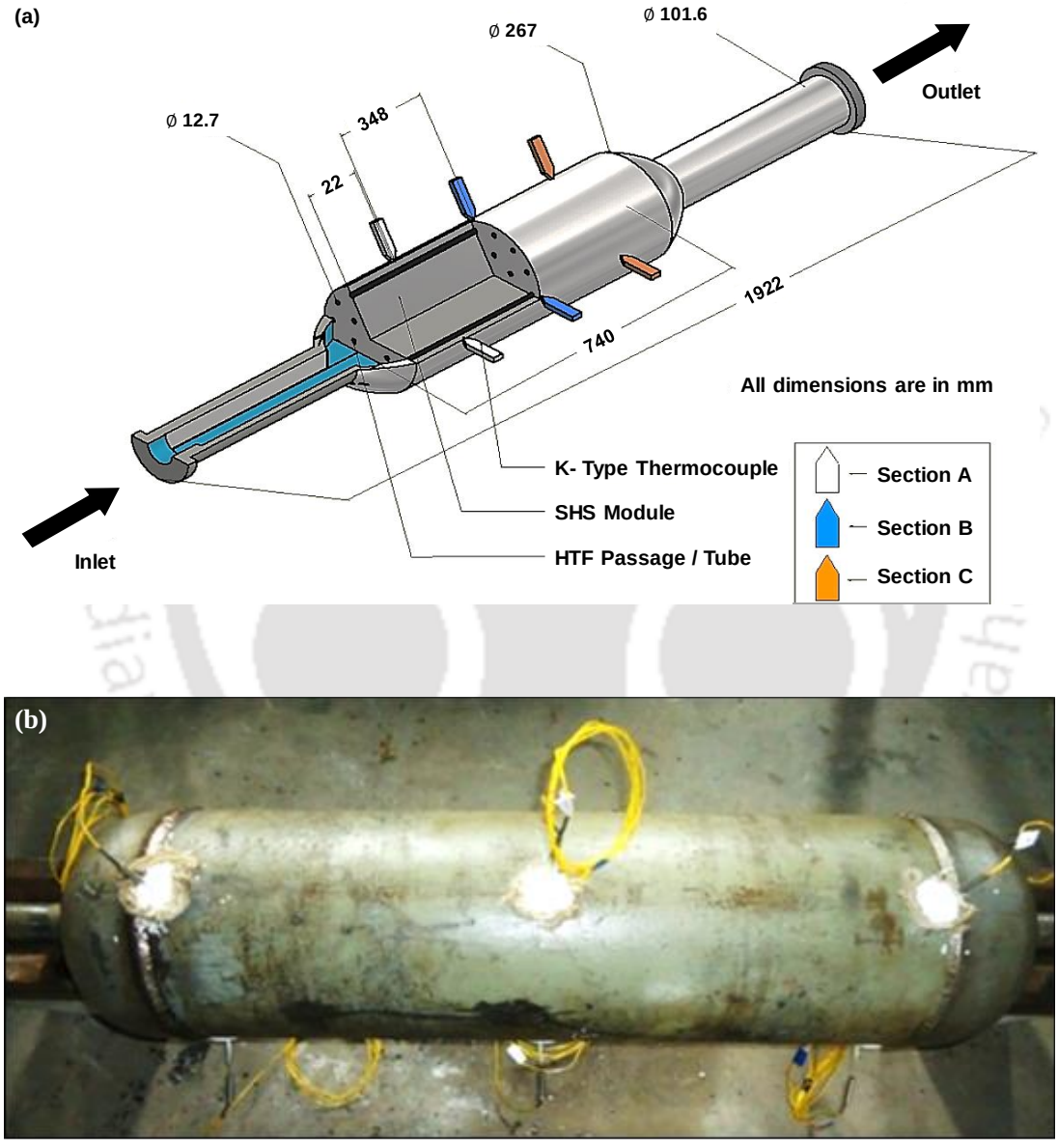

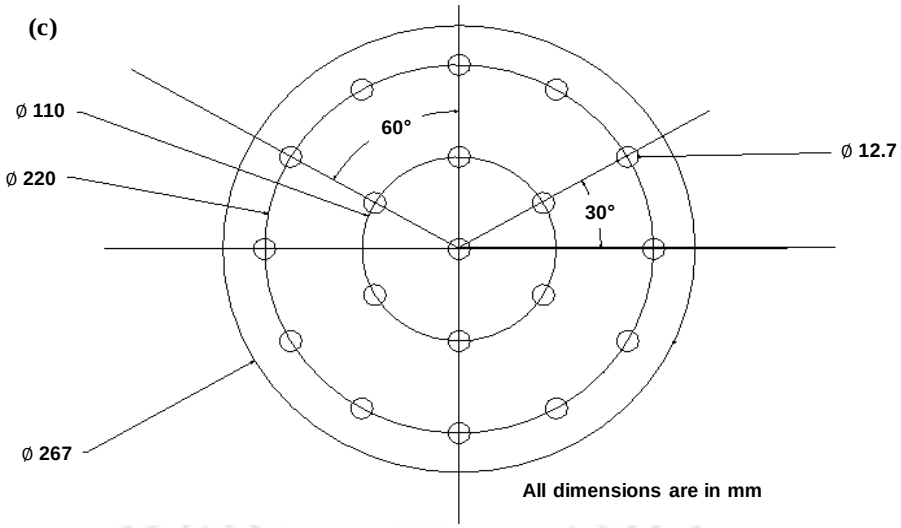

Figure 3-2. (a) Isometric view of the cut sectioned SHS module with thermocouple positions, (b) Picture of SHS module without insulation and (c) Cross-sectional view of HTF passages in the SHS module.

The module is designed by fixing a heat storage capacity as 15 MJ. The estimated mass of the storage medium is 309.28 kg. The volume (V) of the SHS module can be calculated as follows (Prasad and Muthukumar, 2013);

$$V = \frac{\pi}{4}\left(D^2 - nd_{tube}^2\right)L \tag{3.1}$$

where, D and d_{tube} are the diameter of the SHS module and HTF passage, and L is the length of the SHS module.

The amount of heat energy (Q_s) stored and discharged are calculated using the following expressions (Prasad and Muthukumar, 2013);

$$Q_s(t) = \rho_s V_s C_{ps}\left(T_{s,avg}(t) - T_{ini}\right) \tag{3.2}$$

$$Q_s(t) = \rho_s V_s C_{ps}\left(T_{ini} - T_{s,avg}(t)\right) \tag{3.3}$$

where, ρ and C_p, are density and specific heat of SHS material.

3.2.3 Testing procedure

The layout of the experimental setup is shown in Figure 3-3. The experiments can be divided into two major processes; (i) charging and (ii) discharging. The procedures for conducting the charging and discharging experiments are as follows;

Initially, the fresh HTF (air) is drawn inside the centrifugal blower. The air is allowed to pass through the air heater and heated until the air reaches the temperature set point. The set point in the temperature controller is fixed as per the required inlet temperature specified in Table. 3-4 and Table. 3-5. The heated air is supplied to the module through an inlet channel, and later this flow is divided into nineteen passages, as shown in Figure 3-2(a). As the TES system is not equipped with an automated PID controller, to maintain the bulk fluid at a constant temperature is very difficult and hence, a slight variation is observed in the inlet temperature of the HTF. The flow velocity is monitored at the inlet channel, immediately before the storage module. The charging/discharging experiment is started once the module reaches the initial temperature (T_{ini}).

The experiment begins with the supply of the HTF at the required temperature inside the SHS module. The SHS module either absorbs or releases the heat energy from or to the HTF. The experiment is stopped when the SHS module reaches a steady-state volume average temperature ($T_{s,avg}$). After passing through the SHS module, the air is allowed to pass to the atmosphere through the outlet valve. The bypass from the heater towards valve 2 is opened only if the inlet temperature ($T_{f,in}$) does not reach the required operating temperature. In such a case, the air is recirculated to blower and back to the heater to attain the required temperature.

Before starting any charging or discharging experiment, the whole module is brought to a uniform volume average temperature with a minimal temperature gradient. Charging and discharging experiments are conducted with an initial temperature difference of 80 K between the module and air. After conducting charging experiment, discharging does not start immediately. The discharging begins only after the volume average temperature of the SHS module reaches a uniform temperature (T_{ini}), and the same can be estimated once all the

thermocouple placed in the SHS module reaches a steady value. Therefore, charging and discharging experiments are not conducted in a continuous cyclic mode.

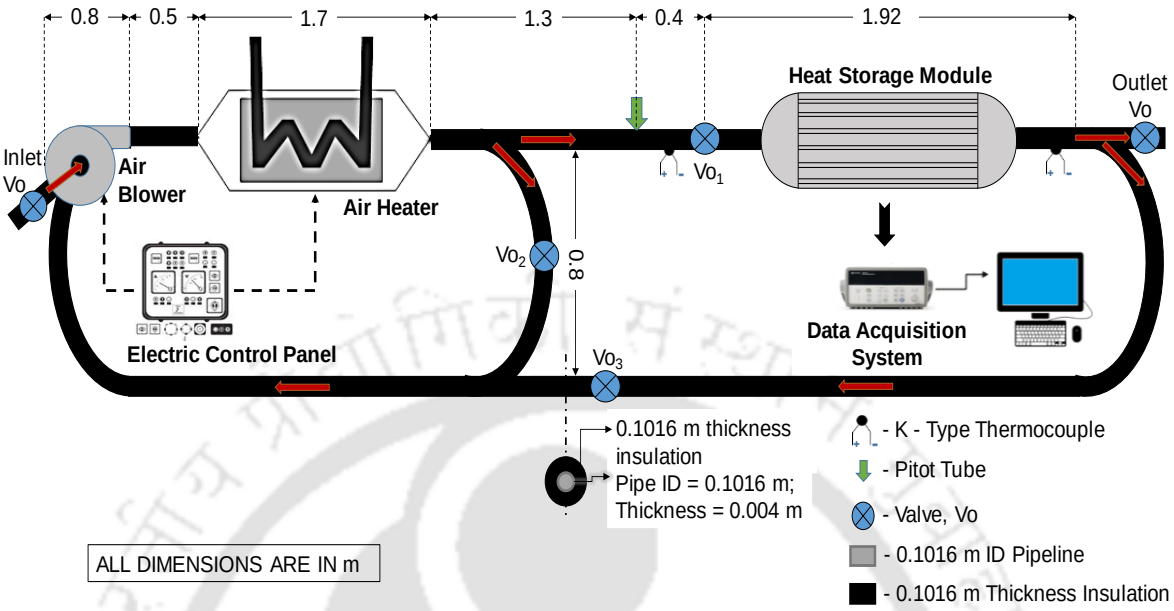

Figure 3-3. Layout of TES system indicating flow directions.

The volume average temperature of the module is estimated by dividing them into nine elements (e) as shown in Figure 3-4. The temperature of the respective element is measured with the corresponding thermocouple placed in that element. The module average is estimated for the complete system including the SHS volume and the HTF passage (tube) volume. The volume average temperature ($T_{s,avg}$) of the module is calculated using below Eq. (3.4);

$$T_{s,avg}(t) = \frac{\sum_{e=1}^{9} V_e T_{s,e}(t)}{V_s} \tag{3.4}$$

To analyse the charging and discharging characteristics of the system, the experiments are conducted for three different HTF velocities and three different operating temperature ranges. All the experimental conditions are described in Table. 3-4 and Table. 3-5.

Table. 3-4 Experimental conditions for the charging process.

Experiment No.	$T_{f,in}$ (K)	T_{ini} (K)	Operating range (80 K)	v_{ch} (m/s)	v_{tube} (m/s)
1	573	493	493-573	4.5	20
2				3.5	15
3				2.5	11
4	523	443	443-523	4.5	20
5				3.5	15
6				2.5	11
7	473	393	393-473	4.5	20
8				3.5	15
9				2.5	11

Table. 3-5 Experimental conditions for the discharging process.

Experiment No.	$T_{f,in}$ (K)	T_{ini} (K)	Operating range (80 K)	v_{ch} (m/s)	v_{tube} (m/s)
10	493	573	573-493	4.5	20
11				3.5	15
12				2.5	11
13	443	523	523-443	4.5	20
14				3.5	15
15				2.5	11
16	393	473	473-393	4.5	20
17				3.5	15
18				2.5	11

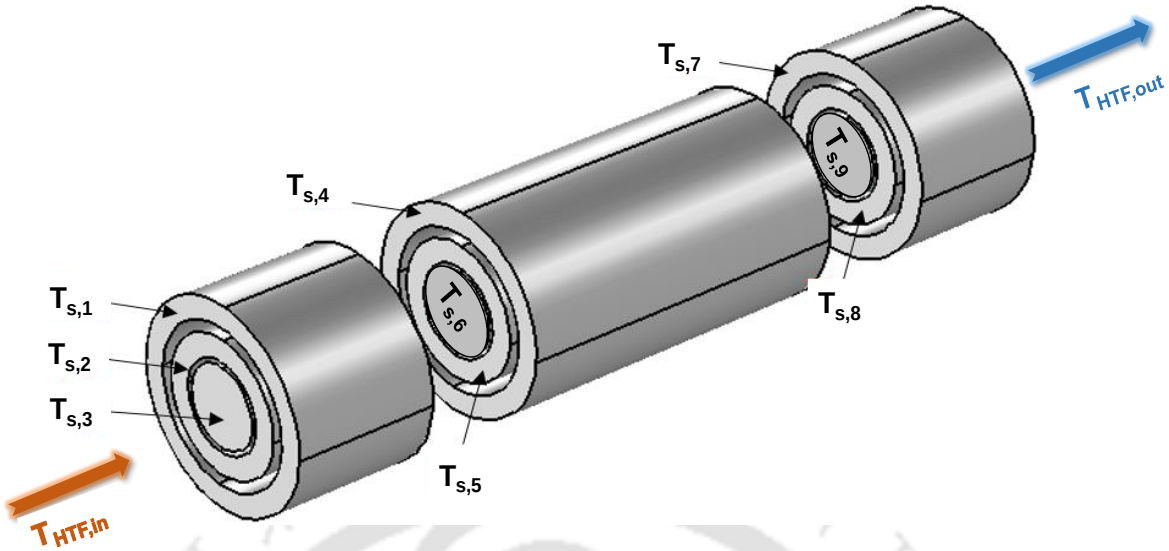

Figure 3-4. The pictorial representation of nine elements of the SHS module representing various thermocouples for determining $T_{s,avg}$.

3.2.4 Error analysis for cast steel module

The uncertainty in the calculated quantities arises due to the error associated with the various measured quantities (obtained from measurement devices). The methodology for estimating the uncertainty which is reported by Kline and Mcclintock, (1953) is used to determine the uncertainty of any dependent parameter (E), which depends on independent measured quantities. If the independent variables such as $w_1, w_2, ...w_n$, are depending upon the 'E', the function can be expressed as given in Eq. (3.5). The uncertainty of any parameter (ΔE) is given by Eq. (3.6).

$$E = E\left(w_1, w_2, ...w_n\right) \tag{3.5}$$

$$\Delta E = \left(\left[\frac{\partial E}{\partial w_1} \Delta w_1 \right]^2 + \left[\frac{\partial E}{\partial w_2} \Delta w_2 \right]^2 + ... + \left[\frac{\partial E}{\partial w_n} \Delta w_n \right]^2 \right)^{0.5} \tag{3.6}$$

The estimated maximum experimental error on the mass flow rate is ± 2.2% (± 0.00109 kg/s), and on energy stored and discharged are ± 4.9% (± 0.7 MJ).

3.3 3-D model of the SHS system

The three-dimensional (3-D) model is useful to understand the spatial behaviour of heat storage material during the energy exchange between the HTF and SHS module. The 3-D modelling of the system is carried out using the simulation tool Comsol Multiphysics 4.3a (COMSOL Multiphysics, 2017).

The conjugate heat transfer problem combining the HTF flow and energy exchange is solved by imposing different initial and boundary conditions on the governing equations. The HTF flow and energy interactions between the HTF and SHS module are governed by the following set of equations (Niyas et al., 2015);

Continuity equation for flow:

$$\nabla.(\rho_f \vec{v}_f) = 0 \tag{3.7}$$

Momentum equation for flow:

$$\frac{D(\rho_f \vec{v}_f)}{Dt} = -\nabla P + \mu_f \nabla^2 \vec{v}_f \tag{3.8}$$

The energy equation for flow:

$$C_{p,f}\left(\frac{D(\rho_f T_f)}{Dt}\right) = k_f \nabla^2 T_f \tag{3.9}$$

Heat conduction for SHS module is given by;

$$\rho_s C_{p,s}\left(\frac{\partial T_s}{\partial t}\right) = k_s \nabla^2 T_s \tag{3.10}$$

where, ρ , C_p and k represent density, specific heat and thermal conductivity of the cast steel, respectively. P and v represent the pressure and velocity. T_s and T_f represent the temperature of solid (cast steel) and fluid (air).

The numerical analysis is conducted on the basis of the following assumptions:

1. The model is perfectly insulated, i.e. heat loss from the model to the surrounding is zero.

2. The storage material is isotropic and homogenous.
3. Effect of radiation heat transfer from the system is neglected.

The flow of air through the inlet channel is assumed to be perfectly divided into 19 passages inside the SHS module based on the below equation.

$$nA_{tube}v_{f,in} = A_{ch}v_{ch} \tag{3.11}$$

where n represents the number of HTF passages and, A_{tube} and A_{ch} represent the cross-section area of tube and channel.

3.3.1 Initial and Boundary conditions

The initial and boundary conditions used for solving mass, momentum and energy equations are given in Table. 3-6.

Table. 3-6 Initial and boundary conditions for the 3-D model.

For charging and discharging (Initial condition)	$At\ t = 0;\ T = T_{ini},\ \vec{v}_f = 0$
For SHS	$At\ z = 0;\ \frac{\partial T(r,\theta,z,t)}{\partial z} = 0$ $At\ z = L;\ \frac{\partial T(r,\theta,z,t)}{\partial z} = 0$ $At\ r = D/2;\ \frac{\partial T(r,\theta,z,t)}{\partial z} = 0$ (*Adiabatic)*
For HTF	$At\ z = 0;\ v_f(r,\theta,z,t) = v_{f,in},\ T_f(r,\theta,z,t) = T_{f,in}$ $At\ z = L;\ \vec{n}(k_f \nabla T_f) = 0,\ P(r,\theta,L,t) = P_{atm}$ *(Atmospheric pressure)* $At\ r = d_{tube}/2;\ v_f(r,\theta,z,t) = 0$ *(no-slip)*

3.3.2 Computational methodology

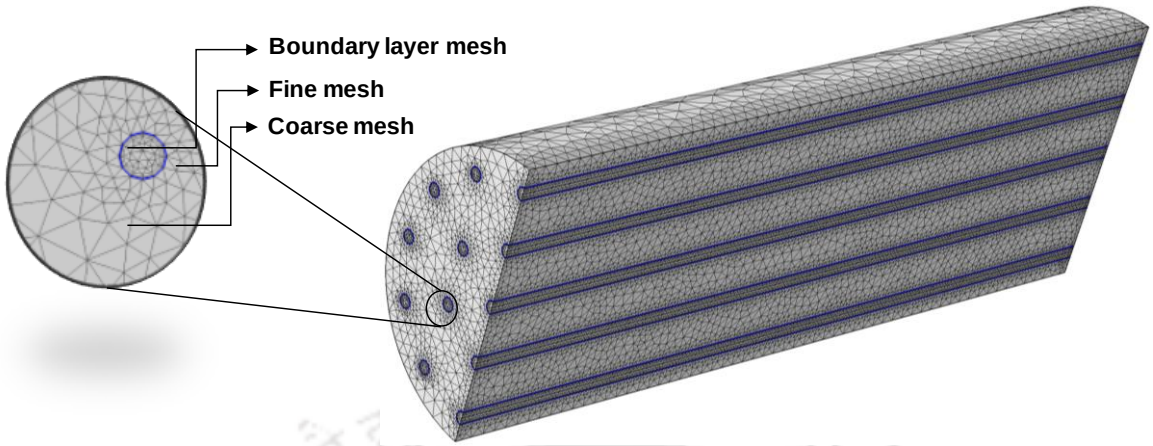

Figure 3-5. 3-D model of the SHS system displaying the mesh features.

The computational model is shown in Figure 3-5. The implicit scheme Backward Differentiation Formula is used for solving Eqs. (3.7) - (3.11). A parallel direct solver available in Comsol Multiphysics is used. Instead of using a constant time step, dynamic time stepping is adopted to save the computational time. The initial minimum time step and the maximum automatic time step are 0.001 s and 0.1 s, respectively. Since the module is symmetric to 'θ', only half diameter SHS model is simulated.

Triangular and free tetrahedral elements are used to generate the mesh of the model. To take care of boundary layer effects, the fine mesh is generated near the walls, whereas, it is coarse in the core of the domains in order to reduce the total number of elements. The cost of handling computation relies upon the total number of elements. Also, the quality of the grid chosen to be optimum in order to match the real-time experimental data. Therefore, the grid is made independent of the solution quality, so that the results do not vary much after selecting the best possible grid size. The numerical model is solved for different grid sizes by varying the total number of elements as follows; 208922, 327000, 376838 and 567068. The variation in the volume average temperature of the module with respect to time for all grid sizes is plotted in to find an optimal number of elements. It is observed that the predicted volume average temperature is independent of the grid size for 376838 elements and above. So, in order to solve in lesser computation time, all subsequent simulations are carried with 376838 elements.

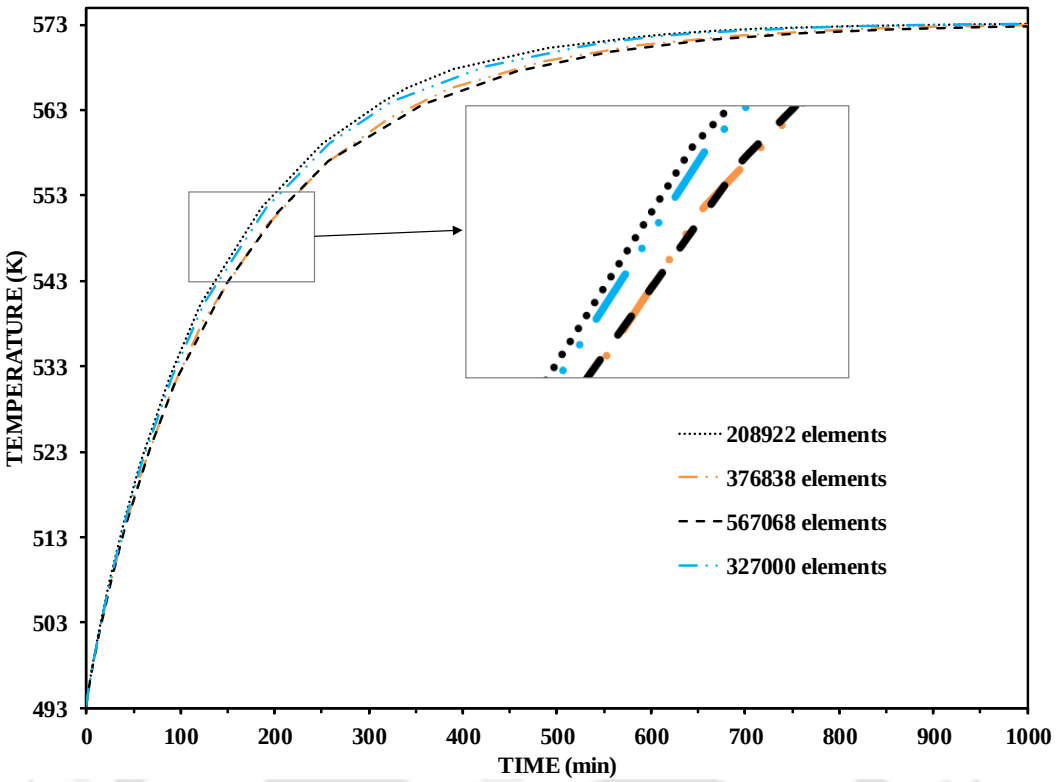

Figure 3-6. Volume average temperature of the module for different grid sizes.

3.4 1-D Mathematical model and parameter estimation

In general, 3-D models provide flexibility in terms of variation in geometrical design features, but due to high computational time, they cannot be employed for real-time monitoring and optimization. In this respect, 1-D dynamic modeling is advantageous over 3-D modeling. Further, the 1-D model has the following advantages:

(i) It is possible to input the dynamic fluctuations in the HTF inlet temperature observed during the real-time experiments. This helps in predicting the SHS system behaviour more realistically, which is not possible in the case of 3-D modeling.

(ii) 1-D simulations are several hundred times faster than 3-D simulations.

(iii) It is highly feasible to integrate the developed 1-D model with a real-time application to study the dynamic behaviour of the system.

(iv) Based on the downstream requirement, system capacity modulation can be varied easily using 1-D modeling.

The Modelica language is widely adopted in the automation industry to develop the real-time monitoring and optimization tool. Therefore, in this work, a simplified 1-D dynamic model for the SHS system is developed and implemented using Modelica language in Dymola software tool (Dassault systems, 2018).

The objectives of the 1-D model are (i) to predict the temperature variation along the length of the SHS, and (ii) to estimate the output power of the HTF and charging/discharging time for monitoring and optimization application. To incorporate the temperature variation along the length, the concept of multiple Continuous Stirred Tank (CST) in series is used by adopting an object-oriented framework of Modelica language. From experimental results, it is observed that the temperature variation in the radial direction is negligible. Therefore, elements 1, 2 and 3 are modelled as 'CST-1', elements 4,5,6 are modelled as 'CST-2' and elements 7,8,9 are modelled as 'CST-3' (refer Figure 3-4). All three CST's are connected in series. The model equations for a single CST are as given below;

The unsteady-state mass and heat balance for HTF is given below;

$$nV_{tube}\frac{d}{dt}(\rho_{f,out}) = nA_{tube}\left(\rho_{f,in}v_{f,in} - \rho_{f,out}v_{f,out}\right) \tag{3.12}$$

$$nV_{tube}\frac{d}{dt}(\rho_{f,out}c_{pf,out}T_{f,out}) = nA_{tube}(v_{f,in}\rho_{f,in}C_{pf,in}T_{f,in} - v_{f,out}\rho_{f,out}C_{pf,out}T_{f,out}) - q \tag{3.13}$$

The volume average temperature of the storage module is estimated by the heat balance between the HTF and the storage module.

$$m_s C_{ps}\frac{dT_{s,avg}}{dt} = q \tag{3.14}$$

$$q = \left(\frac{U_o A_{tube} n(\Delta T_{in} - \Delta T_{out})}{\ln\left(\frac{\Delta T_{in}}{\Delta T_{out}}\right)}\right) \tag{3.15}$$

where n and V represent the number and volume of the HTF passages. ρ, v, C_{pf} and T_f represent density, velocity, specific heat and temperature of the HTF, respectively. U_o and q represent the overall heat transfer coefficient and heat transfer rate.

The temperature difference between HTF inlet temperature and module average temperature is given by;

$$\Delta T_{in} = T_{f,in} - T_{s,avg} \tag{3.16}$$

The HTF passage consists of drilled holes in the storage module. Hence, the conductive resistance due to the tube material is not taken into consideration. So, the overall heat transfer coefficient is estimated only based on the convective heat transfer (h_i) resistance existing in the fluid (Bergman et al., 2011).

$$U_o = h_i \tag{3.17}$$

The HTF pressure (P) drop is calculated by using the Hagen- Poiseuille equation (Bergman et al., 2011).

$$\frac{P_{out} - P_{in}}{L} = \left(\frac{128}{\pi}\right)\left(\frac{\mu_{f,avg}}{d_{tube}^4}\right) A_{tube} v_{f,avg} \tag{3.18}$$

The density of air at inlet and outlet of the storage module is estimated using ideal gas law (Bergman et al., 2011),

$$\rho = \frac{PM}{RT} \tag{3.19}$$

where, P, R and M represent the pressure, universal gas constant and molecular weight of the air respectively.

Heat transfer coefficient is estimated from the dimensionless parameter Nusselt number (Nu) which is further expressed as a function of Reynolds number (Re) and Prandtl number (Pr) number in the Dittus-Boelter equation (Bergman et al., 2011).

$$Nu = aRe^b Pr^c \tag{3.20}$$

$$h_i = \frac{Nu\, k_f}{d_{tube}} \tag{3.21}$$

Table. 3-7 Parameter values in the Dittus-Boelter equation.

Parameters	Values
a	0.023
b	0.8
c	0.4

The maximum estimated value of the Reynolds number for the flow conditions inside the HTF passage is 5048. Reynolds number (*Re*) and Prandtl number (*Pr*) are calculated as (Bergman et al., 2011);

$$Re = \frac{\rho_{f,avg} d_{tube} V_{f,avg}}{\mu_{f,avg}} \tag{3.22}$$

$$Pr = \frac{\mu_{f,avg} C_{pf,avg}}{k_f} \tag{3.23}$$

where μ_f represents the dynamic viscosity of the fluid (air).

The average velocity of air is given by;

$$v_{f,avg} = \frac{v_{f,in} + v_{f,out}}{2} \tag{3.24}$$

The total mass of the storage module (m_s) is estimated by;

$$m_s = \left(\frac{\pi}{4}\right)\left[D^2 - d_{tube}^2 n\right] L \rho_s \tag{3.25}$$

Mass of SHS material per HTF passage,

$$m_{s/tube} = \frac{m_s}{n} \tag{3.26}$$

The temperature difference between the module average and module initial temperature is given by;

$$\Delta T = T_{s,avg} - T_{ini} \tag{3.27}$$

The heat gained/released by the SHS module is calculated using Eqs. (3.2) and (3.3), respectively. Different properties of the HTF are estimated as the function of temperature through the following empirical equations (Zografos et al., 1987).

$$\rho = 345.57(T - 2.6884)^{-1}, \quad 150\,K \le T \le 3000\,K \tag{3.28}$$

$$\mu = 2.5914\times10^{-15}T^3 - 1.4346\times10^{-11}T^2 + 5.0523\times10^{-8}T + 4.1130\times10^{-6} \tag{3.29}$$

$$C_p = 1.3864\times10^{-13}T^4 - 6.4747\times10^{-10}T^3 + 1.0234\times10^{-6}T^2 - 4.3282\times10^{-4}T + 1.0613 \tag{3.30}$$

$$k = 1.5797\times10^{-17}T^5 + 9.46\times10^{-14}T^4 + 2.2012\times10^{-10}T^2 - 2.3758\times10^{-7}T^2 + 1.7082\times10^{-4}T - 7.488\times10^{-3} \tag{3.31}$$

The model parameters of the heat transfer coefficient are unknown and have to be estimated from experimental data. The Dymola's design library is used to minimize the error between the model prediction and the experimentally measured temperature along the length of the module. The decision variables for optimization are *'a'*, '*b*' and '*c*' of the Dittus-Boelter equation (refer Table. 3-7). The error function is given below (Dassault systems, 2018);

$$Error(t) = \sum_{t=1}^{t}\left(\sqrt{\left(1 - \frac{(T_{s,avg}(t))_{Sim}}{(T_{s,avg}(t))_{Exp}}\right)^2} + \sqrt{\left(1 - \frac{(T_{f,out}(t))_{Sim}}{(T_{f,out}(t))_{Exp}}\right)^2}\right) \tag{3.32}$$

where, *Sim* and *Exp* represent the Simulation value and Experiment value, respectively.

The methodology for 1-D dynamic model simulation is described as a flowchart given in Appendix-B of the thesis.

3.5 Results and discussion

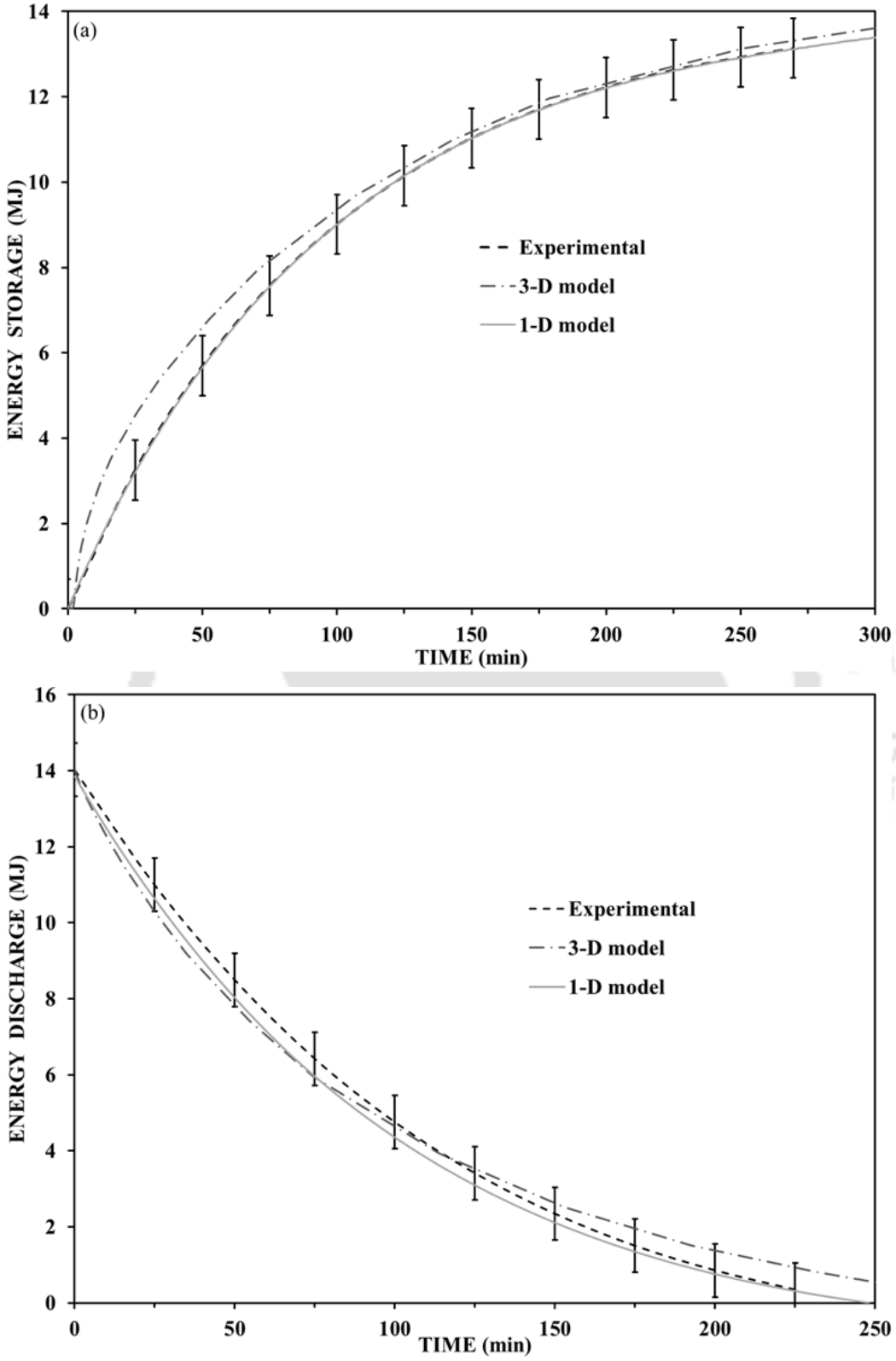

Figure 3-7. Validation of numerical 3-D and 1-D dynamic models with experiment results during (a) charging and (b) discharging processes.

In this section, results obtained from 3-D and 1-D mathematical models, and experimental studies are presented. The performance characteristics of SHS such as the energy stored and discharged during charging and discharging processes are also discussed in detail. The experiments are performed as per the design of experiments reported in Table. 3-4 and Table. 3-5.

Numerically predicted energy storage and discharge rates are validated with the experiment data. Experiment Nos. 7 and 16 are considered for the validation of numerically predicted charging and discharging rates, respectively. In the numerical simulation, the initial temperature (T_{ini}) of the SHS module and the HTF inlet temperature ($T_{f,in}$) are fixed as 393 K and 473 K during charging and 473 K and 393 K during discharging. For both 1-D and 3-D validation studies, the velocity of the HTF (v_{tube}) is maintained at 20 m/s. Figure 3-7(a) and (b) illustrates the validation of the developed thermal models with the corresponding experimental data in terms of energy storage and discharge rates. The flowchart given in the Appendix-B provides the various steps involved in the validation of 1-D dynamic modelling. It is observed that predictions from both 1-D and 3-D models match closely with experimentally estimated values within the error of ± 3.3% for the 1-D model and ± 9% for the 3-D model. The dynamic fluctuation in the air inlet temperature is not possible to include in the 3-D model simulation due to limitations in the Comsol Multiphysics 4.3a software tool. Even if it is possible, due to the large computational requirement, the simulation may require huge computational time. Therefore, the more deviation is observed in 3-D model prediction as compared to the 1-D model.

3.5.1 Experimental results

3.5.1.1 Temperature variation during charging and discharging processes

The variation in air inlet temperature ($T_{f,in}$), air outlet temperature ($T_{f,out}$) and module volume average temperature ($T_{s,avg}$) with respect to time are shown in Figure 3-8. The air inlet temperature fluctuated within a temperature range of 5-8 K while conducting both charging and discharging experiments due to practical limitations of the temperature controller.

During the charging, the storage module was maintained at an initial temperature of 493 K (for instance, *Experiment No. 1* is taken for discussion). $T_{f,in}$ and $v_{f,in}$ were maintained at 573 K and 20 m/s, respectively. It is observed that the module temperature increases linearly with time till 100 min, later follows the non-linear profile and reaches an asymptotic value. Approximately, 70% of the total module energy is stored within 40% of the total time (119 min) and remaining 30% of the total energy storage takes 60% of the total time (159 min). Similarly, for discharging, the initial module temperature was maintained at 573 K (for instance, *Experiment No. 10* is taken for discussion), whereas $T_{f,in}$ and $v_{f,in}$ were maintained at 493 K and 20 m/s, respectively. Also, the temperature profile shown in Figure 3-8(b) reflects that the discharging process is found to be similar to charging, but with heat flow from the module to the HTF.

The charging and discharging experiments are stopped once the module reaches a steady-state condition, such that no heat exchange takes place between the air and the SHS module. Therefore, the net heat loss from the air decreases with a reduced temperature gradient between the module and air. Further, this can be verified from the variation of ΔT (HTF), which tends to zero at the end of the experiment. Thus, the temperature of the air at the outlet tends towards the inlet temperature as shown by $T_{f,out}$ in Figure 3-8(a) and (b). The temperature profiles measured at different thermocouple locations during the charging and the discharging processes are shown in Figure 3-9(a) and (b).

'Section-A', 'Section-B' and 'Section-C' represent temperature data of three thermocouples located in each of these sections (as illustrated in Figure 3-4). It is observed from the temperature data measured at 'Section-A' that the heat transfer in this section is faster as compared to 'Section-B and Section C'. Such an increased heat transfer rate is observed due to the high-temperature difference between the air and the module at 'Section-A'. As expected from the direction of heat transfer, the air temperature drops along the length of the HTF passages during the charging process and increases during the discharging process.

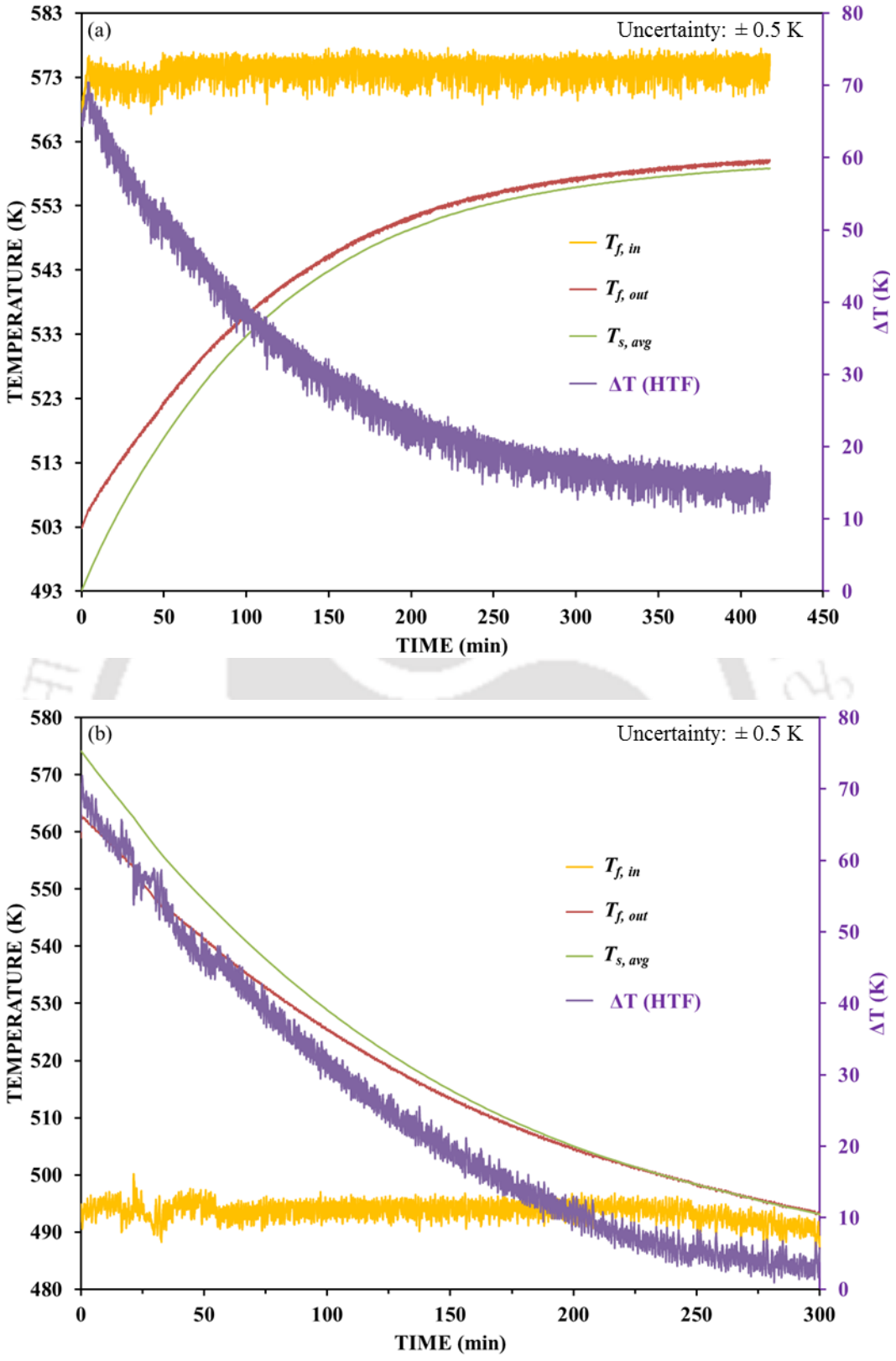

Figure 3-8. Variation in module volume average temperature with time during (a) charging and (b) discharging processes.

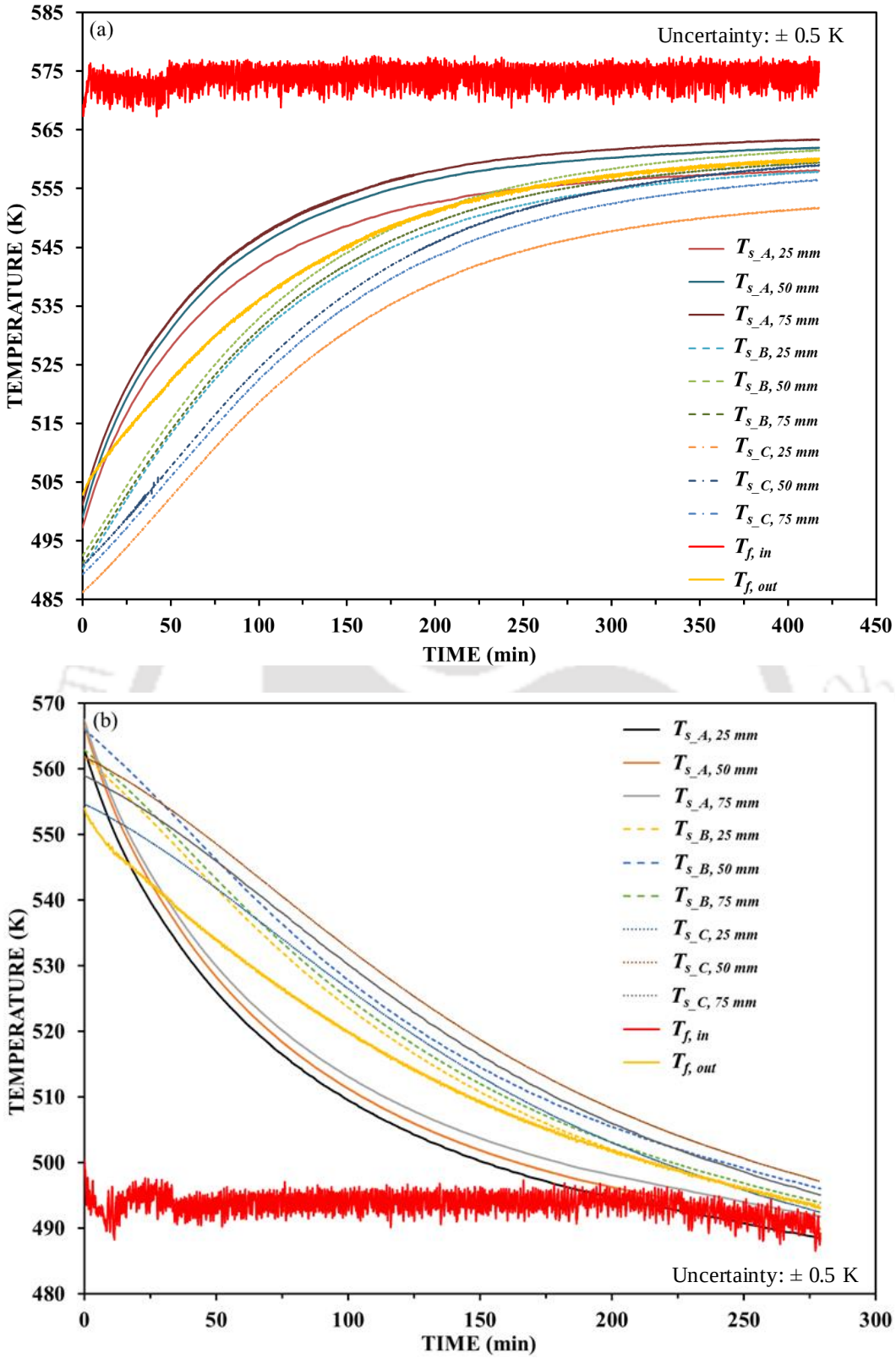

Figure 3-9. Variation in temperature at different thermocouple positions of the SHS module during (a) charging and (b) discharging.

3.5.1.2 Energy stored and energy discharge rates

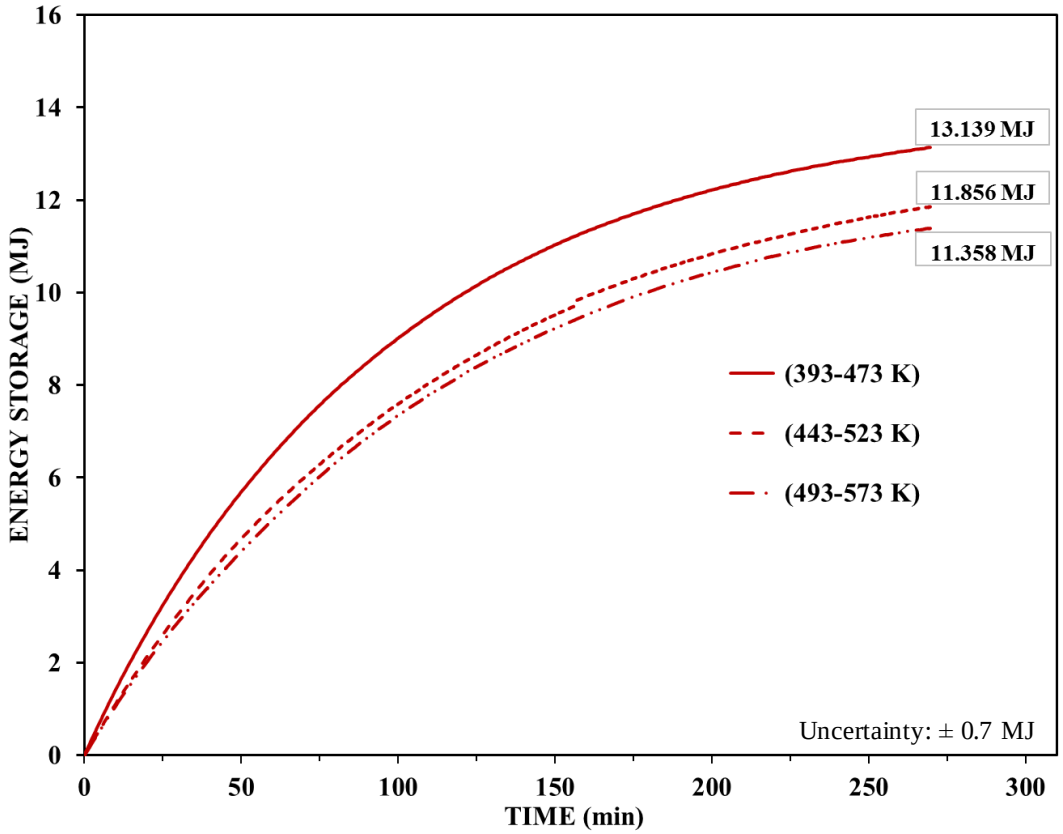

Figure 3-10. Energy profile for charging - *Experiment Nos. 1/4/7.*

Figure 3-10 provides details about the amount of energy stored during the charging process. During this process, $v_{f,in}$ was maintained at 20 m/s and $T_{f,in}$ was varied at three different inlet conditions 393 K, 443 K and 493 K and their respective T_{ini} were 473 K, 523 K and 573 K. As a result, the total energy stored during charging *Experiment Nos. 1/ 4 / 7* was calculated as 13.14 MJ/ 11.85 MJ/ 11.36 MJ, respectively. For all temperature ranges discussed in the experiments, the rate of heat transfer and quantity of energy transfer by the air are higher at lower temperature range as compared to the higher temperature range. This happens primarily because the density of air is relatively high at low temperature. Thus, the mass flow rate and the amount of energy transferred by the air is higher. Hence, better system performance is observed at relatively lower temperatures of the air.

While discharging, achieving a constant power output is one of the vital aspects to run any downstream process at steady state. To accomplish a steady-state operation, both the HTF flow rate and temperature need careful manipulation. Higher flowrates lead to high rate of

charging and discharging, but at the same time, the temperature difference between the HTF inlet and outlet will be less, resulting in less utilisation of supplied heat. Higher HTF inlet temperature increases both the quality and the quantity of the heat stored. In the context of the present study, increasing the flow rate restricts the rise in HTF temperature due to lesser residence time inside the air heater.

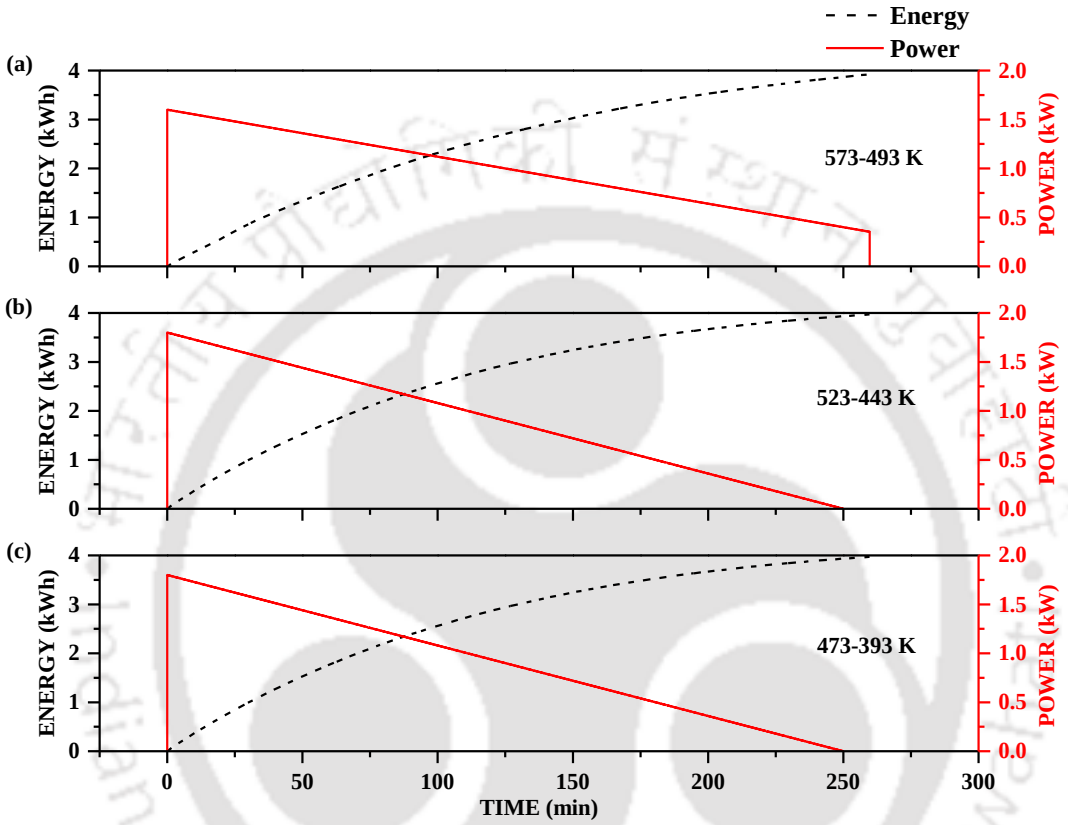

Figure 3-11. Energy and power profile for discharging - *Experiment Nos. 10/13/16.*

On the contrary, reducing the flowrate helps to attain higher HTF inlet temperatures. In the current experimental investigations, flowrate and temperature of the air were manipulated and accordingly, different experiments were performed. For a fixed airflow rate, the heat transfer rate between the HTF and SHS module decreases with time due to drop in a temperature gradient. Hence, the obtained output power decreases linearly with time, as illustrated in Figure 3-11. The peak power discharged at lower operating temperature range is observed to be high due to the high amount of energy discharged. The trend of power (rate of energy discharged) and energy discharged for the temperature range of 473-393 K is almost similar to the range of 523-443 K. The beginning of the discharging is marked by peak power, which gets reduced gradually towards the end. In a sensible heat storage system, the peak power

output is delivered at the start of the discharging process, and this may be an advantage for balancing the peak load during intermittent operation. The sensible heat storage may not be suitable for steady power output conditions for a longer duration.

3.5.1.3 Axial temperature variation in SHS module during charging and discharging processes

The variation in temperature along the axial direction of the SHS module with time, during both charging and discharging processes are illustrated in Figure 3-12 (a) and (b). During the charging process, $T_{f,in}$ and T_{ini} were fixed as 573 K and 493 K (*Experiment No. 1*), respectively; and vice-versa in discharging (*Experiment No. 10*). As shown in Figure 3-2 and Table. 3-2, the thermocouples were located in three different axial positions at 22 mm, 378 mm and 718 mm from the inlet of the SHS module. After 60 min of the charging process, approximately 18 K of temperature difference exists consecutively between the three sections (A, B, C) in the axial direction. This behaviour was observed until 120 min, after which the temperature difference between consecutive sections reduces. This happens because the heat transfer between the HTF and SHS module reduces gradually over time. Finally, at steady state, as $T_{f,out}$ approaches close to $T_{s,avg}$, the temperature difference between consecutive sections is only 2 K. The trend of axial variation during the discharging process is similar to the charging process. Therefore, significant temperature variations are observed along the length of the SHS module during the initial period of charging and discharging processes, which are found to reduce over time.

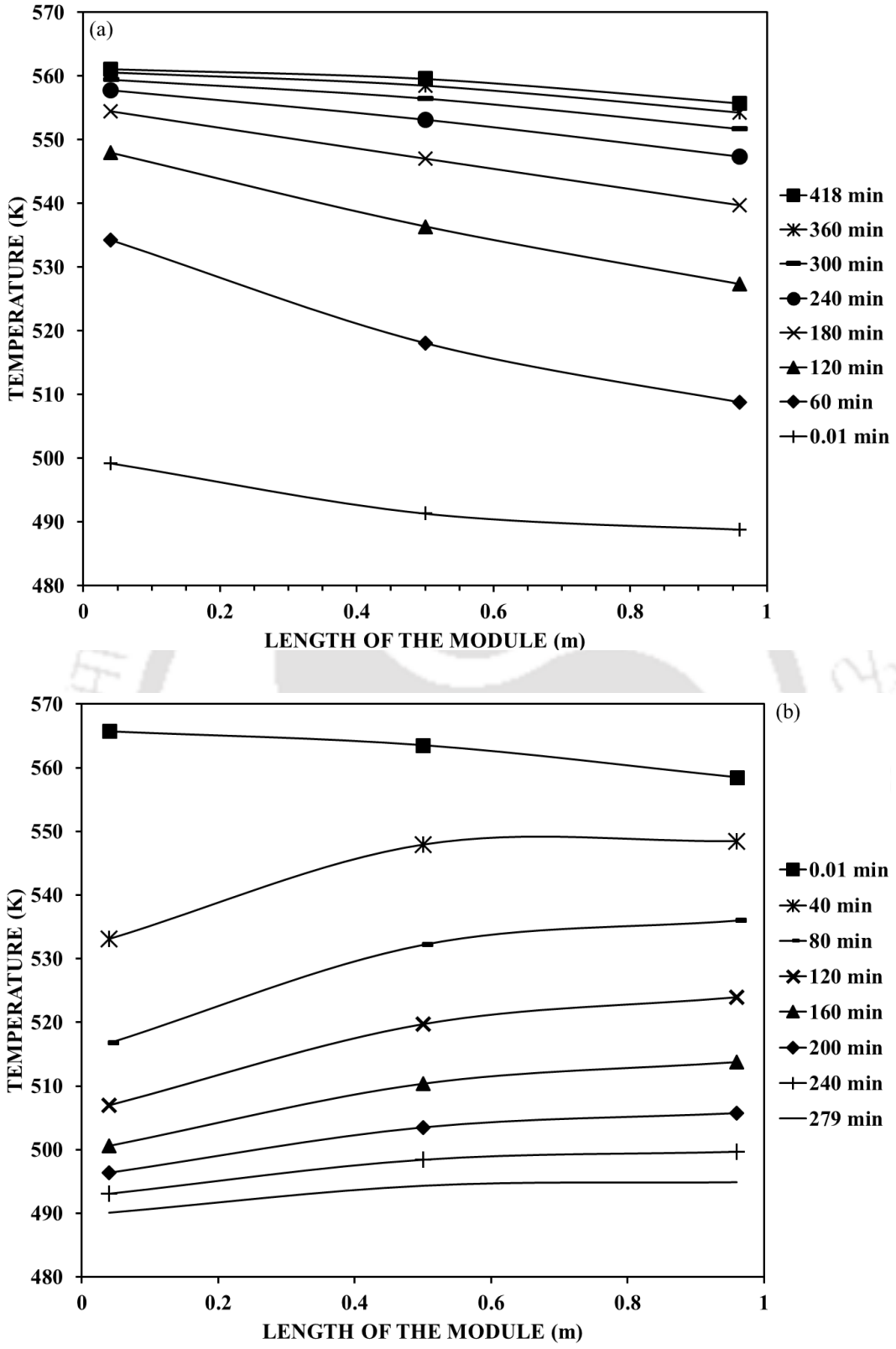

Figure 3-12. Axial temperature variation in SHS module during (a) charging and (b) discharging processes.

3.5.1.4 Radial temperature variation during charging and discharging processes

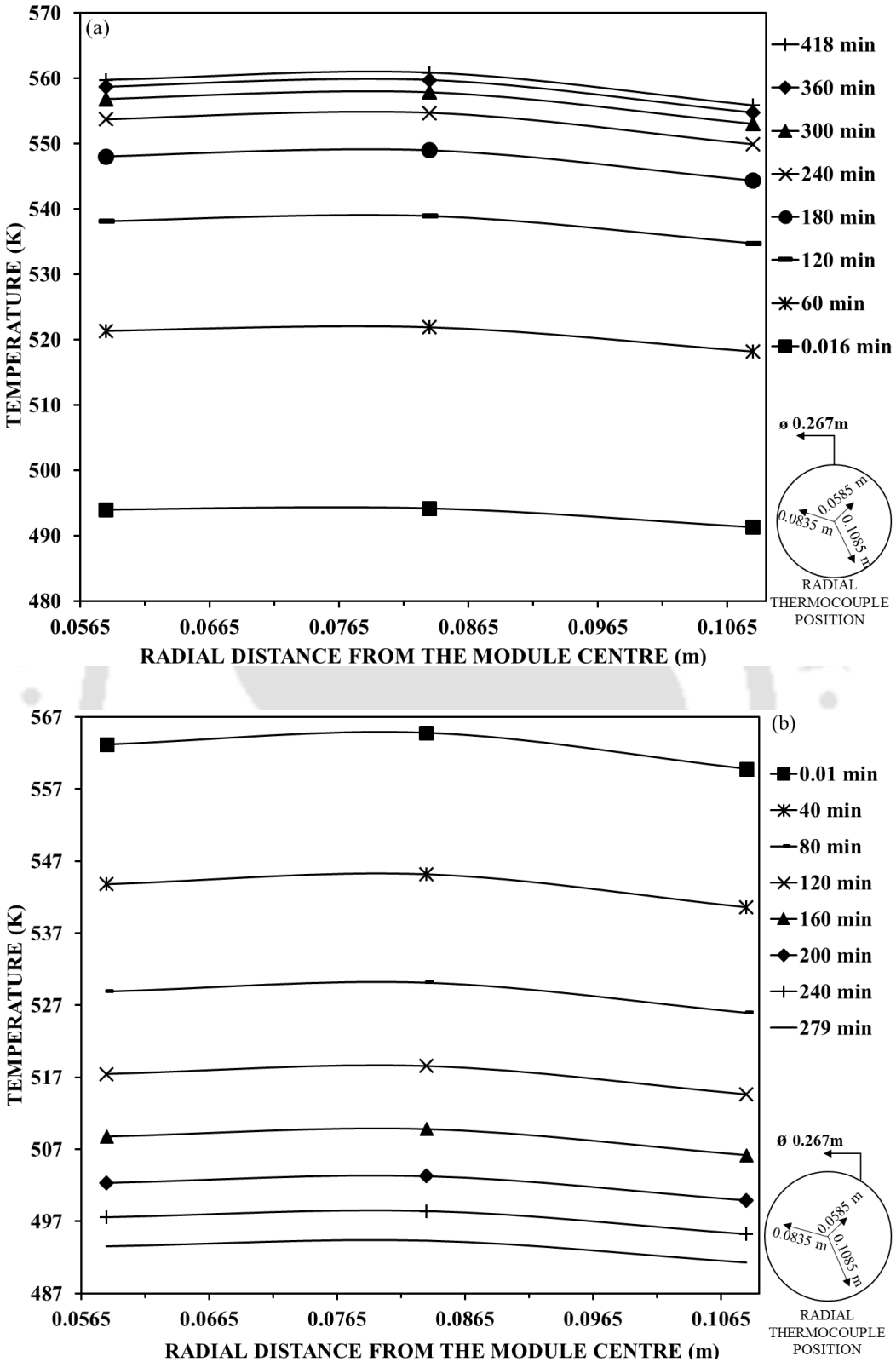

Figure 3-13. Radial temperature variation in SHS module during (a) charging and (b) discharging processes.

To understand the thermal behaviour of the system in the radial direction, the temperature variations along all the radial thermocouple locations for *Experiment Nos. 1 and 10* are analysed. The thermocouple positions are illustrated at the bottom right corner in Figure 3-13 (a) and (b). Due to the distribution of HTF passages uniformly in the radial direction, the conduction heat transfer rate is faster in all the sections. Therefore, the temperature gradient between any radial location is negligible at any time interval throughout charging and discharging processes. The same observations are conferred from the 3-D modelling results. This concludes that the heat transfer does not vary significantly in the radial direction as compared to the axial direction.

3.5.1.5 Influence of the HTF velocity

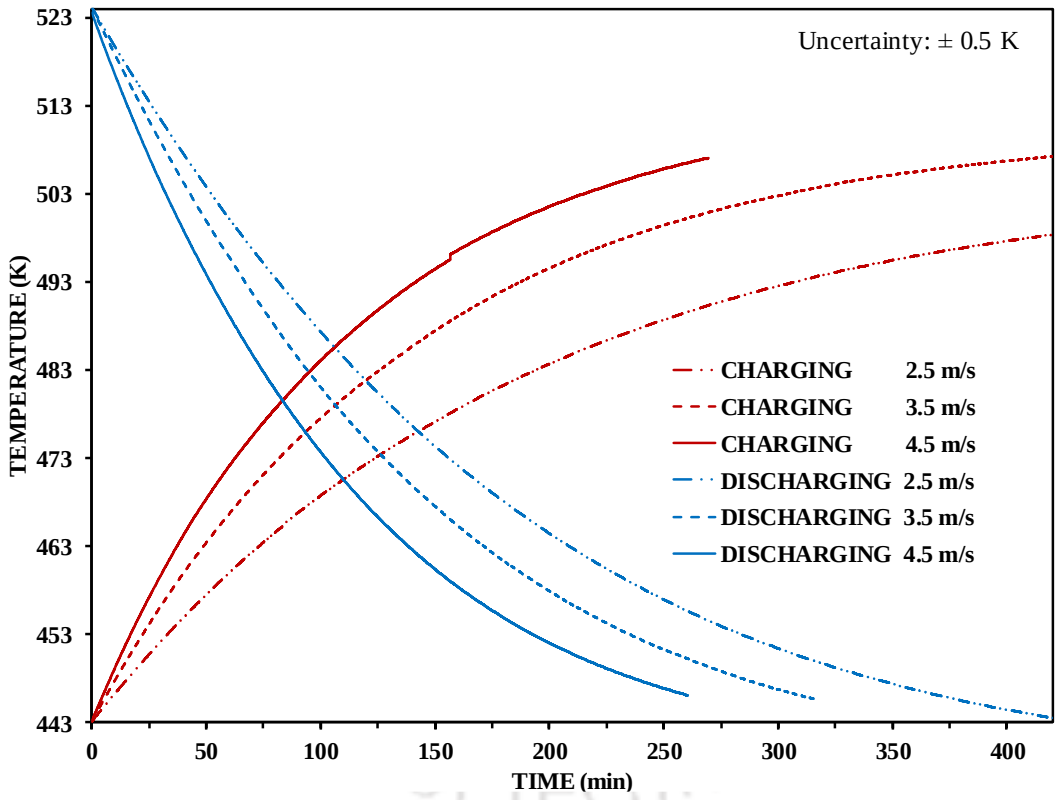

Figure 3-14. Influence of HTF velocity on $T_{s,avg}$ during charging (red line) and discharging (blue line) between the temperature range of 443- 523 K.

During experiments (*Experiment Nos. 4/5/6* and *13/14/15*), the influence of different HTF velocities on volume-averaged temperature ($T_{s,avg}$) of the SHS module throughout the charging and discharging processes are described as red and blue colour, respectively in Figure 3-14. The velocity of the HTF is varied to 2.5 m/s, 3.5 m/s and 4.5 m/s for both processes. As expected, a higher velocity of HTF increases the mass flow rate of the HTF,

which leads to rapid heat transfer from the HTF to the storage module. The increased heat transfer rate ensures that the steady-state of $T_{s,avg}$ at a faster rate. The observations are the same in both charging and discharging processes. The rate of charging and discharging increases with HTF velocity and such increment is observed due to higher heat transfer coefficient and mass flow rate. However, based on the downstream and upstream application requirements, the temperature and flow rate of HTF have to be well adjusted.

3.5.2 Analysis of SHS performance using the 3-D model

The three-dimensional model of the SHS system is useful to visualise the physical behaviour of the module during the energy interactions. Additionally, it is highly useful to study the axial and radial temperature variations in the SHS module. The simulation result of SHS module for higher operating temperature range is shown in Figure 3-15. It is observed that there is a negligible variation of temperature in a radial direction than axial direction. This behaviour has also been verified from experimental observation. This is mainly due to the domination of conduction heat transfer in radial directions as shown in Figure 3-15. Whereas along the axial direction, the heat transfer rate drops gradually along the length due to the reduction in the temperature gradient between the HTF and the SHS module. It should be noted that similar behaviour is observed for other operating temperature ranges, with the only difference is their respective charging and discharging times.

The numerical simulations at all three velocities namely; 11 m/s, 15 m/s and 20 m/s are performed. The predicted temperature contours along the module length show that the front end of the module attains high-temperature much faster for charging and vice-versa for discharging. The percentage completion of the charging and discharging processes in the operating temperature range of 493-573 K at different flow velocities is mentioned in Figure 3-15.

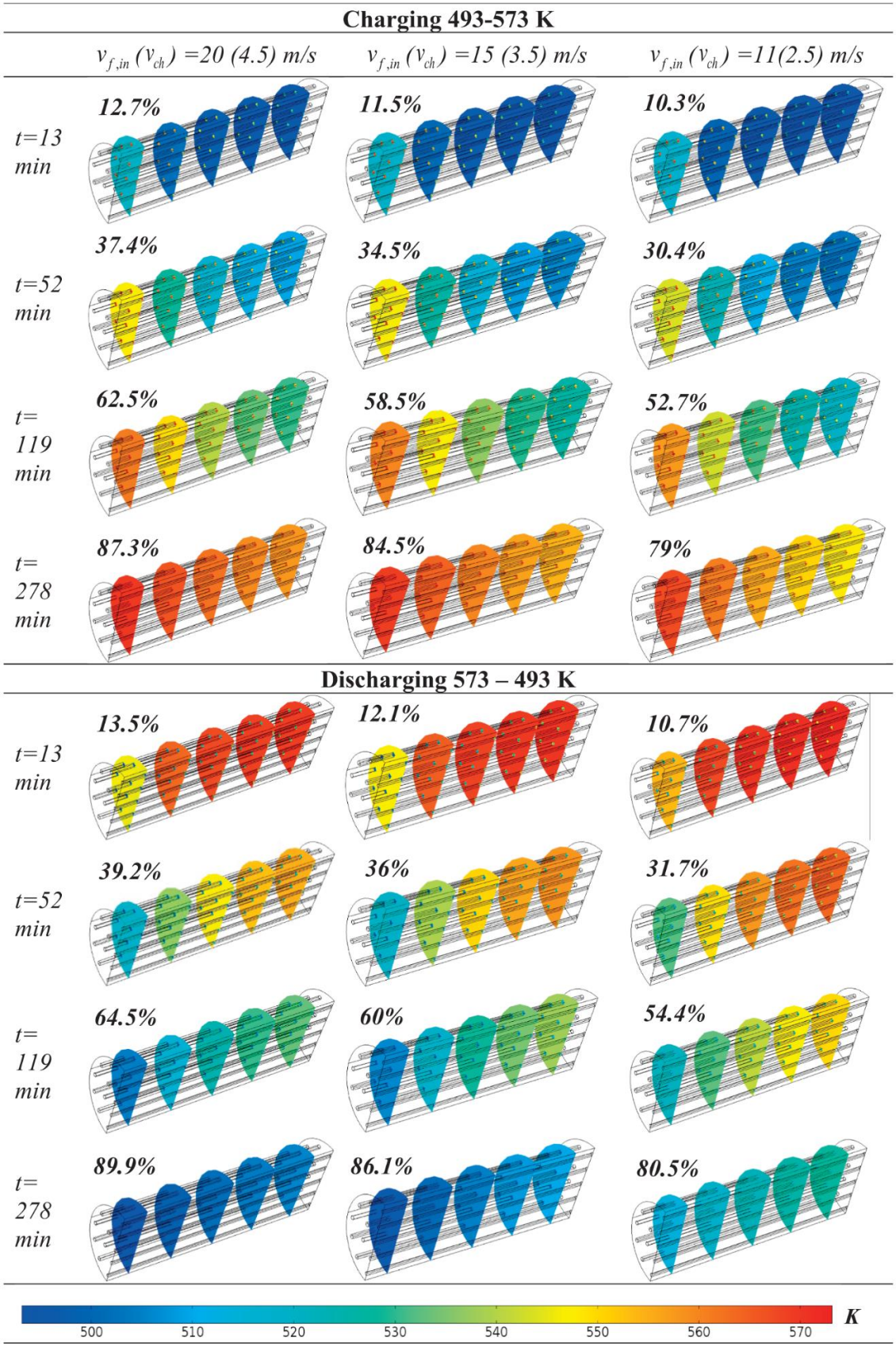

Figure 3-15. Temperature contours obtained from the 3-D model results during charging and discharging processes at different inlet HTF velocities.

The predicted charging and discharging rates are found to be similar to the experimental results reported in Section 3.5.1. A decrease in time is observed due to an increase in the heat transfer rate between the air and the SHS module. At t = 13 min, the temperature contours during charging and discharging reveal that the heat transfer starts in a similar fashion at all the velocities. At t = 52 min, the charging and discharging for 20 m/s is only 7% faster than 11 m/s. The maximum variation in the percentage charging (approximately 8.3%) between the highest and lowest velocity is only seen at t = 278 min. Hence, a very less reduction in charging or discharging time is observed with an increase in velocity.

3.5.3 Analysis of SHS performance using the 1-D dynamic model

The result obtained from the 1-D model is validated by comparing the model prediction with experimentally measured temperature of three CST's and air outlet temperature. Here, the dynamic variation of the air inlet temperature during experiments is given as an input. The experimental CST temperature is estimated by calculating the module volume average temperature using the temperature readings measured at different radial locations. In the 1-D model, the notations A, B and C stand for CST 1,2 and 3 respectively. The variations observed in the volume average temperature of different sections of the SHS module are denoted by A (red), B (blue) and C (yellow) as shown in Figure 3-16 and Figure 3-17. The dotted lines and continuous lines represent the variation of $T_{s,avg}$ for each section obtained through the 1-D simulation data and experiment data, respectively. After obtaining the initial $T_{s,avg}$ and $T_{f,out}$ profiles, the software design library follows specific procedures (refer Appendix-B section) to reduce the error in the profiles with reference to actual experimental $T_{s,avg}$ and $T_{f,out}$ data. After fulfilling this objective, the final simulated values of $T_{s,avg}$ and $T_{f,out}$ are plotted in Figure 3-16 and Figure 3-17. During the mathematical model validation, parameters ('a', 'b' and 'c') in the Dittus- Boelter equation are updated and tabulated in Table. 3-8. The values of 'b' and 'c' are estimated to be 0.8 and 0.4, respectively. The value of 'a' is varying in the range of 2.4 to 2.72 in the case of the charging, and from 2.51 to 3 in the case of discharging. While charging, the coefficient 'a' is always increasing with respect to velocity. But in the case of discharging, coefficient 'a' is found to be constant for high HTF temperature. The updated values of parameters 'a', 'b' and 'c' are the final model variables representing the validated condition of the mathematical model with experimental data. The results conclude that the developed 1-D dynamic model can predict both charging and discharging temperature profiles closely, and it is feasible to integrate them with real-time applications and processes.

Table. 3-8 Estimation of the Dittus-Boelter co-relation parameter 'a' during charging and discharging processes.

Charging Experiment No.	$v_{f,in}$ (m/s)	Simulated '*a*' value	Discharging Experiment No.	$v_{f,in}$ (m/s)	Simulated '*a*' value
1	20	2.72	10	20	3.00
2	15	2.62	11	15	3.00
3	11	2.45	12	11	3.00
4	20	2.60	13	20	2.95
5	15	2.50	14	15	2.89
6	11	2.50	15	11	2.51
7	20	2.50	16	20	2.73
8	15	2.48	17	15	2.67
9	11	2.40	18	11	2.51

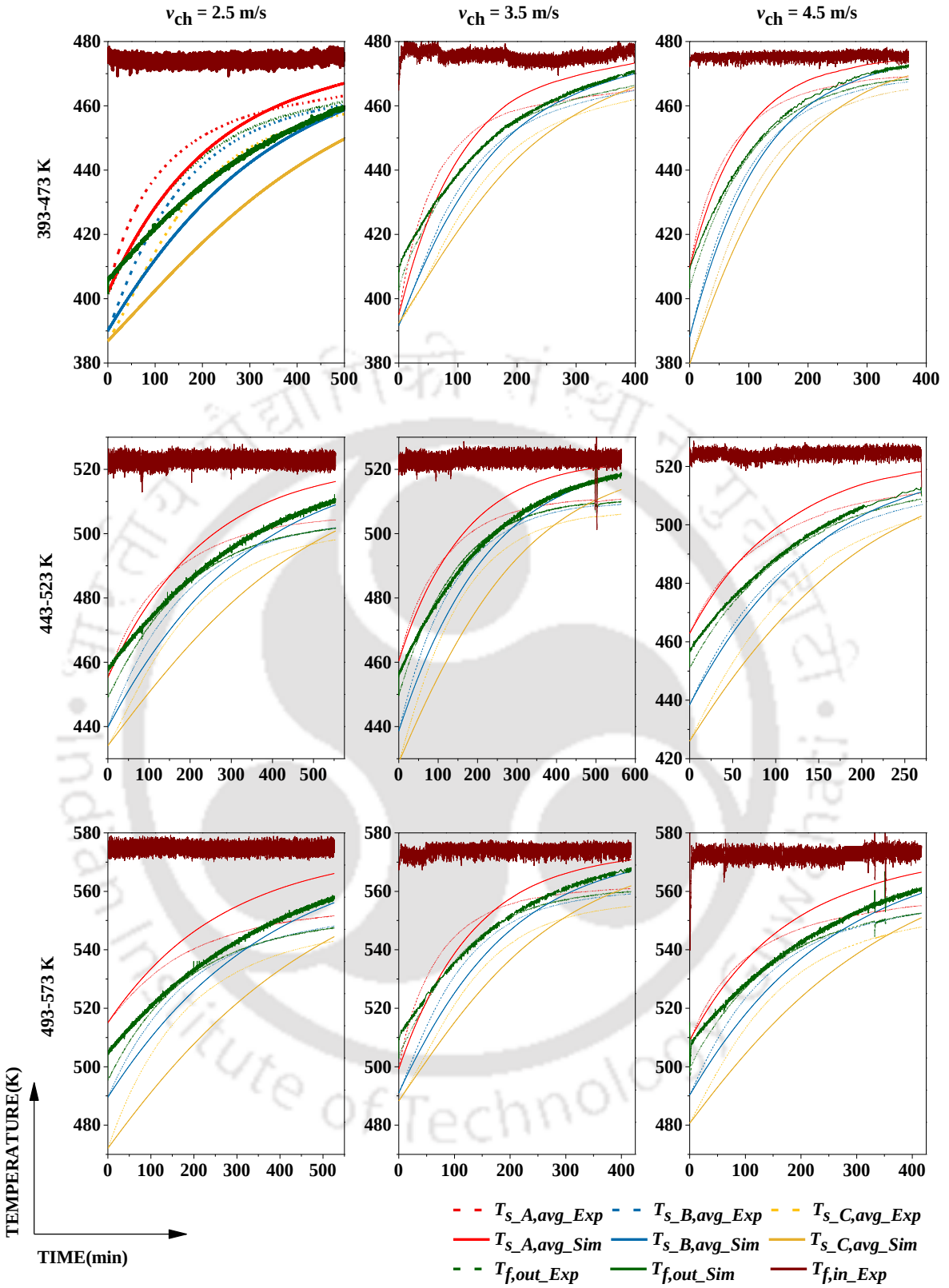

Figure 3-16. 1-D model simulation results during charging (*Experiment Nos. 1-9*): variation of volume average temperature of 3 CST's representing Section-A, Section-B and Section-C of the storage module.

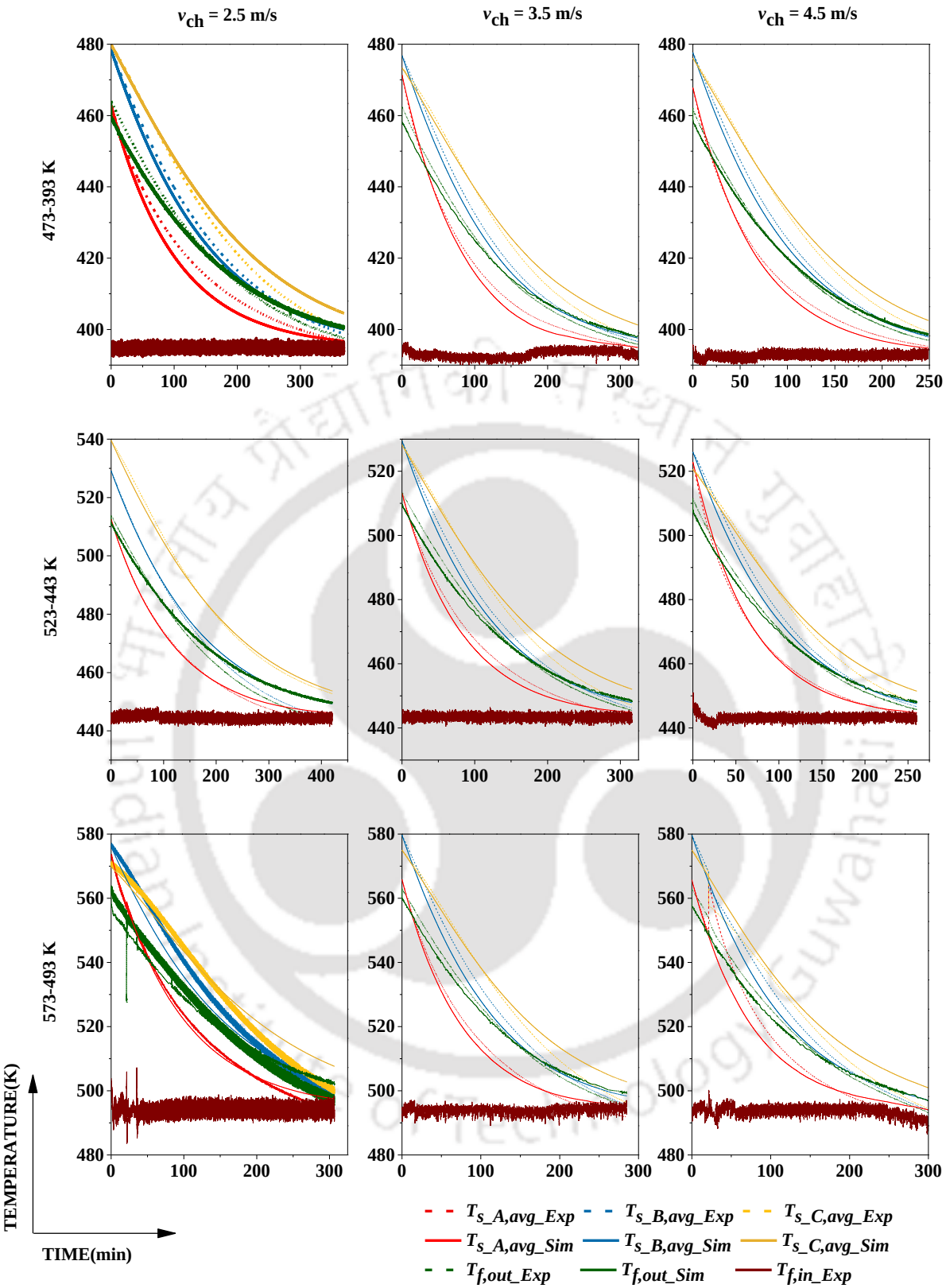

Figure 3-17. 1-D model simulation results during discharging (*Experiment Nos. 10-18*): variation of volume average temperature of 3 CST's representing Section-A, Section-B and Section-C of the storage module.

3.6 Summary

In this chapter, details of experimental and numerical studies carried out on cast steel based high-temperature thermal energy storage system are presented. The study is mainly focused to understand the thermal behaviour of the storage system during the energy storage and discharge processes. The storage module is designed based on the shell and tube configuration. The shell side is composed of storage material (cast steel) and through holes are drilled to pass the heat transfer fluid (air). Detailed parametric investigations have been conducted to evaluate the variation of average temperature energy storage and discharge rate, axial and radial temperature distributions during charging and discharging processes. An experimental study was conducted at various HTF inlet temperatures and flow rates. A 3-D numerical model is developed using the modeling tool COMSOL Multiphysics. The developed model is used to understand the spatial temperature variation and heat transfer between HTF and storage material. Based on the experimental results obtained, a 1-D dynamic model is developed to study the transient behaviour of the storage module. The model is useful to scale up the storage characteristics to match various application and demands less computational time. The net storage unit cost of the cast steel module is 18.43 US$/ MJ.

CHAPTER 4

STUDIES ON CONCRETE BASED SHS SYSTEM[2]

4.1 Foreword

The current chapter focuses on the detailed parametric investigation on Concrete Thermal Energy Storage (CTES) using air as HTF. The heat transfer between the HTF and the storage medium is enhanced by using high thermal conductivity HTF passage/tube made of copper and brazing copper fins on the outer periphery of the HTF passage. Experiments were performed on CTES system by varying HTF inlet temperature up to 688 K and velocity up to 14.9 m/s. A dynamic thermal model for predicting the real time performance of CTES is developed by considering the actual experimental conditions. There is also an apparent need to study the thermal behaviour of high-temperature CTES through the finite element based three-dimensional numerical model. Therefore, a 3-D model to evaluate the spatial behaviour of temperature inside the CTES module is also developed. The results of both the 3-D and 1-D dynamic models have been validated with the experiments.

[2]Content in this chapter has been published as the following research article:

- Vigneshwaran, K., Sodhi, G.S., Muthukumar, P. and Subbiah, S., 2019. Concrete based high temperature thermal energy storage system: Experimental and numerical studies. *Energy Conversion and Management*, 198, p.111905.

4.2 A 3-D numerical model of the CTES module

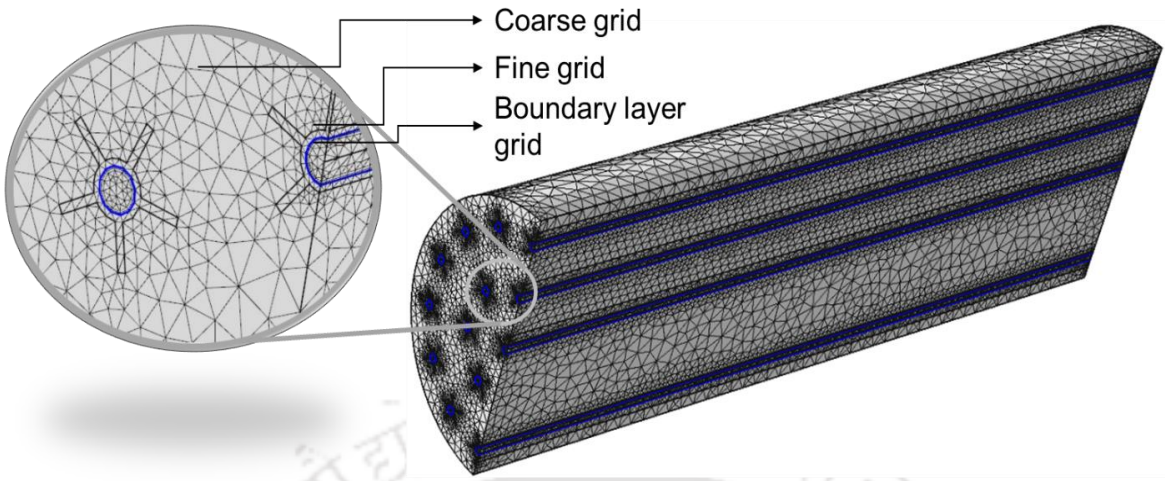

Figure 4-1. Model view after the development of mesh.

The 3-D model for the CTES module is developed and the heat transfer behaviour during the charging and discharging processes are analysed using the Comsol Multiphysics software 4.3a platform (COMSOL Multiphysics, 2017). Figure 4-1 shows a picture of the meshed CTES model. Dimensions of the developed 3-D model are equivalent to the CTES module discussed in Section 4.3.1. Considering the thermal symmetry of the module concerning the vertical axis, a half section of the CTES module is simulated to reduce the computational effort. The mesh is built using tetrahedral and triangular elements. As shown in Figure 4-1, the mesh is distributed in different domains. For example, the mesh is fine close to the fins in order to maintain the solution quality close to the walls and boundaries, while the mesh is relatively coarse in the rest of the domains. In addition, a fine boundary layer mesh is developed in the HTF domain close to the solid wall for better analysis of the boundary layer flow.

The following assumptions are considered while performing the 3-D numerical simulation:

1. The boundary at the air outlet and outer shell of the CTES module are considered as adiabatic.
2. The CTES material is homogenous and isotropic.
3. The radiation heat transfer is neglected.
4. The air passing through the main channel is equally divided through various passages designed in the CTES module.

The heat transfer inside the CTES module is governed by continuity, momentum and energy equations for air and energy equation for CTES material (Niyas et al., 2015):

$$\nabla.(\rho\vec{v})_{air} = 0 \tag{4.1}$$

$$\frac{D(\rho\vec{v})_{air}}{Dt} = -\nabla P + \mu_{air}\nabla^2\vec{v}_{air} \tag{4.2}$$

$$c_{p,air}\frac{D(\rho T)_{air}}{Dt} = k_{air}\nabla^2 T_{air} \tag{4.3}$$

$$\rho_c c_{p,c}\left(\frac{\partial T_{c,avg}}{\partial t}\right) = k_c \nabla^2 T_{c,avg} \tag{4.4}$$

The above-mentioned governing equations of the CTES module are solved using the initial and boundary conditions, as stated in Table. 4-1.

Table. 4-1 Initial and boundary conditions.

Domain	Description
Initial conditions of CTES material and air	at t = 0; $T_{c,avg} = T_{ini}$ and $\vec{v}_{air} = 0$
Boundary condition for CTES material	at z = 0; $\frac{\partial T(r,\theta,z,t)}{\partial z} = 0$ at z = L; $\frac{\partial T(r,\theta,z,t)}{\partial z} = 0$ at r = D/2; $\frac{\partial T(r,\theta,z,t)}{\partial r} = 0$ (Adiabatic)
Boundary condition for air	at $z = 0$; $v(r,\theta,z,t) = v_p$ and $T_{air}(r,\theta,z,t) = T_{air,in}$ at $z = L$; $\vec{n}(k_{air}\nabla T_{air}) = 0$ and $P(r,\theta,L,t) = P_{atm}$ (Atmospheric pressure) at $r = d_i/2$; $v_p(r,\theta,z,t) = 0$ (no slip)

Based on Eq.(4.5), the air passing through the 0.1016 m channel (*ch*) is equally divided to the 22 passages (*p*) inside the CTES module.

$$(Av)_{ch} = (Av)_p\, n \tag{4.5}$$

Multiple simulations are performed to check the variation in results due to the change in the grid size. The primary purpose of this test is to select an optimum mesh, such that there is a

minimal change in the solution quality with a change in the mesh properties. In this study, the simulation for the charging process is conducted for three grid sizes having a different number of elements, namely: 853230, 902446 and 1085157.

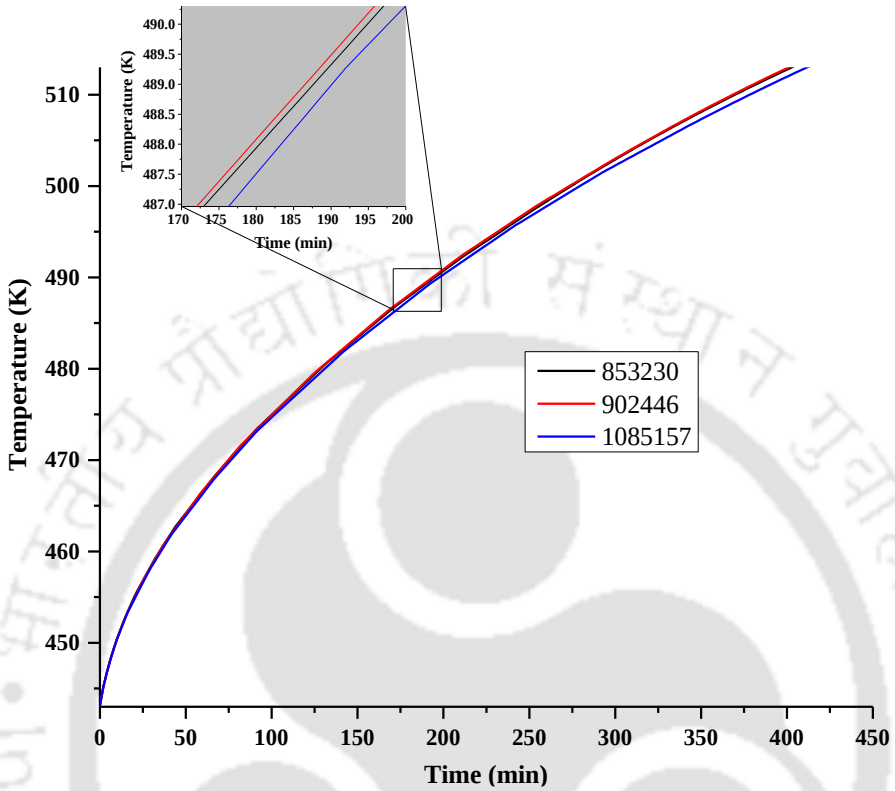

Figure 4-2. Volume average temperature of CTES module vs time for three grid sizes.

The charging temperature with respect to time for the CTES model at all three grids is plotted in Figure 4-2. It is observed that there is a definite reduction in charging time by changing the grid from 8,53,230 to 9,02,446, but there is no significant change thereafter from 9,02,446 to 10,85,157. Therefore, the solution quality is almost independent of the change in the grid from 9,02,446 to 10,85,157. Hence, it is concluded that grid with 9,02,446 number of elements is optimum and is selected for numerical simulations. The time step is set to 0.001 s. However, the parallel direct solver in the Comsol library employs a dynamic time step, which can mainly decrease the total simulation time.

4.3 Experimental setup and methodology

The information about the experimental setup and the operating methodology are explained in Section 3.2. Considering the difficulties involved in the cyclic operation of charging and discharging processes, both experiments were performed independently. Therefore, the initial volume average temperature value of the CTES module is different for both the charging and

discharging processes and maintained at different values. The HTF velocity, operating temperature range, and the HTF inlet temperature are the possible process parameters used for testing the CTES in charging and discharging processes. The testing conditions are given in Table. 4-2 and Table. 4-3.

Table. 4-2 Testing conditions for the charging process.

Case. No.	HTF inlet temperature $T_{air,in}$ (K)	CTES initial temperature T_{ini} (K)	Module average temperature at the end of charging (K)	Operating range [70 K]	Velocity at 0.1016 m channel v_{ch} (m/s)	Velocity at each HTF passage/ tube v_p (m/s)
1	553	443	513	443-513	2	9.9
2	573	443	513	443-513	2	9.9
3					2.5	12.4
4					3	14.9
5	593	443	513	443-513	2	9.9

Table. 4-3 Testing conditions for the discharging process.

Case No.	HTF inlet temperature $T_{air,in}$ (K)	CTES initial temperature T_{ini} (K)	Module average temperature at the end of discharging (K)	Operating range [70 K]	Velocity at 0.1016 m channel v_{ch} (m/s)	Velocity at each HTF passage/ tube v_p (m/s)
6	403	513	443	513-443	2	9.9
7					2.5	12.4
8					3	14.9
9	383	513	443	513-443	2	9.9
10	363	513	443	513-443	2	9.9

4.3.1 Concrete thermal energy storage module

Figure 4-3(a) depicts the isometric view of cut sectioned CTES module. Due to easy availability, low price and higher specific heat capacity, concrete has been selected as the energy storage material. The geometric configurations of the CTES module are given in Table. 4-5. The high-temperature CTES material mixtures have been finalised based on the maximum value of the material's compressive strength to the cost (3158 kN/$) (Rao et al., 2018). During the construction of the CTES module, to avoid the voids inside materials, a vibration mechanism had been employed while filling concrete mixture around the twenty-two copper HTF passages. Five copper fins having 10 mm height and 2 mm thick were brazed on the outer surface of the HTF passage tubes for improving the effective thermal conductivity of the concrete. The number HTF passages and number of fins on the HTF tube were optimized (in the present case, number of HTF passage is 22 and number of fins on each HFT tube is 5) based on minimum charging and discharging times (Prasad and Muthukumar, 2013).

The performance of the CTES module is mainly analysed by monitoring the HTF velocity and temperatures measured at different locations of the system. The heat transfer inside the CTES module was measured by mounting nine Type-K thermocouples at different locations. The temperature of the CTES material in different radial and axial locations were recorded by dividing the total storage volume into three equivalent sections such as: 'Section-A', 'Section-B' and 'Section-C' as shown in Figure 4-5. Considering the midpoint of each section and element temperature were recorded at a different radial depth of 25 mm, 50 mm and 75 mm from the outer periphery of the CTES module, as shown in Table. 4-6. Furthermore, at each section, the temperature at the midpoint of the outer peripheral surface of the CTES module was also measured.

Table. 4-4 Thermal properties of CTES material (Tian and Zhao, 2013).

Storage medium	$C_{p,c}$ **(kJ/kg-K)**	ρ_c **(kg/m^3)**	k_c **(W/m-K)**
Concrete	0.85	2200	1.5

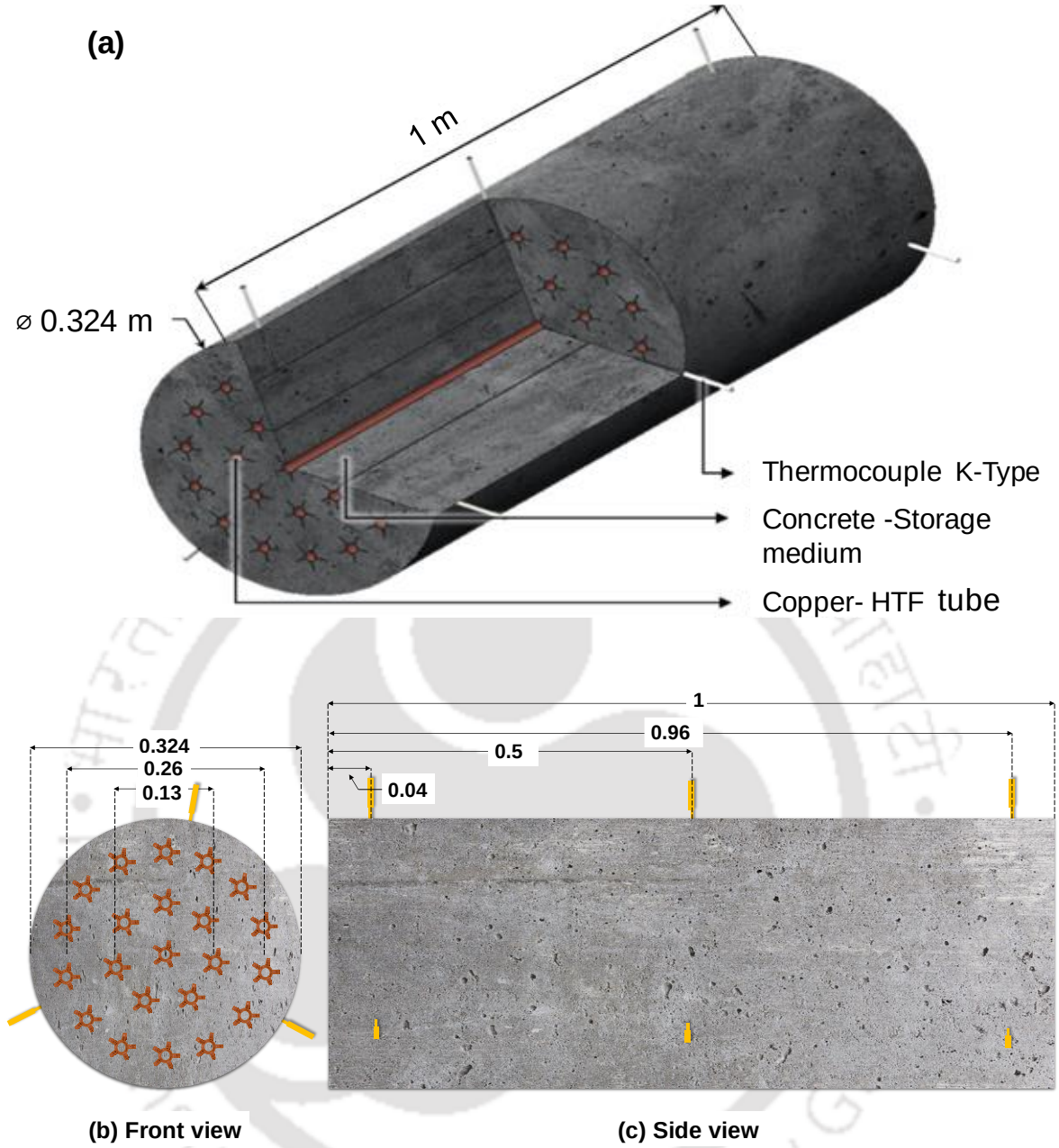

Figure 4-3. (a) Isometric view of cut sectioned CTES module, (b) front view and (c) side view of the CTES module (all dimensions are in m) with the distribution of thermocouples (in yellow colour) (for radial depth and angle, please refer Table. 4-6).

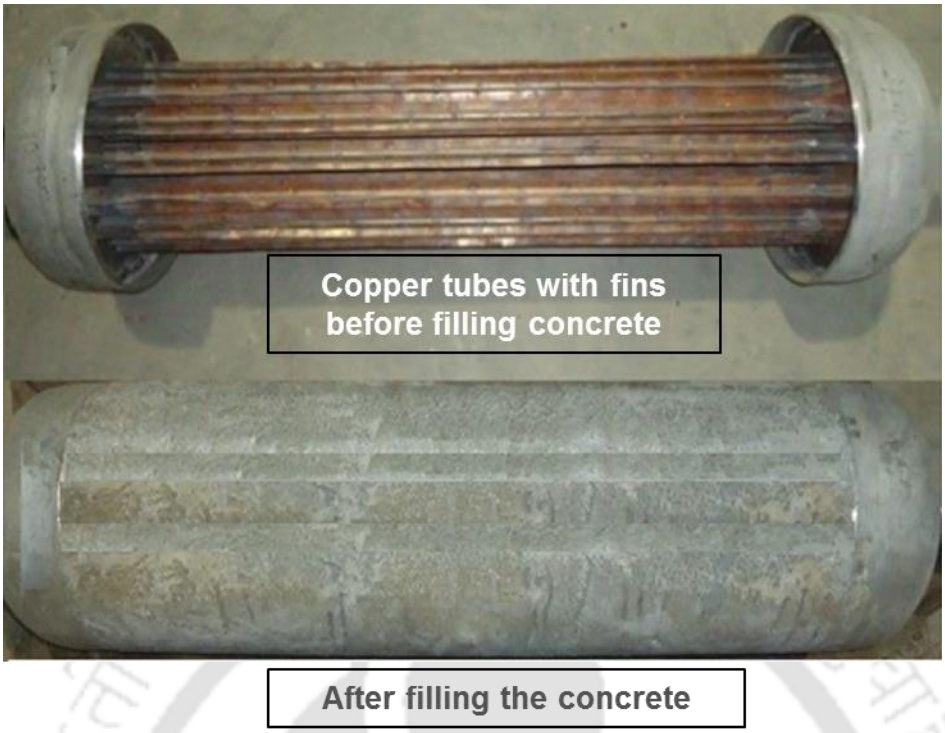

Figure 4-4. Snapshots of the CTES module before and after filling the concrete.

Table. 4-5 Dimensions of the CTES module.

Specification	Values
Length	1 m
Diameter	0.324 m
Thickness of HTF passage	0.0015 m
Outer diameter of HTF passage	0.0127 m
Number of fins on each tube	5
Height of fin	0.01 m
Thickness of fin	0.002 m
Inner pitch circle diameter	0.13 m
Outer pitch circle diameter	0.26 m
Total HTF passages	22

Table. 4-6 Thermocouple positions in the CTES module.

CTES module Section	Thermocouple nomenclature	Radial distance from module outer periphery (mm)	Axial length position from module inlet section of HTF (mm)	Angle between each thermocouple at any Section
Section-A	$T_{c,1}$/ $T_{c,2}$/ $T_{c,3}$	25/50/75	40	
Section-B	$T_{c,4}$/ $T_{c,5}$/ $T_{c,6}$	25/50/75	500	120°
Section-C	$T_{c,7}$/ $T_{c,8}$/ $T_{c,9}$	25/50/75	960	

The thermo-physical properties of concrete have been described in Table. 4-4. The CTES module has been designed based on the total energy storage capacity of the system. The mass of concrete, which is determined based on the storage capacity is estimated to be 170.41 kg. Based on the density of concrete, the volume of concrete (V_c) is calculated. The outer diameter of the CTES module (D_c) is calculated using Eq. (4.6) below;

$$V_c = \left(\frac{\pi}{4} L \left(D_c^{\,2} - d_p^2 n \right) \right) - V_{fin} \tag{4.6}$$

where L is the length of the CTES and d_p, n and V_{fin} are diameter of HTF tube, number of tubes and total volume of fins, respectively. The amount of heat energy stored and discharged is calculated using the following expressions;

Energy charged, $Q(t) = V_c \rho_c C_{p,c} \left(T_{c,avg}(t) - T_{ini} \right)$ (4.7)

Energy discharged, $Q(t) = V_c \rho_c C_{p,c} \left(T_{ini} - T_{c,avg}(t) \right)$ (4.8)

As shown in Figure 4-5, the CTES module is divided into elements (e) to estimate the volume average temperature ($T_{c,avg}$). By using Eq. (3.4), the $T_{c,avg}$ is estimated for the whole CTES module volume and HTF passage volume.

Volume average temperature, $T_{c,avg}(t) = \dfrac{\sum_{e=1}^{9} V_e T_{c,e}(t)}{V_c}$ (4.9)

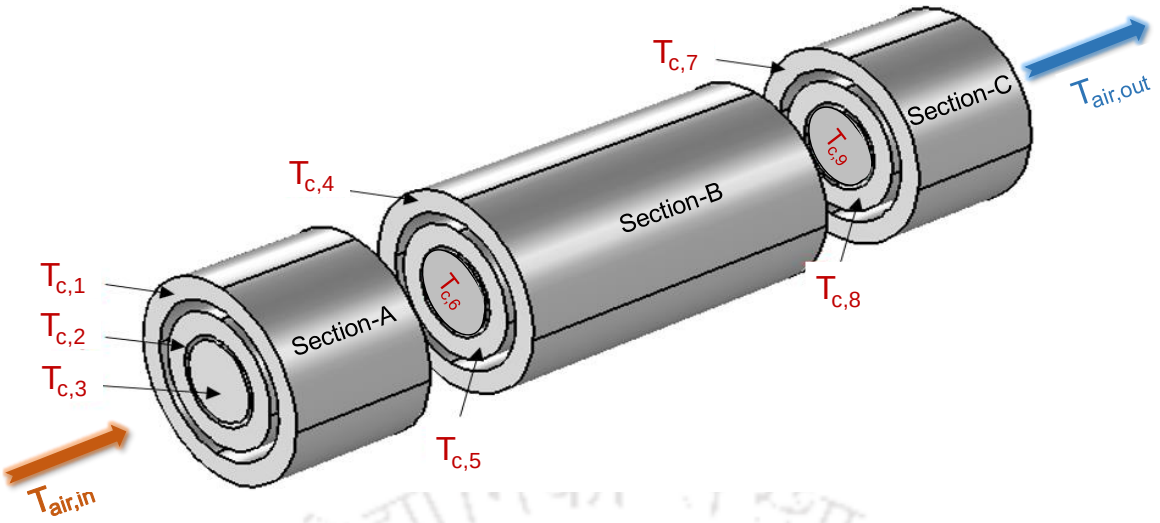

Figure 4-5. The graphical representation of thermocouple nomenclature in CTES module with different sections and elements.

4.3.2 Error analysis for CTES module

The uncertainty analysis is performed in order to determine the error in the estimated quantities such as mass flow rate, energy-charged/discharged, etc. The error persists due to inaccuracy in the measured quantities recorded by different instruments. The different measured quantities, the instruments used to measure them and their accuracy are presented in Table. 4-7. Using these values, the uncertainty arising in the estimated quantities are determined by the using method proposed by Kline and Mcclintock, (1953).

Table. 4-7 Accuracy of the instruments.

Measured Quantity	Units	Instrument/Sensor	Accuracy
Temperature	K	K-type thermocouple	±0.5
Mass of concrete	kg	Industrial weighing scale	±0.5
Velocity	m/s	Testo pitot tube meter	±0.1

The maximum error in the estimated quantities are; energy stored = ±0.36% (±0.1206 MJ), energy discharged = ±0.77% (±0.0783 MJ) and mass flow rate = ±3.33% (±0.0492 kg/min).

4.4 A 1-D dynamic model of the CTES module

Generally, two or three-dimensional mathematical models are employed for predicting the performance of any thermal systems. However, due to the high computational power, it is practically challenging to simulate the applications of CTES and monitor their performance in real-time using the mathematical models. Therefore, it is very important to predict the optimum operating range of the CTES module by developing a 1-D dynamic model. The real-time monitoring and optimization of operating parameter's ranges are made possible through the tool developed using the Modelica language. Therefore, the complex model has been simplified into a 1-D dynamic model by implementing the code developed using the Modelica language in Dymola software tool (Dassault systems, 2018). The objectives of the 1-D dynamic model of CTES module are (i) to envisage the temperature behaviour along the length and (ii) to evaluate the outlet temperature of the air, along with the charging and discharging times for real-time monitoring. In Modelica language, for evaluating the temperature variation along the length of the CTES module, an object-oriented framework is adopted by implementing the theory of Continuous Stirred Tank (CST) in series. It is evident from the 3-D numerical and experimental results that the heat transfer rate is fast and uniform in the radial direction as compared to the axial direction. Hence, Section-A, B and C are arranged in series and modelled as CST-1, 2, and 3, respectively. For each CST, the mass and energy equations are solved to calculate the outlet air and concrete temperature. The schematic diagram given in Figure 4-6 describes the charging processes of the CTES module, respectively. The analysis is made based on assumptions such as (i) T_{ini} is considered uniform throughout the CTES module, (ii) properties of CTES material are maintained constant and (iii) air properties are considered as a function of temperature. The methodology for 1-D dynamic model simulation is described as a flowchart given in Appendix-B of the thesis.

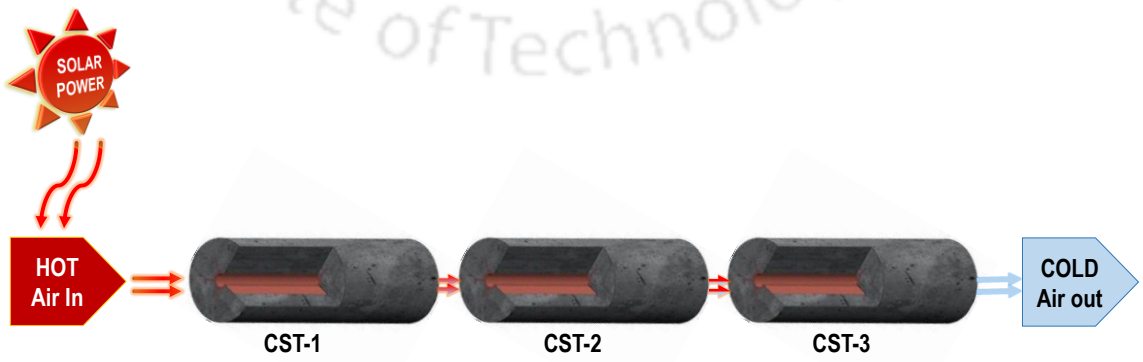

Figure 4-6. Simplified dynamic modeling of CTES module during the charging process

In this structure, the air entering the CTES module is heated or cooled by flowing through the HTF passages. Step by step, the temperature of the storage material increases or decreases and approach towards the steady-state conditions, based on experimental design strategy.

The heat and mass balance for single CST is given below:

$$V_p \frac{d(\rho C_p T)_{air,out}}{dt} n = A_p n\left((v\rho c_p T)_{air,in} - (v\rho c_p T)_{air,out}\right) - q \tag{4.10}$$

$$V_p n \frac{d\rho_{air,out}}{dt} = A_p n\left((v\rho)_{air,in} - (v\rho)_{air,out}\right) \tag{4.11}$$

Eq. (4.12) of heat balance between the HTF passages and the CTES model provides the possibility of calculating the volume average temperature of the CTES module.

$$q = \left(mC_p \frac{dT_{avg}}{dt} \right)_c \tag{4.12}$$

The heat transfer rate from the air to the CTES module can also be written as,

$$q = \left(\frac{U_o A_{sur} (\Delta T_{in} - \Delta T_{out}) n}{\ln\left(\Delta T_{in} / \Delta T_{out} \right)} \right) \tag{4.13}$$

The temperature difference between the air and CTES module is given below,

$$\Delta T_{in} = T_{air,in} - T_{c,avg} \tag{4.14}$$

$$\Delta T_{out} = T_{air,out} - T_{c,avg} \tag{4.15}$$

The HTF passages are made up of copper tubes of thickness = 0.0015 m. Therefore, the overall heat transfer coefficient of the CTES module is estimated using Eq. (4.16),

$$\frac{1}{U_o} = \left(\left(\frac{d_o}{h_i d_i} \right)_p + \left(\frac{d_o \ln\left(d_o / d_i \right)}{2k} \right)_p + \left(\frac{d_{p,o} \ln\left(D_{c,avg} / d_{p,o} \right)}{2k_c} \right) \right) \tag{4.16}$$

where, subscripts *p* and *c* represents the HTF passage/tube and concrete, respectively. The pressure drop of the air across the CTES module is calculated using the Hagen- Poiseuille equation (Biswas, 2003),

$$\frac{P_{air,out} - P_{air,in}}{L} = \left(v_{air,avg} A_p\right)\left(\frac{128}{\pi}\right)\left(\frac{\mu_{air,avg}}{d_{p,i}^4}\right) \tag{4.17}$$

The ideal gas law, Eq. (4.18), is used for calculating the density of air.

$$\rho_{air} = \frac{PM}{RT_{air}} \tag{4.18}$$

The Nusselt number is estimated using the Dittus-Boelter equation (Bergman et al., 2011), where, a = 0.023, b = 0.8, c = 0.4 (heating) and 0.3 (cooling) are the standard value of parameters in the Dittus-Boelter equation.

$$Nu = aRe^b Pr^c \tag{4.19}$$

Further, the heat transfer coefficient is estimated using Eq. (4.20),

$$h_i = \frac{Nu\, k_{air}}{d_p} \tag{4.20}$$

By using the data obtained through the experiments, it is possible to estimate the unknown model parameter values of heat transfer coefficient equation such as 'a', 'b' and 'c'. The error between the predicted model and the experimental values are minimized using Dymola's design library and using the error function in Eq. (4.21), where, *1D* and *Exp* represent the result values of 1D dynamic modeling and experiments, respectively.

$$Error(t) = \sum_{t=1}^{t}\left(\sqrt{\left(1 - \frac{(T_{c,avg}(t))_{1D}}{(T_{c,avg}(t))_{Exp}}\right)^2} + \sqrt{\left(1 - \frac{(T_{air,out}(t))_{1D}}{(T_{air,out}(t))_{Exp}}\right)^2}\right) \tag{4.21}$$

During 1-D model simulations, the initial conditions considered are (i) velocity of air: $v_{out} = v_{in}$ and (ii) initial temperature of CTES module: 443 K (for charging process) and 513 K (for discharging process).

4.5 Results and discussion

The results obtained from the numerical models and experimental studies are described in this section. Figure 4-7 details about the validation of numerically predicted volume average temperature of CTES module versus time with experimental measurements. The results obtained from 3-D and 1-D numerical models are matching closely with the experimental values with a maximum error of ±6 K for the 3-D model and ±4.9 K for the 1-D model. The

deviation observed in the 1-D model is less because of the dynamic real-time inlet temperature of the air, whereas the tool used for the 3-D model has a limitation with the same.

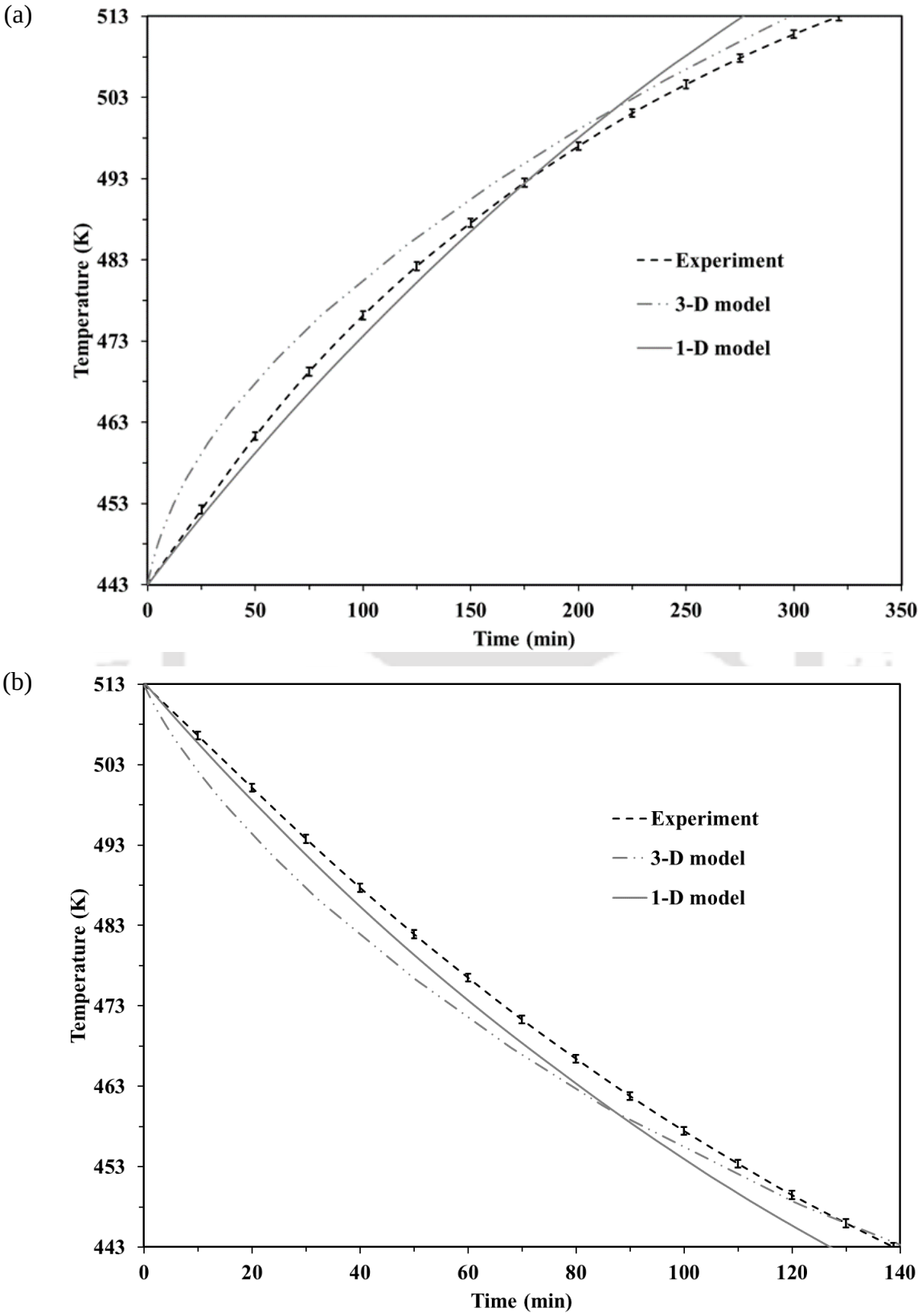

Figure 4-7. Validation of numerical models (a) charging and (b) discharging processes.

4.5.1 Results of 3-D modeling of CTES module

The 3-D numerical model result describes the physical behaviour of the module subjected to charging and discharging conditions of velocity and inlet temperature of the air. All charging and discharging simulations are performed as per experimental conditions described in Table. 4-2 and Table. 4-3. The temperature contours and percentage of charging completion at different intervals during the charging process are plotted in Figure 4-8. Simulations are performed at three different HTF inlet temperatures: 553 K, 573 K and 593 K. In all the simulations, the initial and final volume average temperatures of the module are considered as 443 K and 513 K, during the charging process and vice-versa for the discharging process. The HTF inlet velocity is fixed as 9.97 m/s in all the three cases. It is to be noted that velocity of 9.97 m/s in every single tube having a diameter of 9.7 mm, is an equivalent of the flow velocity of 2 m/s in the main air supply channel having a diameter of 0.1016 m. It is observed that there is a significant variation in temperature development across all the three cases having the different inlet temperatures mentioned above.

During charging, it is observed that the heat transfer rate is relatively higher for a high inlet HTF temperature. When the charging approaches the end, the heat transfer rate becomes slower with a decrease in HTF temperature. This happens due to the decrease in the temperature difference between the HTF and the volume average temperature of the module. At t = 234 min, the model with an inlet temperature of 593 K is charged completely, whereas the models with inlet HTF temperature of 553 K and 573 K are charged by 74.7% and 87.4%, respectively. The temperature variation scale reflects that the temperature varies from higher to lower values from the inlet section to the outlet section. When the volume average temperature of the concrete reaches 513 K, then the charging process is completed. As shown in Figure 4-9, during discharging, the inlet HTF temperature is varied in a similar fashion with values; 403 K, 383 K and 363 K. A similar result is observed during discharging, wherein the case with inlet HTF temperature of 363 K discharges rapidly as compared to other cases. At t = 96 min, the model with an inlet temperature of 363 K is discharged completely with a volume average temperature of 443 K, whereas 85.1% and 70.5% of discharging are completed for inlet temperature of 383 K and 403 K, respectively. Also, one can observe that the discharging is relatively faster than charging for all the cases within a fixed temperature range of 443 K – 513 K. This may happen due to a higher density of air at lower inlet HTF temperatures during discharging, which increases the flow rate of air passing through the tubes. The same can be observed in the experimental results presented in Section 4.5.2.

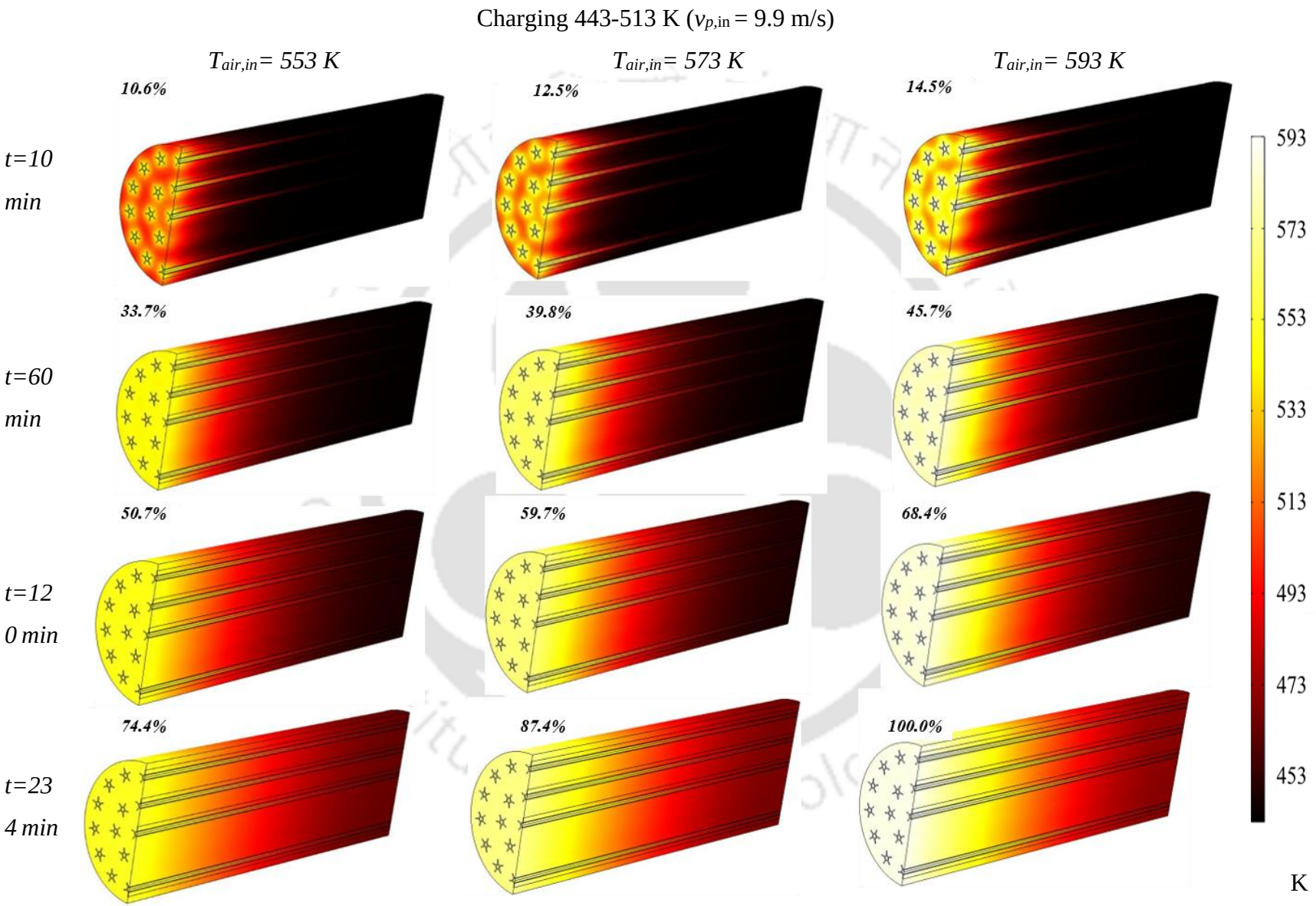

Figure 4-8. Graphical view of the 3-D model result: charging processes.

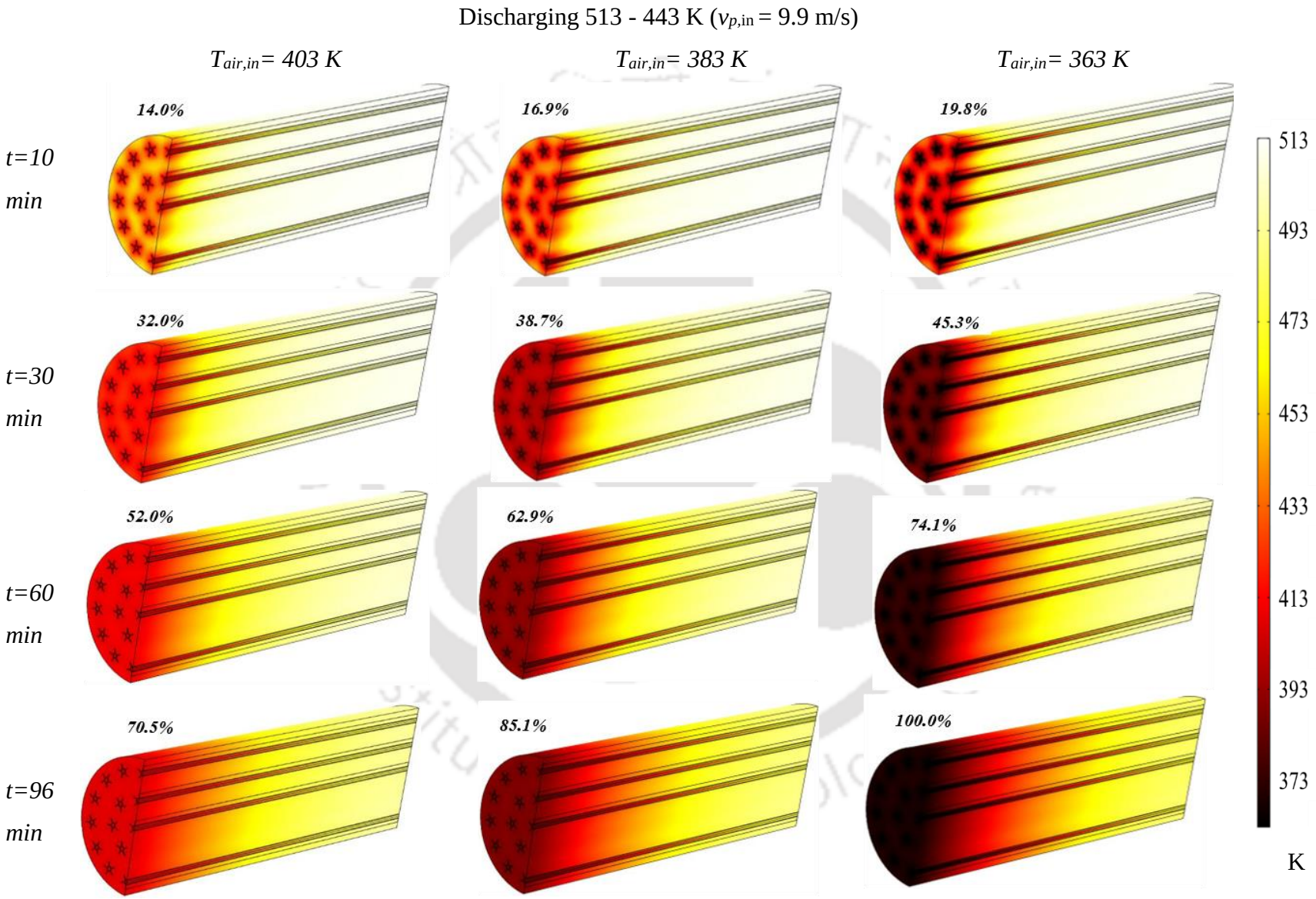

Figure 4-9. Graphical view of the 3-D model result: discharging processes.

4.5.2 Experimental results of the CTES module

Several experimental studies have been conducted on the CTES module by varying HTF velocity and HTF inlet temperatures with an objective to analyse the thermal performance of the CTES module. The charging and discharging conditions are reported in Table. 4-2 and Table. 4-3. The charging and discharging experiments are said to be complete once $T_{c,avg}$ reaches 513 K and 443 K, respectively. It should be noted that the pressure drop across the CTES module is found to be insignificant with respect to the variation in the operating parameter. The observed pressure drop across the CTES module varies between 100 – 120 Pa.

4.5.2.1 Variations of the surface temperature of CTES during charging and discharging processes

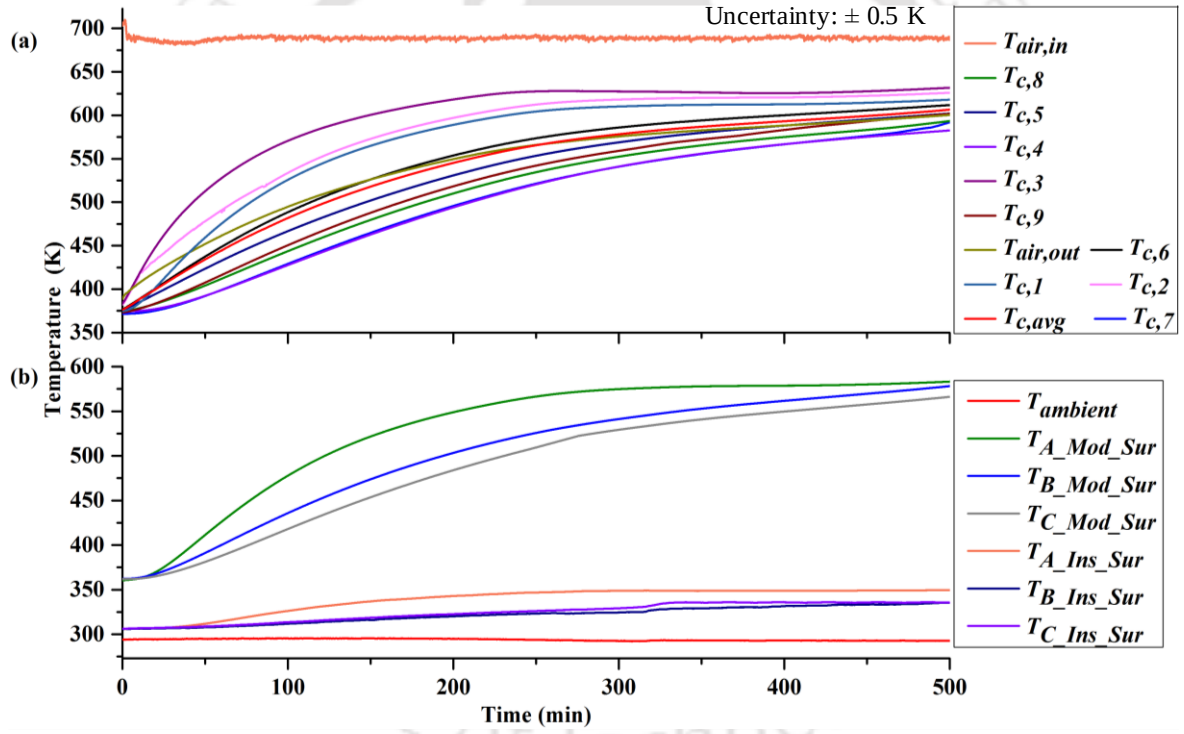

Figure 4-10. Variations of local temperatures in the charging process (a) CTES module and (b) Ambient, module and insulation surface.

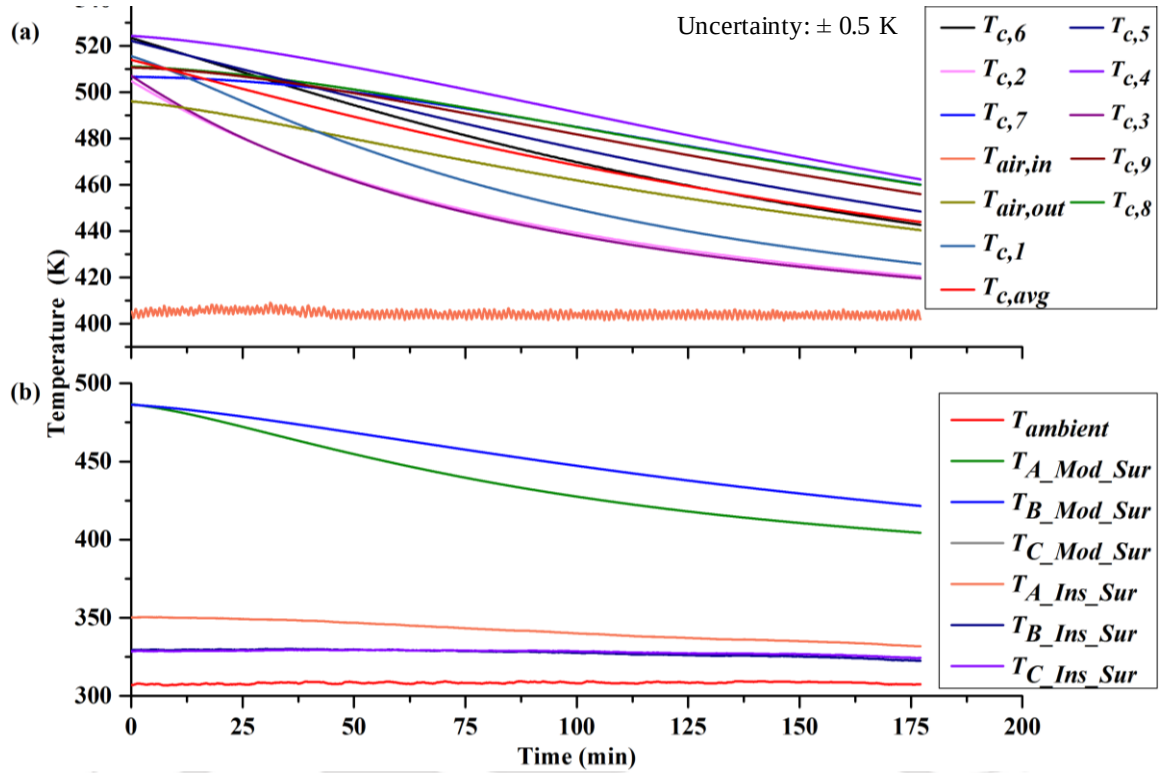

Figure 4-11. Variations of local temperatures in the discharging process (a) CTES module and (b) Ambient, module and insulation surface.

Figure 4-10 shows the temperature profile across the module length and diameter, along with module average temperature $T_{c,avg}$, air inlet temperature $T_{air,in}$ and air outlet temperature $T_{air,out}$. A slight fluctuation was observed in the air inlet temperature due to the practical difficulty in maintaining an isothermal condition. To analyse the thermal behaviour of the CTES module in high-temperature applications, air was maintained at 688 K ($T_{air,in}$) and 2.5 m/s velocity at the inlet of the CTES module. The module was charged by increasing the temperature from 373 K to 603 K. The charging is stopped when the module average temperature reaches to an asymptotic value, and the variation in $T_{c,avg}$ is minimal after this point, and thus the net heat transfer between the air to the module is minimal. By using Eq. (4.7), the total energy stored in the module is calculated as 32.8 MJ. It is prominent from the $T_{c,avg}$ value in Figure 4-10 that 46 % (i.e. 15.14 MJ) of the energy was stored within 100 min, and rest 54 % (i.e. 17.66 MJ) took 401 min. The fast charging in the initial period is mainly due to the high-temperature difference between air and module. During discharge, the module is cooled from 513 to 443 K, wherein, the $T_{air,in}$ is maintained at 403 K and v_{in} is fixed at 2 m/s. The trend of the discharging curves are shown in Figure 4-11, and it is found to have similar behaviour of the charging process.

4.5.2.2 Effect of HTF velocity on charging and discharging rates

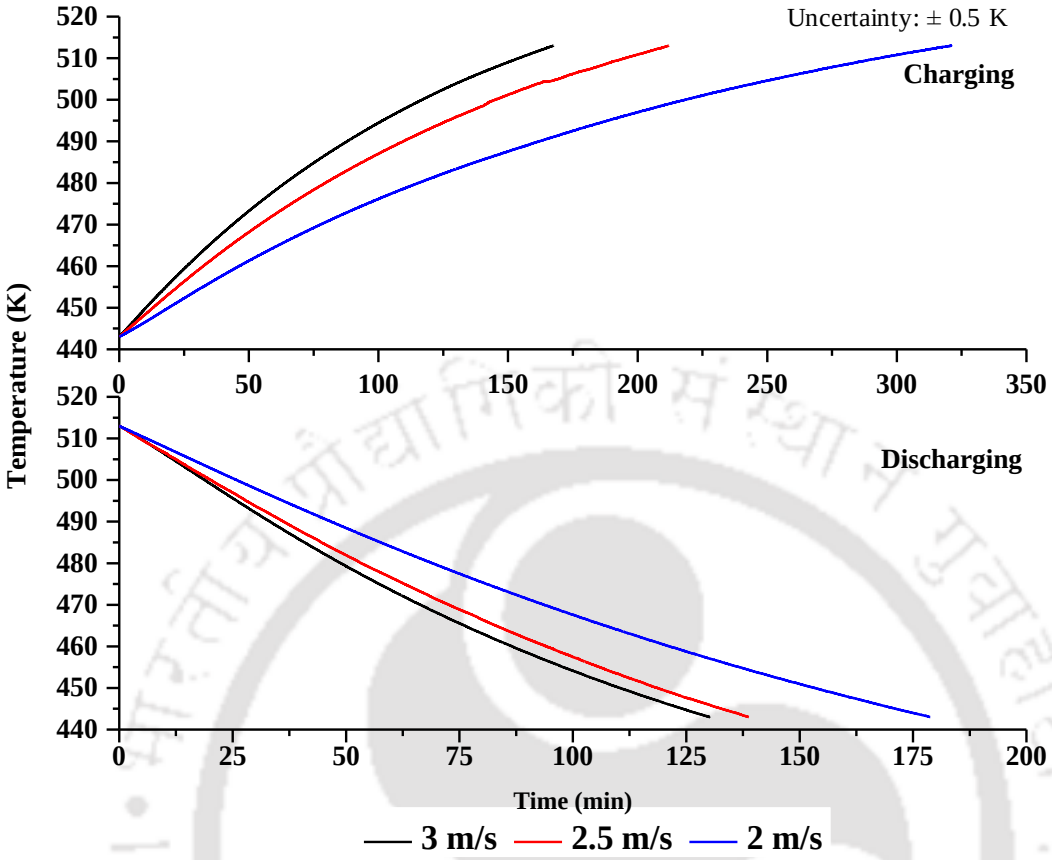

Figure 4-12. Effect of air velocity (v_{in}) on charging and discharging rates.

Figure 4-12 describes the effect of air velocity on the variation in volume average temperature of the CTES module during charging and discharging processes. During this analysis, the inlet temperature of the air ($T_{air,in}$) was maintained constantly at 573 K and 403 K for charging and discharging processes, respectively. The energy was stored in the temperature range of 443-513 K. The charging and discharging experiments were performed for three different velocities (v_{in} = 2 m/s, 2.5 m/s and 3 m/s). By increasing the velocity, the mass flow rate of air increases which leads to the rise in the heat transfer rate.

4.5.2.3 Spatial variations of temperature in the CTES module

In this section, the test result of Case Nos. 5 and 6 are analysed for studying the spatial variations of temperature during charging and discharging processes, respectively. Figure 4-13 and Figure 4-14 depict the change in temperature during charging and discharging processes measured at different sections of the CTES module (illustrated in Figure 4-5). As described in the 3-D simulation results, the experimental results also concluded that 'Section-

A' (nearby air inlet), can absorb and release the heat at a faster rate than 'Section-B' and 'Section-C'.

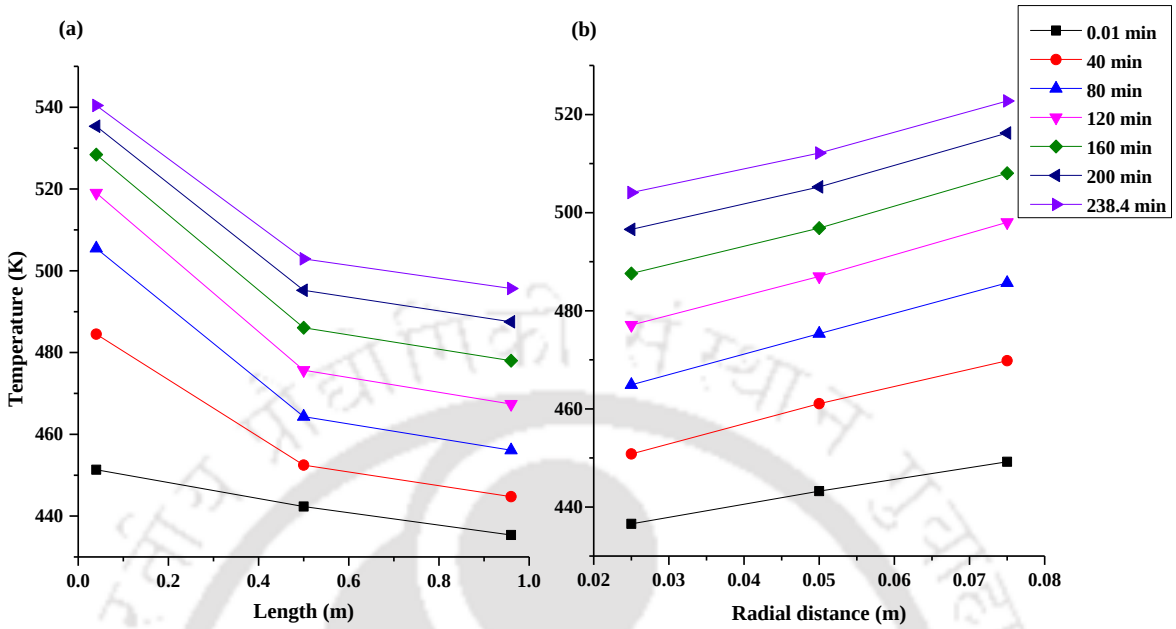

Figure 4-13. Variation in temperature at different sections in the CTES module during the charging process.

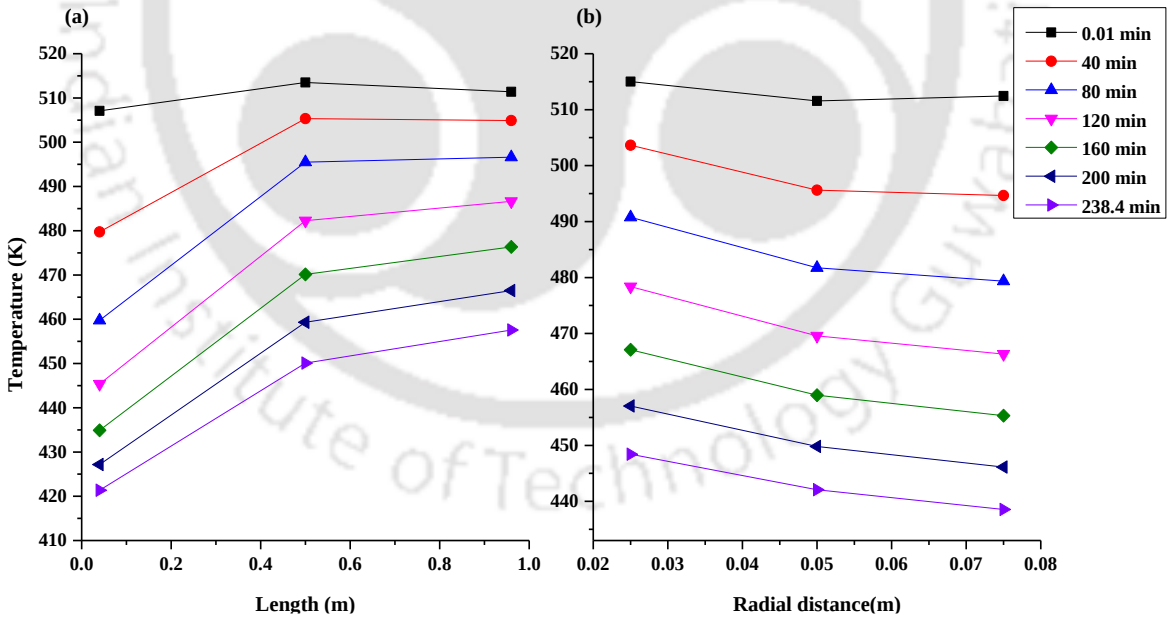

Figure 4-14. Variation in temperature at different sections in the CTES module during the discharging process.

In both charging and discharging processes, a maximum difference of 5 K can be observed between different radial locations. Also, it is observed that the heat transfer is dominating in

the radial direction as compared to the axial direction due to a drop in HTF temperature along the length.

4.5.2.4 Thermal energy storage and discharge rates of the CTES module

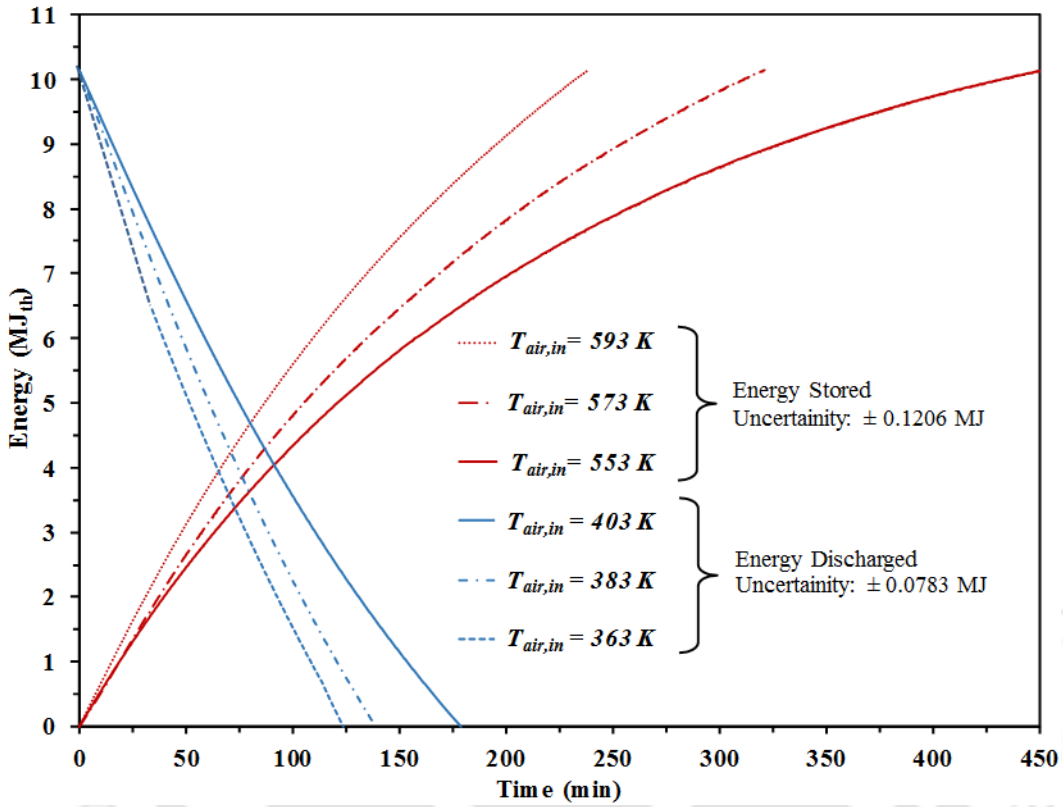

Figure 4-15. Influence of air inlet temperature on energy storage/discharge rate.

The red and blue colour in Figure 4-15 denotes the rate of energy stored and discharged calculated at the different air inlet temperatures, respectively. The amount of energy stored/discharged to/from the CTES module are estimated using Eqs. (4.7) and (4.8). It is observed that the results are directly proportional to the $T_{c,avg}$ of the CTES module. The experimental Case Nos. 1, 2, 5 and 6, 9, 10 as mentioned in and are taken for the analysis of charging and discharging processes, respectively. During charging process, the percentage reduction in charging time when the $T_{air,in}$ is increased from 553 K to 573 K is 28.9% and while further increasing the $T_{air,in}$ to 593 K, the charging time is decreased by 25.9%. Similarly, with reference to $T_{air,in}$ at 403 K, the percentage reduction in discharging time decrease from 22.3% to 10.9% when decreased $T_{air,in}$ from 383 K and 363 K, respectively.

Figure 4-16 depicts the variation of power and energy while discharging the heat from the CTES module for Case Nos. 6, 9, 10. At a fixed velocity, the discharging process always delivers peak power initially; however, the power delivered from the CTES module decreases

over time. Therefore, along the discharging process, achieving constant power output is viable by manipulating the inlet air velocity for the downstream process. Delivering such peak power during the initial phase of discharging is well appropriated for balancing the sudden high power demand during the busy hours.

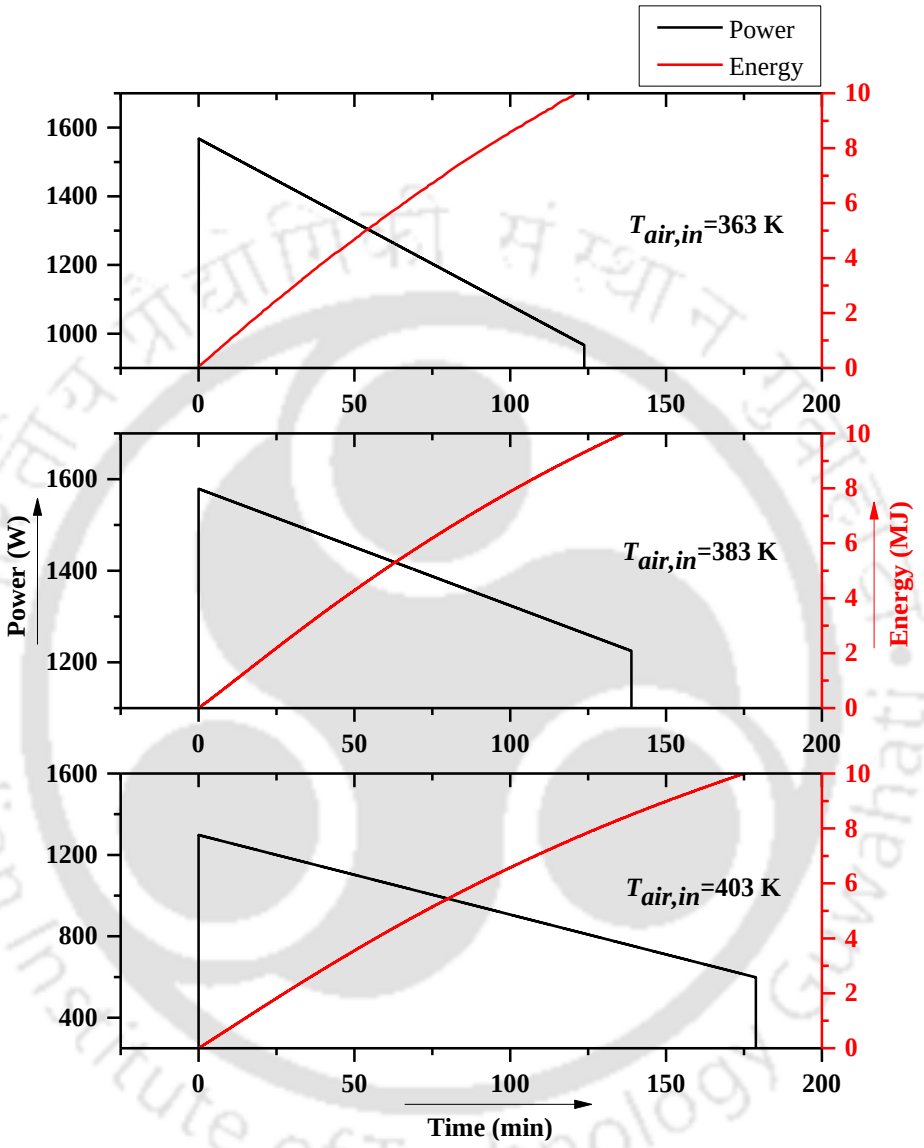

Figure 4-16. Power and energy variation during the discharging process.

Table. 4-8 summarizes the storage and discharge characteristics of the CTES module. In this study, the experiments have been performed for different operating conditions to analyse system performance. However, to adopt this system in industrial application, one has to study the upstream and downstream processes requirements to fix the operating condition (v_{in} and $T_{air,in}$).

Table. 4-8 Measured storage and discharge characteristics of the CTES module during charging and discharging processes.

$v_{ch,}$ (m/s)	$T_{air,in}$ (K)	Initial $T_{c,avg}$ (K)	Final $T_{c,avg}$ (K)	t (min)	Q_c (MJ)	Q_d (MJ)	Q_{CTES} kW.h	Q_{CTES} (kW.h/m^3)	Q_{CTES} (kW.h/kg)
2.5	688	373	603	501	32.8		9.11	117.6	0.0534
2.0	553	443	513	451					
2.0	573	443	513	321					
2.5	573	443	513	212	10.13	-	2.81	36.28	0.0164
3.0	573	443	513	167					
2.0	593	443	513	238					
2.0	403	513	443	179					
2.5	403	513	443	139					
3.0	403	513	443	130	-	10.13	2.81	36.28	0.0164
2.0	383	513	443	139					
2.0	363	513	443	127					

4.5.3 Predicted results - dynamic modeling

The validation of the 1-D dynamic model is confirmed by matching values of $T_{c,avg}$ and $T_{air,out}$ from the predicted model with the experimental outputs. The nomenclature A, B and C used in legends given in Figure 4-17 and Figure 4-18 represent the CST 1,2 and 3, respectively. The individual average temperatures of Section A, B and C computed from the 1-D model have been validated with the average temperature data of these sections obtained from the experiments. In 3-D simulations, $T_{air,in}$ is fixed as a constant value, whereas in 1-D simulation, the air inlet temperature values recorded from experiments are fed as input. This dynamic input reduced the error on predicted CST temperatures. While validating the 1-D model, the estimated model parameters given in Eq. (4.19) are listed in Table. 4-9. Figure 4-17 and Figure 4-18 describe the performance of a 1-D dynamic model with real-time experimental data. It is clear from the predicted 1-D model results that the model is able to closely predict the performance of the CTES module during charging and discharging processes.

Table. 4-9 Parameter estimation in different cases of CTES module.

Case No.	v_p (m/s)	$T_{air,in}$ (K)	model parameter value in simulation		
			'*a*'	'*b*'	'*c*'
1	9.90	553	0.020	0.818	0.403
2	9.90	573	0.023	0.841	0.420
3	12.4	573	0.023	0.851	0.336
4	14.9	573	0.027	0.828	0.347
5	9.90	593	0.026	0.828	0.680
6	9.90	403	0.014	0.890	0.102
7	12.4	403	0.033	0.798	0.133
8	14.9	403	0.045	0.790	0.344
9	9.90	383	0.020	0.705	0.410
10	9.90	363	0.019	0.848	0.100

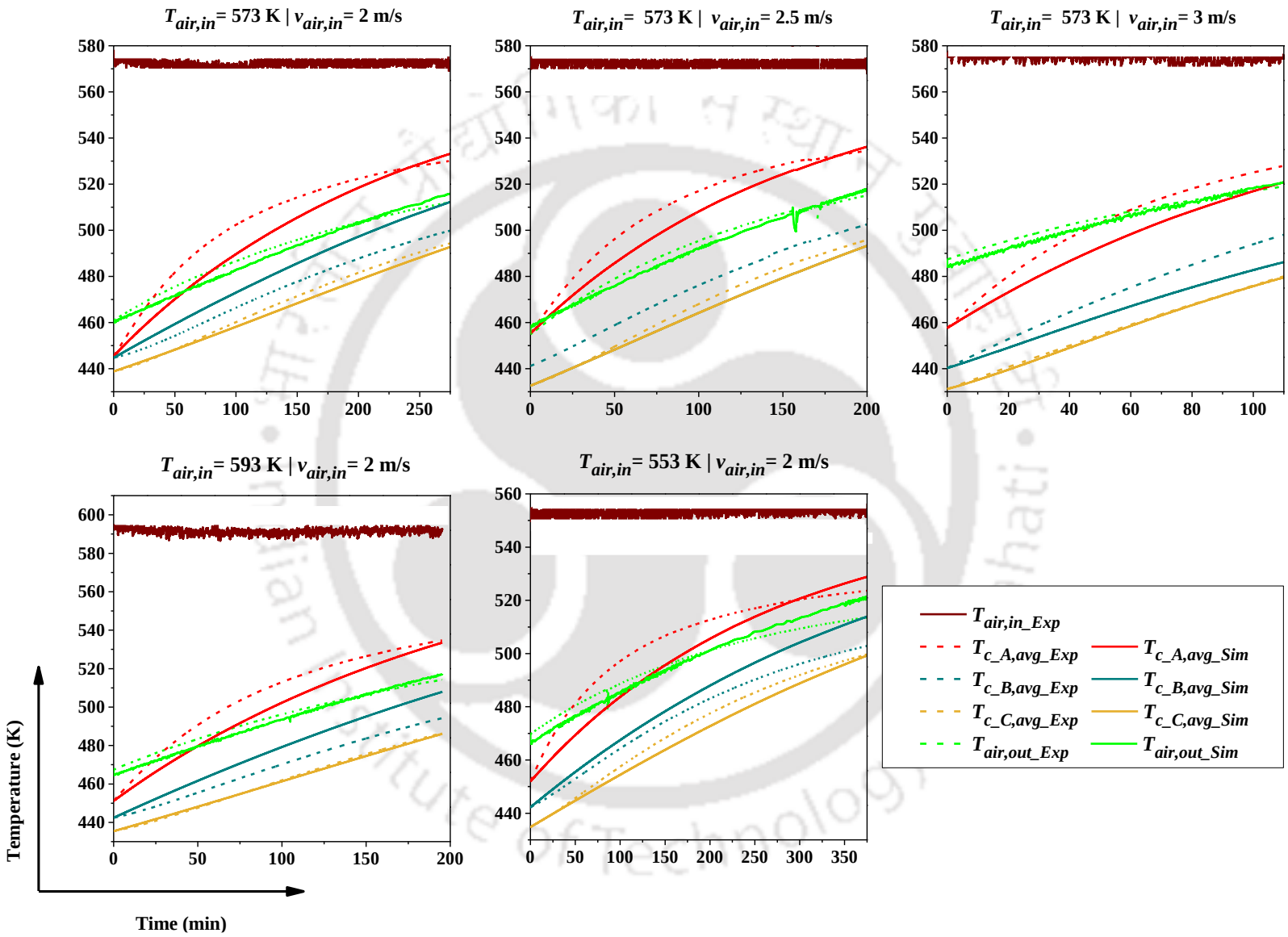

Figure 4-17. Results of 1-D modeling during charging: volume average temperature of CTES module vs time.

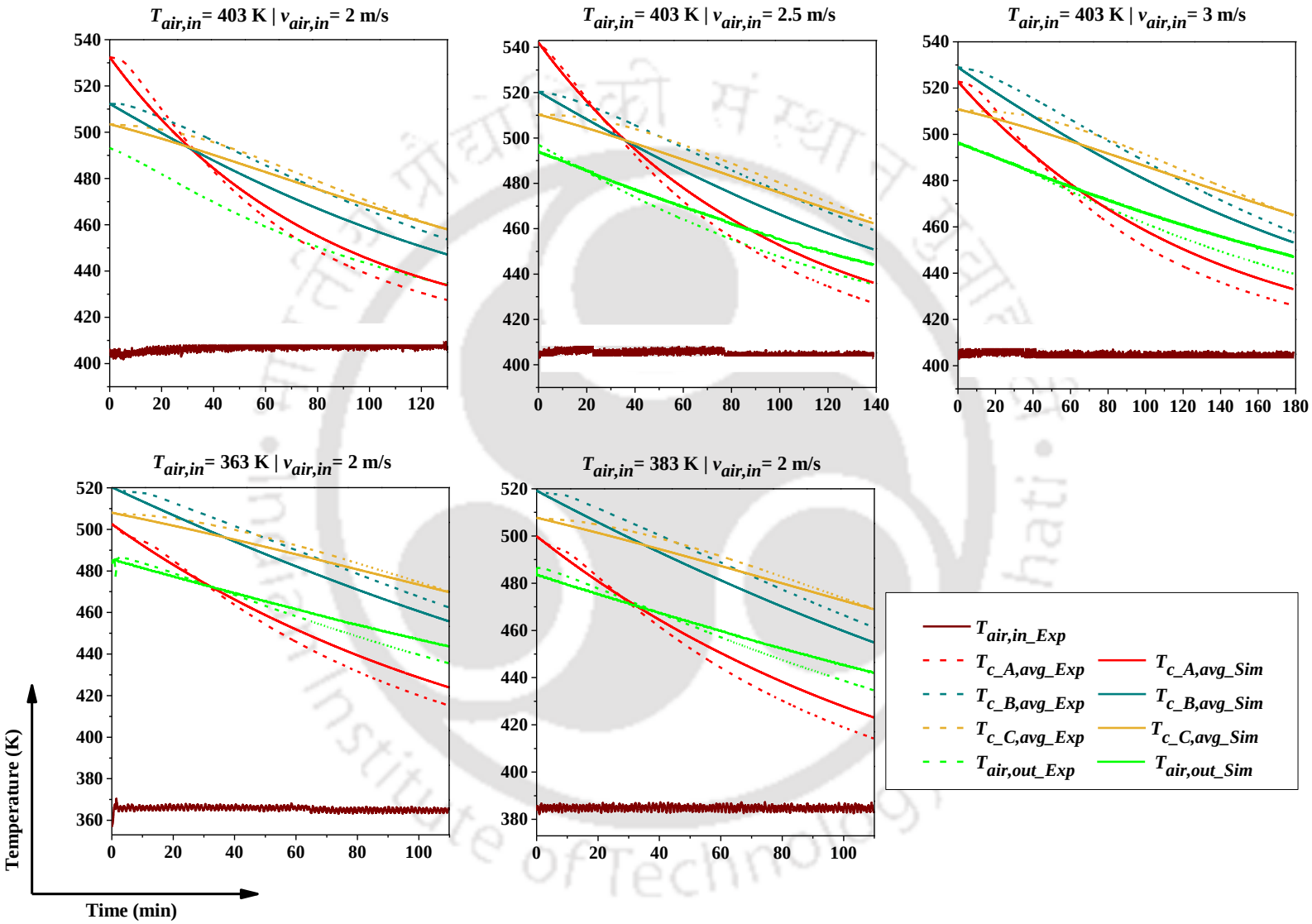

Figure 4-18. Results of 1-D modeling during discharging: volume average temperature of CTES module vs time.

4.5.3.1 Variation in overall heat transfer coefficient (U_o) during charging and discharging processes

The overall heat transfer coefficient is found to vary significantly during both the charging and discharging processes. Since the 1-D model is fitted with the real-time experimental data, estimated U_o values reflect the overall behaviour during the experiments. The effect of velocity on U_o during charging and discharging processes at near-constant inlet temperature are described in Figure 4-19. The value of U_o for charging experiments for Case Nos. 2, 3, 4 and discharging experiments for Case Nos. 6, 7, 8 (refer Table. 4-2 and Table. 4-3) show that U_o increases with an increase in velocity. U_o increases from 25.4 to 32.75 W/m^2-K as the velocity increases from 2 to 3 m/s during the charging process. Whereas, during the discharging process, with an increase in the velocity from 2 to 3 m/s, U_o increases from 32.5 to 42.3 W/m^2-K. As observed in Eq. (4.16), the value of U_o varies only with the air film heat transfer coefficient (h_i). Therefore, with an increase in velocity, U_o increases due to the increase in h_i.

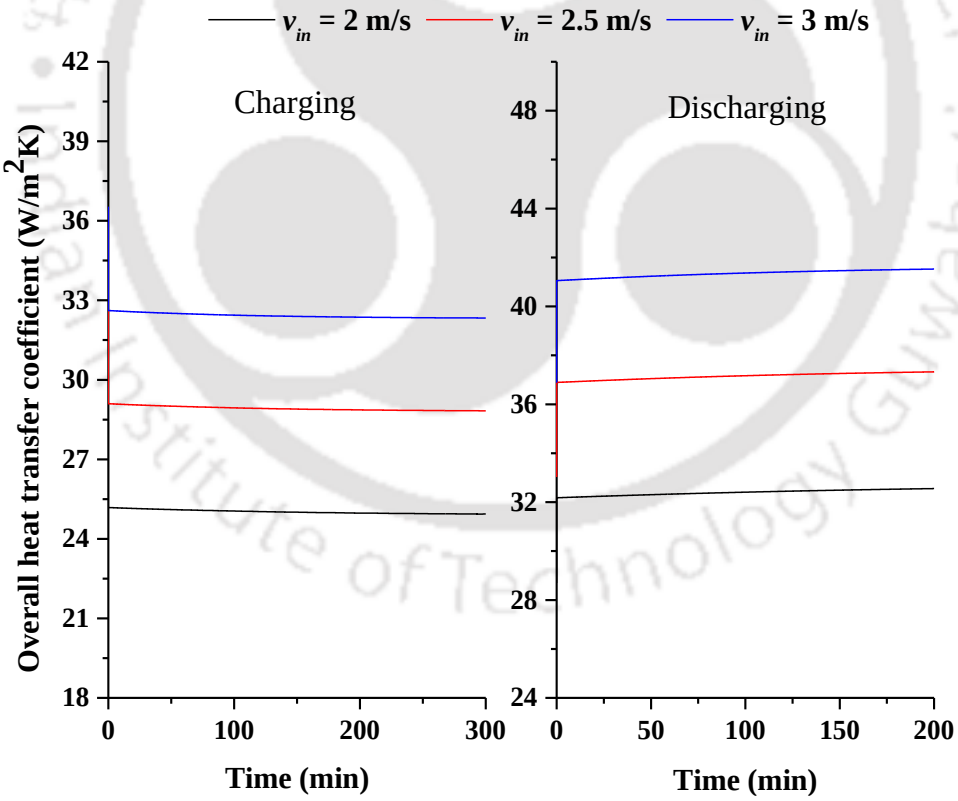

Figure 4-19. Change in overall heat transfer coefficient with respect to the HTF velocity.

From charging experiments namely Case Nos. 1, 2, 5 and discharging experiments namely Case Nos. 7, 9, 10, it is observed that the effect of HTF inlet temperature on U_o is insignificant. In charging process, for a fixed HTF velocity of 2 m/s, with an increase in inlet temperature

($T_{air,in}$) from 553 to 593 K, the value of U_o was found to vary from 24.6 to 25.7 W/m^2-K. Similarly, during discharging, the value of U_o was found to vary from 32.7 to 34.3 W/m^2-K when the $T_{air,in}$ is decreased from 403 K to 363 K. This shows that the effect of $T_{air,in}$ on U_o is almost negligible. The small variations observed in U_o are expected due to the experimental uncertainty and variations in thermo-physical properties of air due to change in temperature. Therefore, the velocity of HTF is the primary factor leading to an observable variation in U_o.

4.5.4 Aftermath of high-temperature CTES module experiments

Figure 4-20 shows the pictorial view of the initial stage of the hairline crack formation. During the experiment study, the CTES module had been subjected to more than 300 charging and discharging cycles over a period of more than 36 months of operation in the temperature range of 333 K and 753 K. The maximum inlet temperature of air supplied to CTES module was 753 K, but due to the practical difficulties in conducting experiments, the results discussed were restricted to the $T_{air,in}$ of 688 K. Due to the high thermal stress formation on the inlet section of the module, a tiny hairline crack was noticed in the 'Section-A' part of the module. Externally, it has been observed that there was no formation of hairline cracks in any other sections of the CTES module. From this observation, it is clear that the developed CTES module is highly durable for operating in a very high-temperature range. This study provides the framework for integrating the CTES module with a very high-temperature application such as super-heated steam generation which can be further connected to applications like power generation, multi-stage flash distillation process, etc.

Figure 4-20. Photographs of minor crack formation in the CTES module.

4.6 Summary

The detailed investigations on the CTES module have been presented in this chapter. The storage module is designed similar to the shell and tube configuration. The shell side is filled with the concrete as storage material and copper HTF passages are embedded inside the storage material. Experimental and numerical investigations were carried out to study the effect of variation in parameters such as HTF inlet temperature and velocity on the thermal storage performances of CTES. The transient temperature variations inside the storage module are examined with the help of a 3-D model developed using modeling tool COMSOL Multiphysics. The performance parameters such as charging time, discharging time, energy storage and discharge rate are evaluated. Based on the developed module, a simplified 1-D numerical model is developed to study the dynamic behaviour of the CTES module. The results obtained from the current study and the condition of CTES material after 300+ cycles show that the developed module is highly durable for high-temperature thermal energy storage application at low cost. The net energy storage unit cost of the CTES module is 2.4 US $/MJ.

CHAPTER 5
ANALYSIS OF MULTI-MODULE SHS SYSTEM PERFORMANCE FOR LARGE SCALE APPLICATION[3]

5.1 Foreword

This chapter focuses on evaluating the performance of a multi-module SHS system using the 1-D dynamic model. The validated 1-D dynamic model developed is adopted to scale-up the module for large scale application. The SHS module is made of materials such as cast steel, cast iron and concrete. Air is used as the heat transfer fluid at a velocity of 15.2 m/s. Six Cases are framed to evaluate the charging (493-573 K) and discharging (373-573 K) performance of multi-module SHS system *in series and/or parallel arrangements. The factors considered during the performance evaluations are HTF flow direction, module arrangements, energy stored, storage rate, energy discharged and energy discharge rate. The cost of the net energy discharged (USD/kW-h) from the storage module of each Case is evaluated and discussed.*

[3] Part of this chapter has been presented in the following conference:

- Vigneshwaran, K., Sodhi, G.S., Muthukumar, P. and Subbiah, S., Experimental study and dynamic thermal modeling of solid sensible heat storage system, *11th International Conference on Applied Energy* (ICAE 2019*)* at Mälardalen University, Västerås, Sweden, Aug 12-15 2019. (Presented work has been recommended for the special edition of Applied Energy Journal).

5.2 Thermal energy storage module

The mathematical models of the concrete and cast steel based SHS systems are validated with experimental results. The validated models are used to simulate the performance of the multi-module SHS system for large scale application. The multi-module SHS system can be designed either using a single SHS material or the combination of multiple SHS material. In this work, both concrete and cast steel were used for the fabrication of a single SHS module. Similarly, cast iron was used for the fabrication of SHS module having cost in between them. For example, concrete provides benefits such as low cost and high energy storage potential. However, the charging and discharging rate are found to be very low. Whereas the cast steel provides benefits such as high charging and discharging rates (Gil et al., 2010; Medrano et al., 2010b). Cast iron is expected to have intermittent cost, energy storage potential, charging and discharging rates which are in between concrete and cast steel. Therefore, the identification of optimal multi-module SHS system configuration is a very important aspect to achieve optimised charging and discharging rates, energy storage cost and energy storage potential.

Table. 5-1 Dimensions of the solid SHS module.

Name of the SHS module	Diameter (mm)	Number of HTF tubes	Length (mm)	Inner diameter of HTF tubes (mm)	Inner pitch circle diameter (mm)	Inner pitch circle diameter (mm)
Cast steel	300	19	340	12.7	110	220
Cast iron	300	19	346	12.7	110	220
Concrete	324	22	1000	9.7	130	260

Six different multi-module configurations are established by using concrete, cast iron and cast steel SHS modules. The dimensions of these modules are given in Table. 5-1. The basis of the dimension is derived by fixing the mass of a single module as 170.85 kg. Accordingly, the volume of the module will be calculated. As reported in the literature, the cylindrical module is found to be superior than other configuration with respect to uniform heat distribution (Rao, 2018). Therefore, all three storage modules are constructed as the

cylindrical module. The thermal properties of all the storage modules required for SHS modelling are given in Table. 5-2.

Table. 5-2 Thermal properties of SHS material (Pilkington Solar International GmbH, 2000).

SHS material	Thermal conductivity (W/m-K)	Density (kg/m^3)	Specific heat (J/kg-K)
Cast steel	40	7800	600
Cast iron	37	7200	560
Concrete	1.5	2200	850

5.3 Potential configurations of integrating multiple TES module

Six different multi-module SHS configurations are derived to identify the best configuration by performing a simulation study. The performance of the multi-module SHS system is benchmarked by calculating the amount/rate of energy stored and discharged, and the cost of the storage. While designing all six configurations, the optimal number of SHS module that can be connected in series has to be calculated. In general, while adding more number of SHS modules in series the HTF temperature will be approaching towards the module initial temperature. In that case, the rear end of the SHS modules is not utilized effectively to store the energy in comparison to front end modules. Therefore, finding an optimal number of modules that can be connected in series is one of the important aspects and it can be achieved by simulating multiple modules in series configuration. The simulations results concluded that the maximum of six modules in series can provide optimum storage performance for concrete, cast steel and cast-iron module. Further, hybrid multi-module configurations are also configured by using six number of SHS module. So, the first three configurations are proposed by connecting six number of cast steel, cast iron and concrete in series, respectively. Remaining three hybrid multi-module configurations are proposed by combining all three modules as described below. The pictorial representations of all six configurations are shown from Figure 5-1 to Figure 5-6.

- In Case 4, two SHS modules of each type (cast iron, cast steel and concrete) are arranged in series in the order of lowest to highest specific heat. Therefore, two cast iron followed by two cast steel and followed by two concrete modules coupled in series (as shown in Figure 5-4).
- In Case 5, the air input goes directly into a splitter, which splits the flow into two parallel branches, and each branch has the same velocity as 15.2 m/s. As illustrated in Figure 5-5, in each branch, three modules are connected in series in the order of lowest to highest specific heat capacity (cast iron-cast steel-concrete).
- In Case 6, splitter divides the air inlet flow into three branches, each branch considered to have the same air inlet velocity as 15.2 m/s through each HTF tube. As illustrated in Figure 5-6, each branch has two modules of different types in series, arranged on the basis of low to high specific heat capacity.

For simulation and benchmark study, flow and temperature conditions are fixed for all six Cases. The inlet air velocity is fixed as 15.2 m/s through the storage module. The temperature range for charging and discharging are fixed as 493-573 K and 393-573 K, respectively. During charging and discharging processes the initial temperature of the module is maintained at 493 K and 593 K, respectively. The inlet temperature of the HTF is maintained at 573 K during the charging process and 393 K during the discharging process.

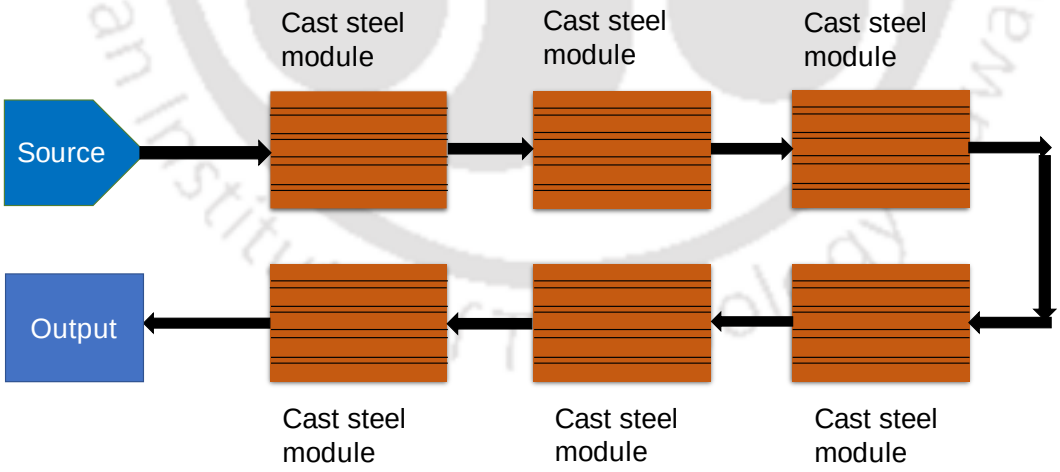

Figure 5-1. Arrangement of six cast steel modules in a series.

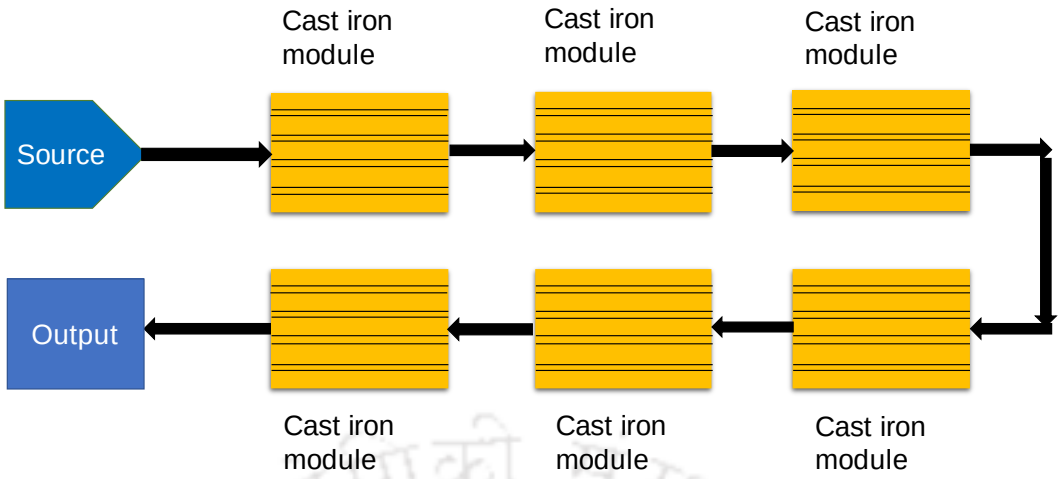

Figure 5-2. Arrangement of six cast iron modules in a series.

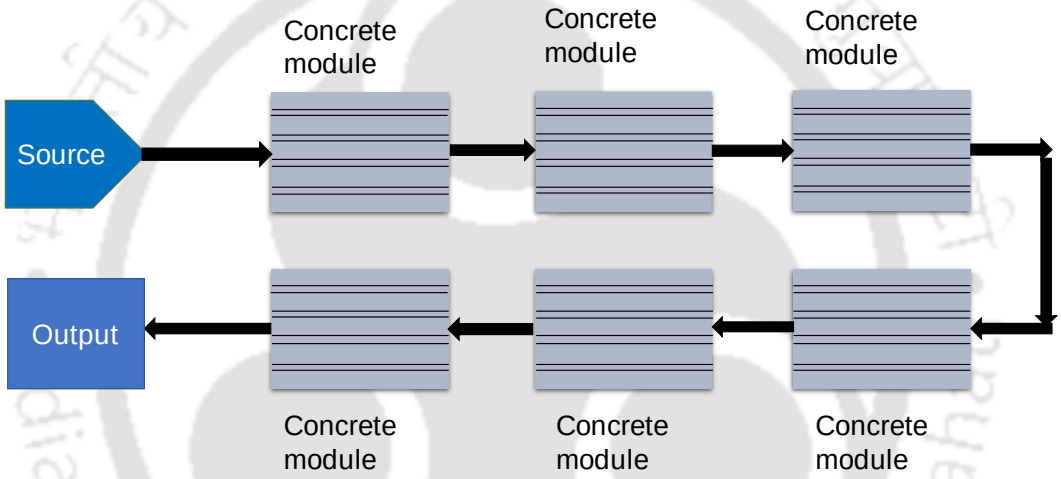

Figure 5-3. Arrangement of six concrete modules in a series arrangement.

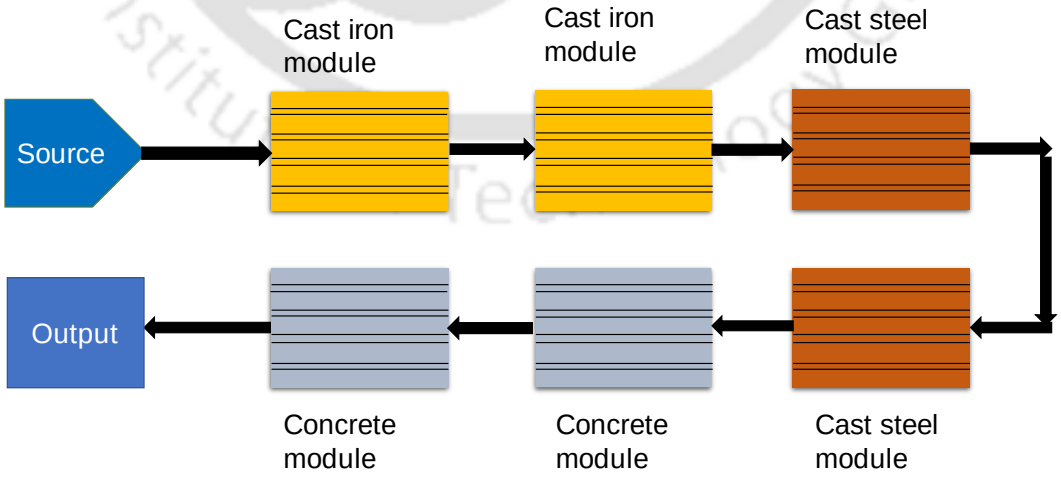

Figure 5-4. Arrangement of SHS modules for Case 4.

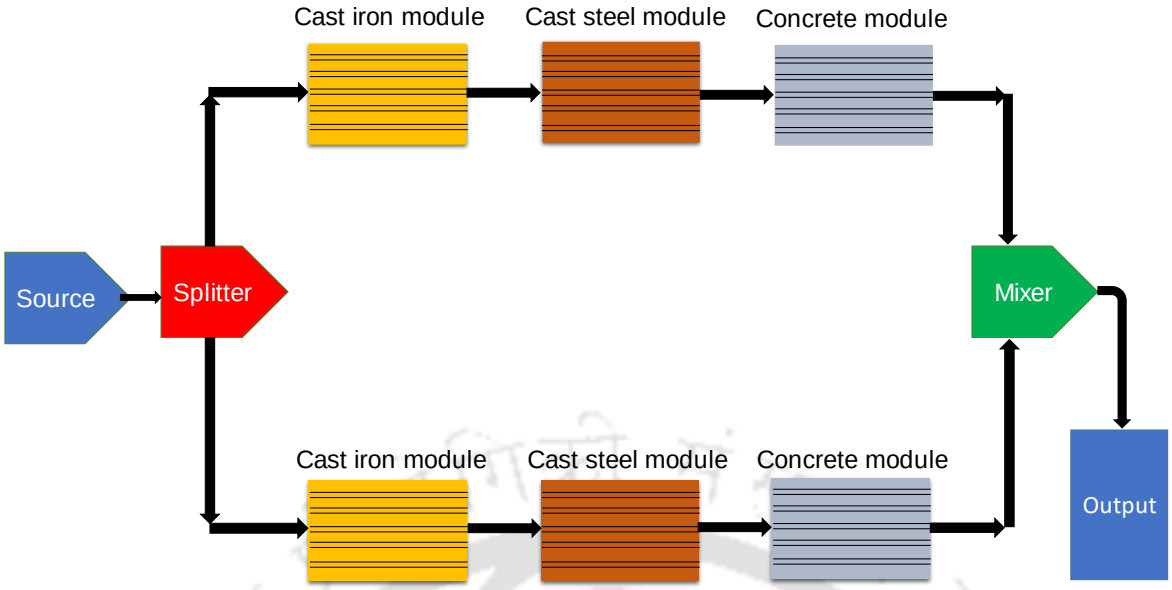

Figure 5-5. Arrangement of SHS modules for Case 5.

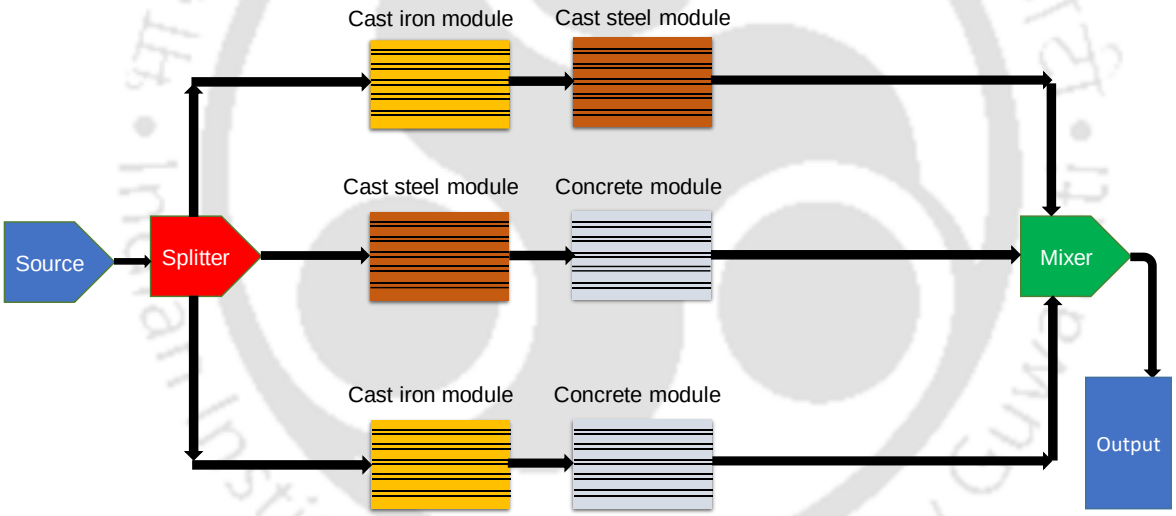

Figure 5-6. Arrangement of SHS modules for Case 6.

5.3.1 HTF flow direction and its impacts

The flow direction of HTF in the SHS module can be manipulated to achieve the desired charging and discharging characteristics. For example, the interchanging of flow direction from forward flow to reverse flow during the charging process may improve the charging rate. Similarly, during the discharging process, the flow reversal may help in achieving the maximum power output. The definitions of forward and reverse flows are given below.

Forward flow: In this flow pattern, different SHS modules are arranged based on the hierarchy from lower to higher C_p values (whereas in Cases 1, 2 and 3, the C_p values are constant), with cold air going from the module of lowest temperature to that of highest temperature.

Reverse flow: The position of the modules remains same as forward flow, but the direction of flow is just opposite; Reverse arrangement: change in arrangements of the modules in series or in each branch of the parallel arrangement Cases, where the modules are arranged based on hierarchy position from higher to lower C_p values, with cold air going from the module of lowest temperature to the module of highest temperature. Figure 5-7 and Figure 5-8 illustrate the forward flow, reverse flow and reverse arrangement.

The effect of flow direction on SHS module performance is simulated for all six Cases to find out if there is any advantage of using reverse-flow configuration compared to the forward flow configuration.

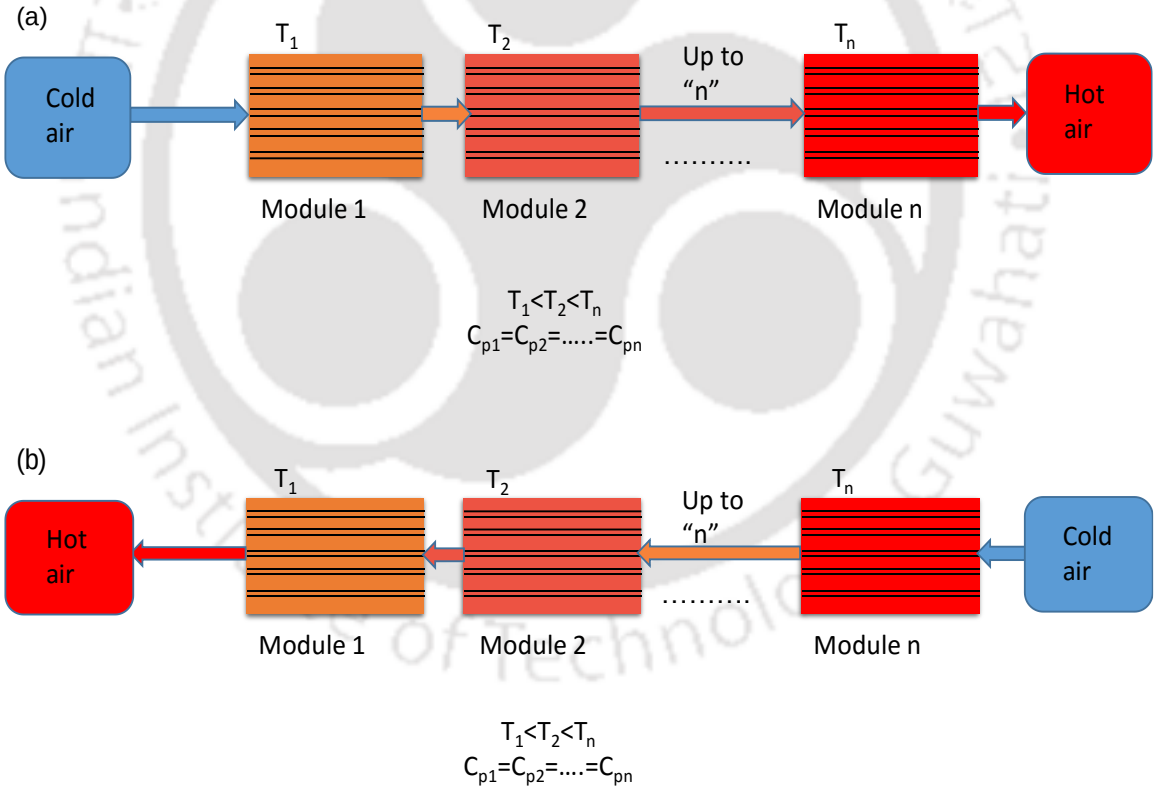

Figure 5-7. (a) Forward and (b) Reverse flow for Cases 1, 2 and 3: Same type of modules in series, where T_n is the temperature of n^{th} module in series. For Cases 1,2 and 3, n=6.

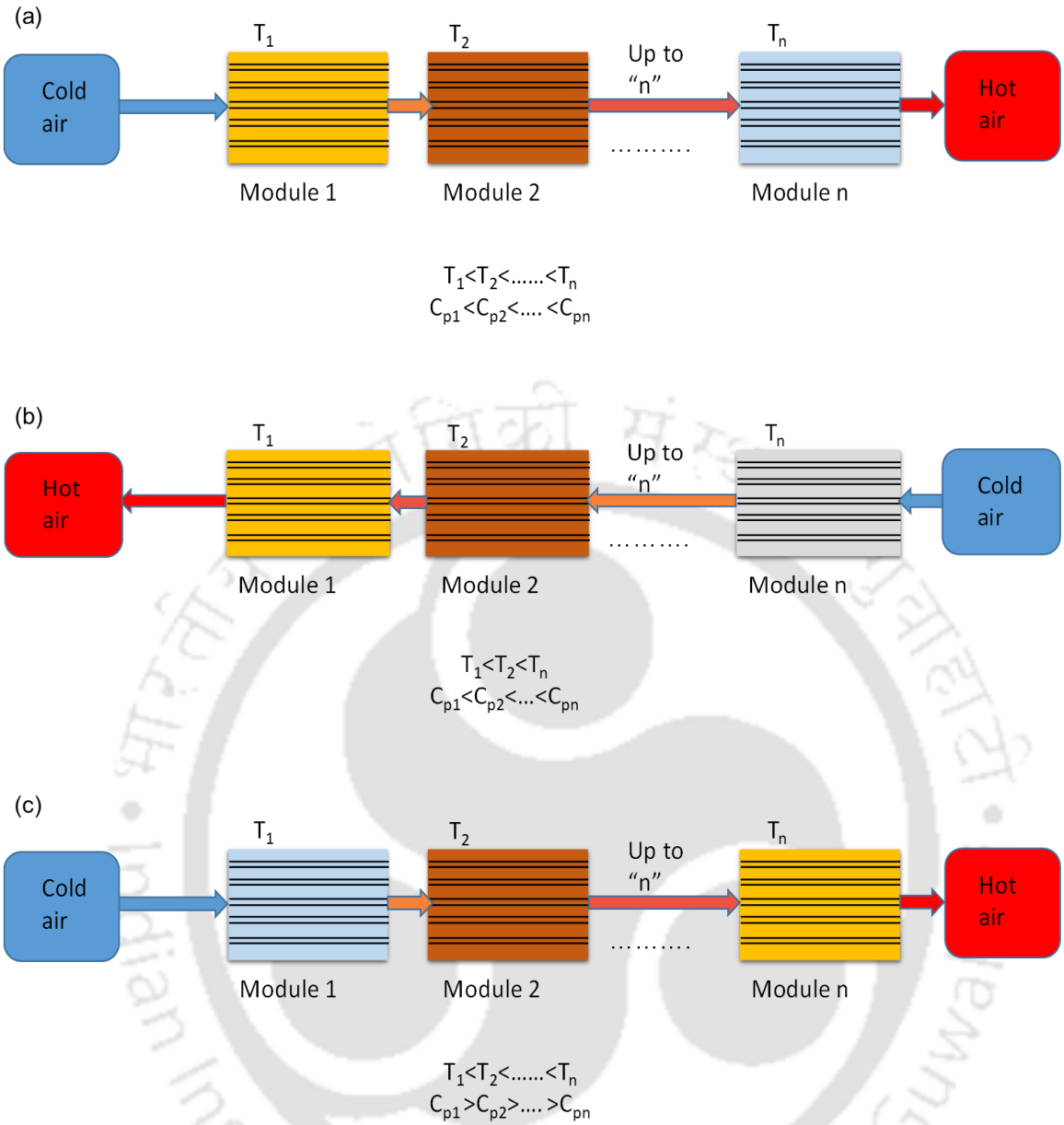

Figure 5-8. (a) Forward, (b) Reverse flow and (c) Reverse arrangements for Case 4, 5 and 6: where T_n is the temperature of n^{th} module in series or in each branch of the parallel arrangements. For Case 4, n = 6, while for Cases 5 and 6, n = 3 and 2, respectively.

The performances of the SHS modules with respect to the forward and reverse flow are analysed for all six Cases by comparing the amount of energy discharged.

5.4 Dynamic modelling of the thermal energy storage module

The experimentally validated 1-D thermal model of cast steel (discussed in Section 3.4) and concrete (discussed in Section 4.4) SHS modules are used for simulation of all six Cases. The model requires initial temperature and HTF flow rate as an operating parameter and other model parameters such as the constants of the heat transfer coefficient correlation used in Eqs. (3.18) and (4.19). These model parameters for both concrete and cast steel are taken from Table 3-7 and Table 4-9. Further, the model parameter for cast iron is expected to be similar to the cast steel module because the geometry and surface nature of both cast steel and cast-iron module are assumed to be same.

5.5 Results and discussions

The results obtained by simulating the numerical models are described in this section. For all the Cases, the performance characteristics of the SHS system such as the amount/rate of energy stored and discharged during charging and discharging processes are also explained in detail. The cost of net unit energy discharged is evaluated and discussed.

5.5.1 The effect of forward flow and reverse flow on multi-module SHS system

Figure 5-9 (a) illustrates the discharging result obtained from the forward and the reverse flow patterns for Case 1. Since all the storage module used in Case 1 are having same properties and configurations, the change in the direction of flow from forward to reverse direction has no effect on the discharging rate. The similar trend is also observed for Cases 2 and 3. Therefore, the corresponding results are not presented.

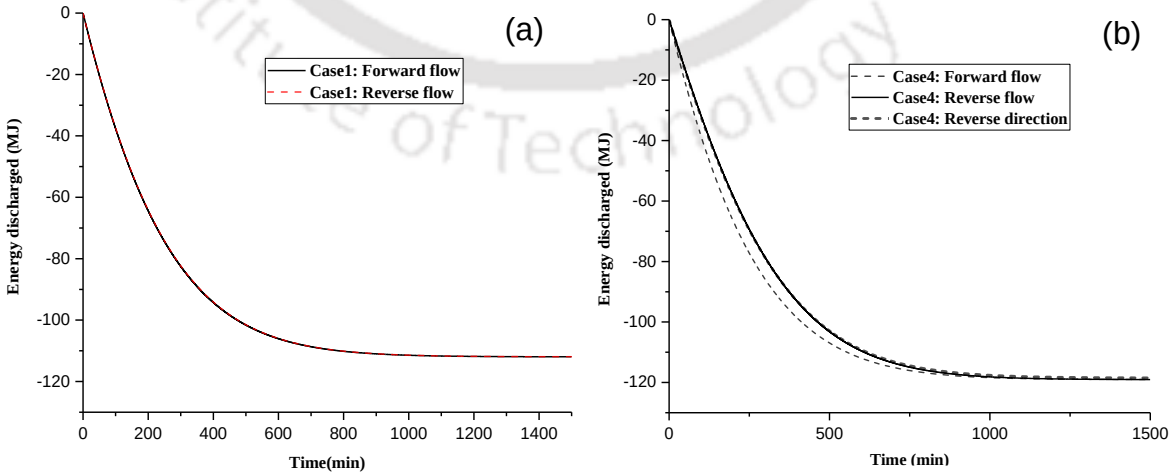

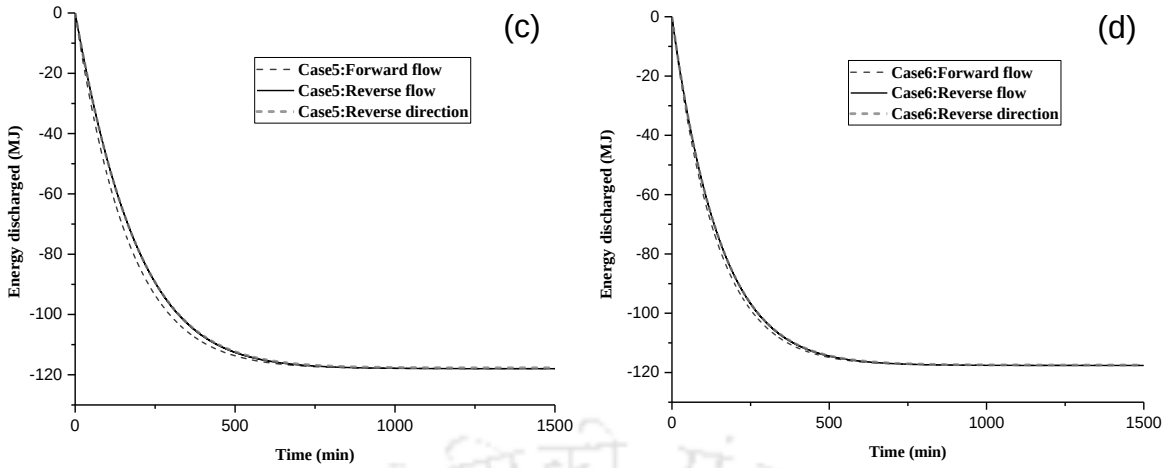

Figure 5-9. Energy discharging pattern (a) result of forward and reverse flow pattern for Case 1, (b) result of forward flow, reverse flow and reverse arrangements for Case 4, (c) result of forward, reverse flow and reverse arrangements for Case 5 and (d) result of forward, reverse flow and reverse arrangements for Case 6.

However, for Cases 4, 5 and 6, it is clear from Figure 5-9 (b), (c) and (d) that the forward flow pattern provides higher discharging rate than the reverse flow pattern and the reverse arrangement Cases. Because the thermal conductivity value of the frontend module is high as compared to the rear-end module. Therefore, the maximum heat dissipation rate is observed for the forward flow pattern.

5.5.2 Energy stored - a comparative analysis of all Cases

All six multi-module SHS systems considered in this study are simulated for forward flow condition. The energy storage capacity of each system has been compared with their charging time, as shown in Figure 5-10. It can be observed that up to 580 min, the energy storage capacity in Case 6 is maximum, later the energy storage capacity of Case 3 (six concrete modules in series) is found to be maximum than the other Cases. Concrete has low thermal conductivity due to which the energy storage rate is low initially for a certain period (310 min). However, in the remaining Cases, the system approaches the steady-state much earlier than the Case 3 due to the presence of cast iron and cast steel which has lower C_p value than the concrete. Later, Case 3 gains maximum energy due to the high specific heat capacity of concrete SHS material.

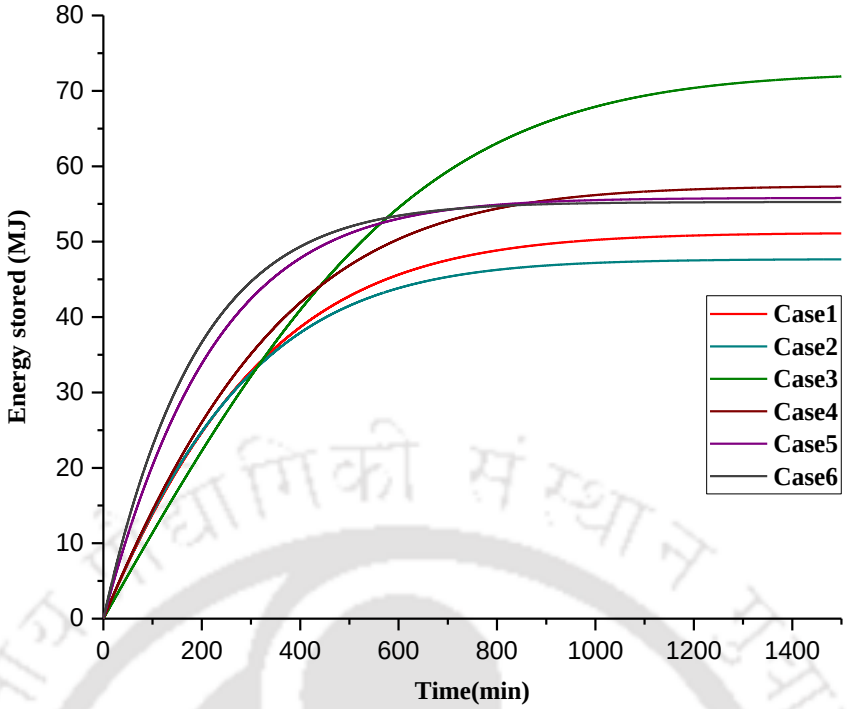

Figure 5-10. Total heat stored - comparison among all six Cases.

5.5.3 Rate of energy stored among all arrangements

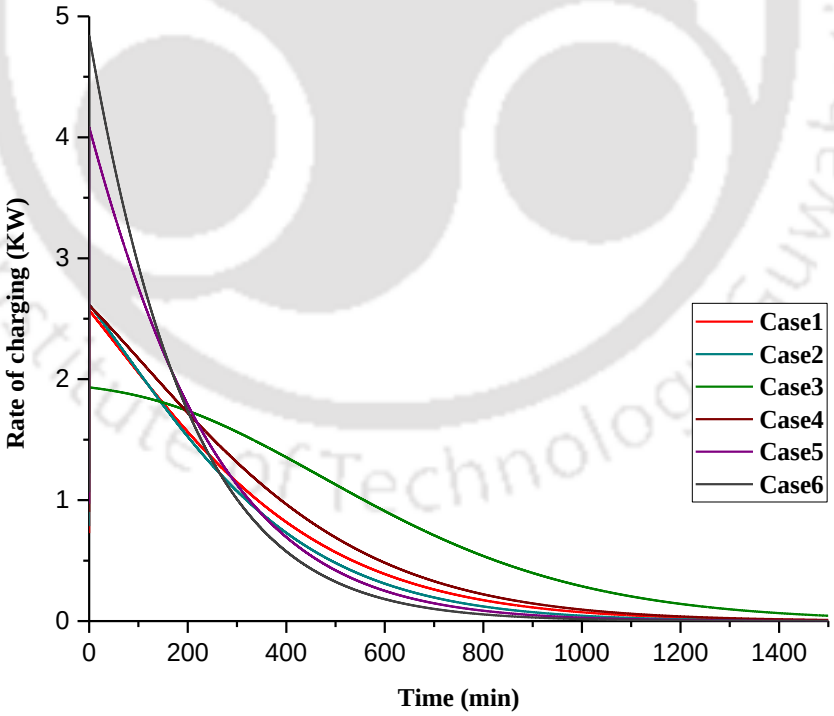

Figure 5-11. Charging rate - comparison among all six arrangements.

From the simulation study, the rate of energy stored in all six Cases of multi-module SHS system is calculated and compared (shown in Figure 5-11). The result concludes that the

concrete module alone Case (3) is able to deliver consistent energy output than all other Cases. For example, other than Case 3, the energy storage rate is found to be very high at the initial stage, later, decreases to lower value. On the other hand, for Case 3, the energy storage rate is found to be consistent with time.

The charging time of the multi-module SHS system is calculated by fixing the temperature difference between the inlet temperature of HTF and temperature of SHS module located in the rear end as 10 K. The calculated charging time is shown in Table. 5-3. From the results, it is noticed that Case 6 gives the lowest charging time. This may be due to the presence of high thermal conductivity material such as cast steel and cast iron.

Table. 5-3 Charging time for all the six arrangements

Cases	Charging time (min)
Case 1	785.68
Case 2	707.62
Case 3	1164.06
Case 4	869.42
Case 5	564.78
Case 6	477.50

5.5.4 Energy discharged - a comparative analysis of all Cases

The results obtained for discharging of all the Cases are shown in Figure 5-12. The discharging profiles of all six Cases are found to be similar to the charging process. While comparing the energy discharged from all the six Cases with their discharging time, in Case 6 the discharging rate is found to be faster till 480 min, later it reaches the steady-state because the maximum heat is discharged by the module. In other hand, Case 3 (concrete module alone) releases the heat slowly due to low thermal conductivity; however the rate of energy discharge is found to be consistent for a longer time due to high C_p.

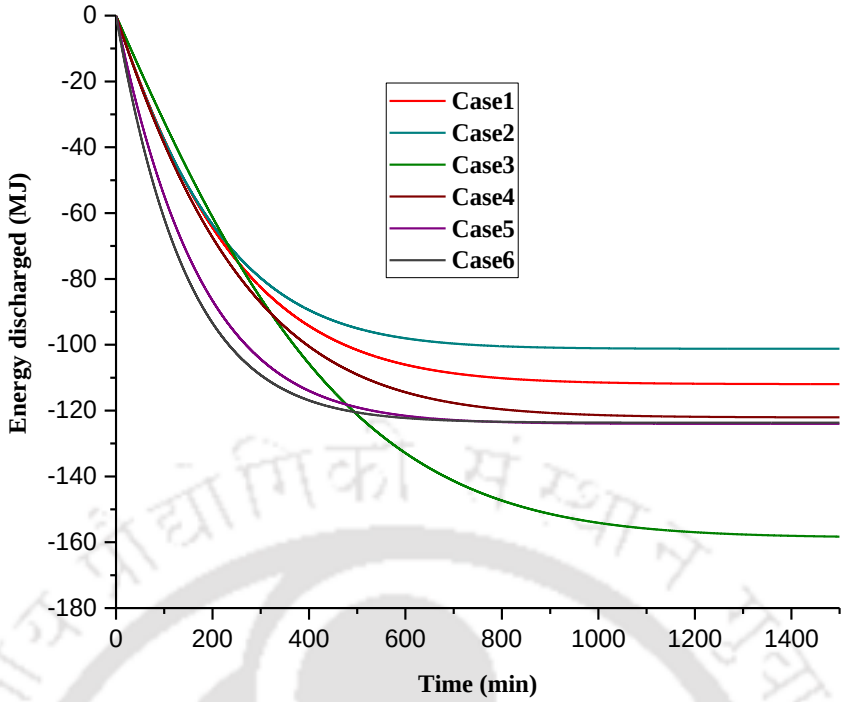

Figure 5-12. Total heat discharged - comparison among all six Cases.

5.5.5 Rate of energy discharged among all arrangements:

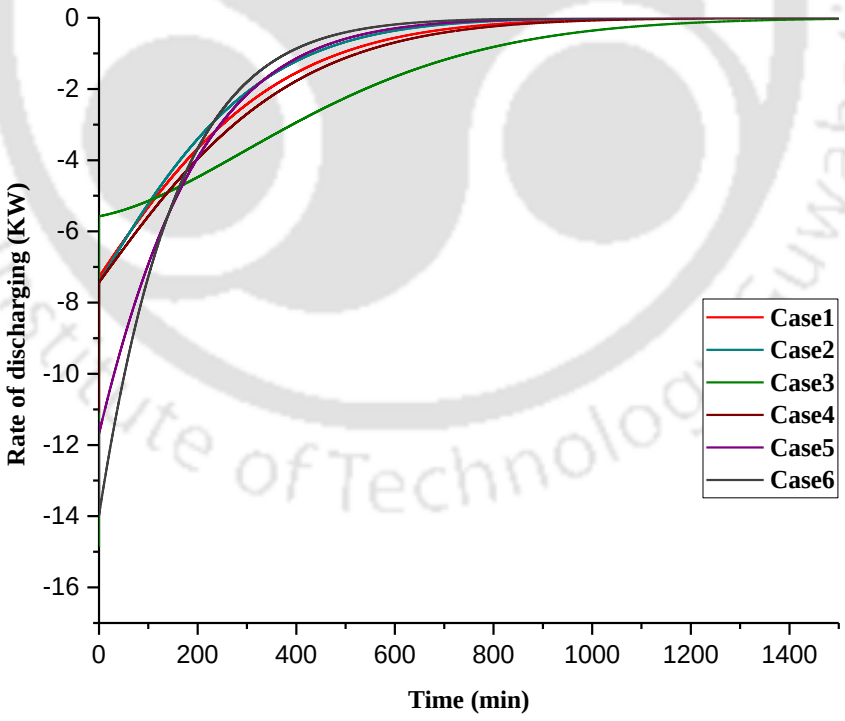

Figure 5-13. Discharging rate - comparison among all six arrangements

The rate of energy discharged obtained from the simulations are found to be similar to the rate of energy stored. The result of the energy discharge rate is shown in Figure 5-13. The details of the discharging time of each Case is given in Table 5-4.

Table. 5-4 Discharging time for all six arrangements

Cases	Discharging time (min)
Case 1	776.17
Case 2	681.37
Case 3	1148.58
Case 4	855.43
Case 5	587.73
Case 6	504.65

5.5.6 Economic Analysis of all six modules:

The cost per unit of heat discharged is calculated for all the six arrangements mentioned in Section 5.3. The cost of the system belongs Cases 1- 3 have been compared and later, the cost comparison for the rest three Cases are presented. Among Cases 1,2 & 3, it has been observed that Case 3 provides the lowest cost per unit energy discharged (USD/kW-h), which is shown in Figure 5-14.

In Cases 4, 5 & 6, the cost of the SHS materials in each arrangement are identical. The variation observed in the net unit cost of energy discharged (as shown in Figure 5-15) is due to a change in the discharging rate of individual Cases. In terms of overall performance, Case 6 could able to store and discharge energy at a faster rate. The cost of net energy discharged from Case 6 arrangement is 62.26 USD/kW-h. The performance of Case 3 is good in terms of the total amount of energy stored and discharged. The cost of net energy discharged for Case 3 is 1.18 USD/kW-h. Cost comparison for all the arrangements is illustrated in Figure 5-14 and Figure 5-15.

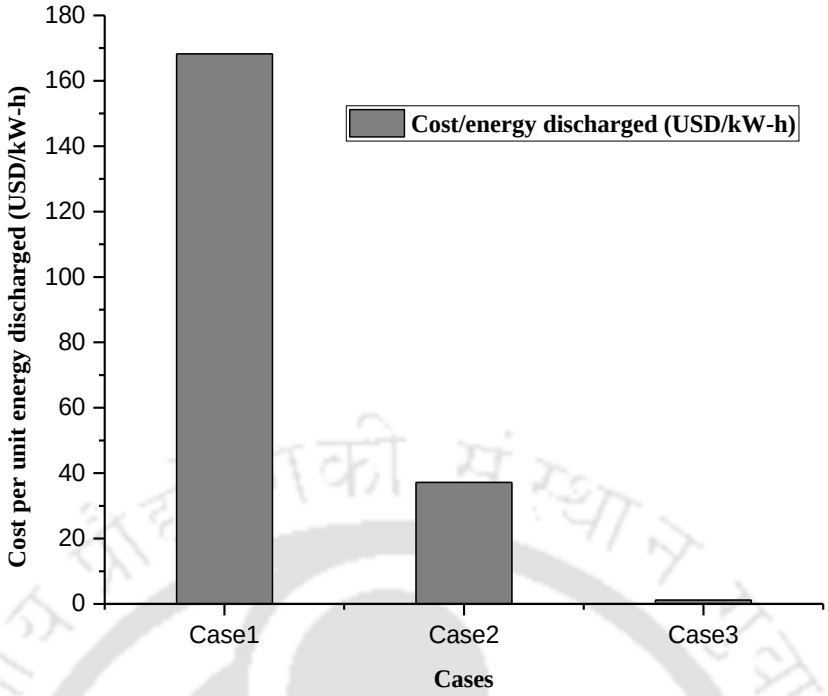

Figure 5-14. Cost analysis comparison among the arrangements: cost per unit energy discharged for the first three Cases (Cases 1, 2 and 3)

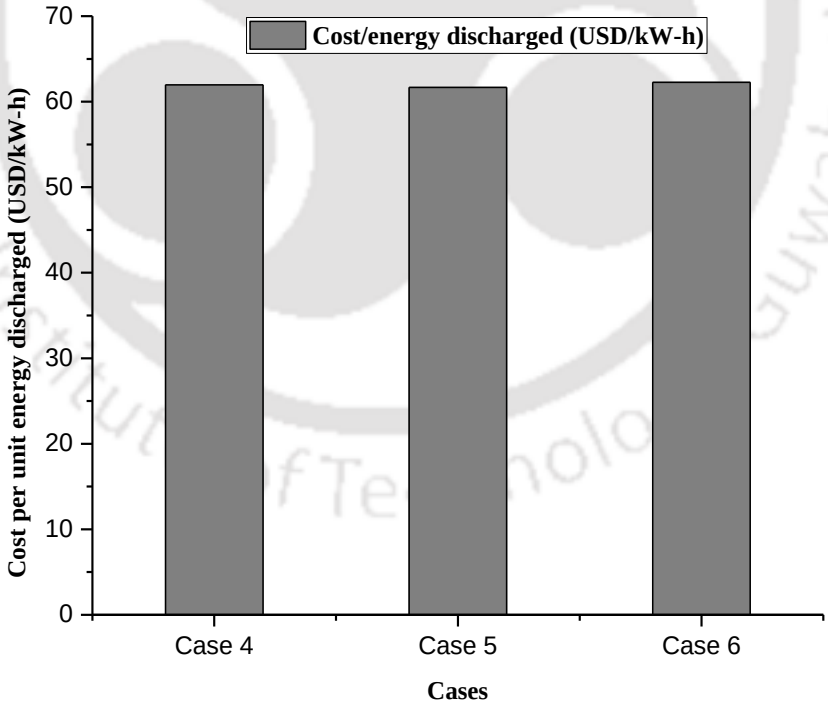

Figure 5-15. Cost analysis comparison among the arrangements: cost per unit energy discharged for the last three Cases (Cases 4,5 and 6).

5.6 Summary

A comprehensive investigation of the multi-module high-temperature SHS system is presented in this chapter. By adopting the 1-D dynamic model developed in the previous chapter, the flowsheet model is framed for evaluating the six Cases, which consist of multiple SHS modules in series and/or parallel arrangements. The SHS module is made of materials such as cast steel, cast iron and concrete, and the air is used as the HTF. The charging and discharging performances of all the Cases are evaluated and discussed. The net discharge unit cost of all Cases is evaluated and discussed.

CHAPTER 6
CONCLUSIONS AND RECOMMENDATIONS FOR FUTURE WORK

The present thesis work contributes to expand the research on the high-temperature thermal energy storage. The thesis work is primarily focused on sensible heat storage, giving special consideration to materials such as cast steel and concrete. The important conclusions obtained from the detailed investigations on experimental and numerical modeling are described in this chapter.

6.1 Studies on cast steel based SHS system

The work is focused on a detailed investigation of high-temperature sensible heat thermal energy storage system. The storage material and heat transfer fluid used for the analysis are cast steel and air. The estimated storage unit cost for cast steel system employed in the present investigation is 18.43 US$/ MJ. In the experiment section, a detailed investigation has been conducted from low temperature to high-temperature charging and discharging processes at different HTF flow velocities. 3-D numerical model and a simplified 1-D dynamic model are developed and simulated using similar conditions as maintained in the experiments. Based on experimental and numerical observations, the following conclusions can be made;

- In all experiments, the time taken for charging to reach a steady-state condition is higher than discharging. Approximately 70% of the total module is charged in 40% of the time and the remaining is stored in 60% of the time. The energy storage and discharge rate are observed to be faster in “Section-A” followed by “Section-B and Section-C” due to the high-temperature gradient between the air and storage module near the inlet section. The temperature profiles of individual thermocouples show that the heat transfer rate is much more uniform in the radial direction than axial direction. Along the axial direction, the heat transfer rate drops along the length causing a fall in the air temperature. The energy charged in the SHS module in the temperature ranges of 393-473 K, 443-523 K and 493-573 K is 13.14 MJ, 11.85 MJ and 11.36 MJ, respectively. The discharging profile of the

cast steel based SHS system recommends that the peak load demand can be achieved for a system with an interrupted power source. However, the SHS system can be adopted for constant power output cases by manipulating the HTF inlet temperature and flow rate. The high velocity of air leads to a higher rate of heat transfer between the air and storage medium.

- 3-D numerical and 1-D dynamic model results are found to be in close proximity with the experimental data. Temperature contours developed using 3-D simulations confirms that the temperature gradient between HTF and cast steel decreases along the length of the storage module. The real-time operation of the SHS system requires real-time monitoring and optimization solution. One can visualize the thermal characteristics of the complete system by coupling the mathematical model with real-time applications, and such a solution can be developed using the 1-D dynamic model. The developed 1-D model is able to predict the temperature profile of the SHS module with minimum error in lesser simulation time.
- Although the cast steel-based TES is a viable option for developing energy storage systems, there is a need to develop systems which are still inexpensive and have a good storage characteristic. This motivated the research work to be further directed towards concrete based storage system, considering the cost of storage material used. The key findings using concrete based TES are presented in the next section.

6.2 Studies on concrete based SHS system

The current study discusses the performance evaluation of the CTES module by conducting experiments and performing 1-D and 3-D mathematical modelings. The CTES module is made up of concrete, and air has been used as the HTF. A parametric study by varying the inlet temperature and velocity of air during charging and discharging processes was conducted. The study concludes the following;

- The thermal behaviour of the CTES observed through 3-D numerical simulations matches closely with the result obtained from experiments.
- During charging and discharging processes of the CTES with the fixed amount of energy, the performance of the CTES module is affected significantly by inlet air conditions. The increase in air inlet temperature from 553 K to 573 K, enhances the rate of energy stored by 28.9%, whereas further increasing air inlet temperature to 593 K, the energy storage rate is enhanced by 25.9%. The energy discharge rate increases by 22.3% with an initial reduction of inlet temperature by 20 K from 403 K, whereas

with further reduction by 20 K, the improvement in energy discharge rate is insignificant.

- The temperature profiles obtained from the various thermocouples located at different axial and radial locations depict a significant variation of concrete temperature primarily along the length of the CTES module.
- The output power profile obtained from all discharging experiments decreases linearly with time, whereas varying inlet airflow rate of the module may lead to constant output power. Considering output, the storage unit cost of the CTES module is estimated as 2.4 US$/MJ.
- The 1D dynamic model of the CTES module has been also validated with experimental data and it is fairly accurate with a maximum error of ±4.9 K. The 1-D model can be developed as per the actual operating process conditions of the storage system, and hence allows the user to estimate the performance of the CTES module during the charging and discharging processes under dynamic condition. Further, the developed dynamic model is also useful for real-time monitoring of any large scale CTES module (CTES is modular in nature) operation and optimization of process parameters without performing the expensive experimental investigations.
- The outcomes from the current study also signify that the developed CTES module is highly durable at high-temperature for more than 300 cycles of charging and discharging processes. Therefore, there is a possibility to integrate the developed CTES module with high-temperature applications such as power generation. The developed CTES module is easily scalable, alterable and the compact design provides an attractive technique for storing the heat.

6.3 Analysis of multi-module high-temperature SHS system

A 1-D dynamic model is developed and simulated to study the performance of different multi-module SHS systems. The models developed in the previous chapters are adopted to investigate the SHS system for large scale applications. The materials such as cast steel, cast iron and concrete are selected with the design similar to shell and tube configuration. Air is used as the heat transfer fluid. The temperature range considered for the charging process is 493 - 573 K and 373 - 573 K for the discharging process. Six Cases are developed using the flowsheet configuration. Each Case consists of different SHS module connected in series/parallel coupling arrangements. Based on the developed flowsheet model, the charging and discharging rates are analysed through the rate and amount of energy stored and

discharged from the SHS modules. Finally, the cost of net energy discharged from the storage module is evaluated for all the Cases. The following are the major observations obtained from the study.

- The overall performance of the individual Cases is evaluated for the flow of HTF in the forward flow pattern, reverse flow pattern and reverse module arrangements. From results, it has been observed that slight or no change in heat storage or discharge by changing the airflow direction or the arrangement of the modules.
- The total energy stored and discharged for Case 3 (six concrete modules in series) are highest among all Cases, i.e. 71.9 MJ and 158.2 MJ, respectively. However, Case 3 consumes more time to store/discharge due to low thermal conductivity. During energy storage, Case 6 stores more energy until 312.8 min and approaches the steady-state, whereas in Case 3, it still accumulates the energy due to high specific heat. The similar trend is observed in energy discharged.
- Rate of energy stored and discharged are found to be highest for Case 6, up to 312.8 min for charging and 231.2 min for discharging, respectively. Beyond that, all Cases (except the Case 3) approaches the steady-state due to a decrease in heat transfer.
- In the cost evaluation, among the coupling arrangements made of identical modules in Case 1 - Cast steel, Case 2 – Cast iron and Case 3- concrete, the cost of net energy discharged is low in Case 3 (i.e. 1.18 USD/kW-h). Whereas, for multiple SHS modules are arranged in series/parallel combinations (Cases 4, 5 and 6), the cost estimated is almost same in all Cases. Slight variation can be observed due to the change in the discharging rate of each Case.

Based on the detailed study on evaluating the different multi-module SHS systems, it is proposed that Case 3 and Case 6 arrangements are the best suitable options for integrating into the large scale application such as power generation, feed water heating for boiler and space heating applications. The developed model can be employed for studying the overall system operation in applications.

6.4 Commercial feasibility of the current research

Based on the demonstrations of thermal energy storage modules at lab scale level, there is a feasibility to commercialize the developed system. Further, the 1-D dynamic model developed in the current work is flexible to simulate and up-scale the capacity of SHS with respect to the application's requirement. By using the flowsheet model explained in Chapter

5, the SHS modules can be integrated and simulated along with the application. Therefore, by simulating the complete system, it is possible to decide the number of modules required for combining different SHS materials (concrete, cast iron and cast steel) in various multi-module arrangements with respect to the application's requirement.

6.5 Recommendation for future work

The work carried out for this thesis provides wide opportunities to expand the research work on the solid thermal energy storage system. At this point, it is essential to outcome that more analysis should be carried out during the commercial operation of TES system. From the research conducted and details reported in this thesis, some ideas have arisen which are not covered in this the present work and may be appropriate for the future developments:

- Based on the developed model, the possibility of coupling the developed low cost and high-temperature module with the high-temperature applications like steam generation, process heat and large-scale thermal desalination can be explored.
- The thermal behaviour and stability of the storage module developed in the current study could be explored by design scale-up and test in the temperature condition closer to 1000 K. The performance of the concrete and the cast steel TES system developed in the present study could prove the possibilities of using at very high-temperature conditions.
- The performance of the CTES system could be improved by mixing the high thermal conductivity material such as copper powder, graphene and high-grade stainless-steel scraps to enhance the heat transfer, and mixing of high thermal capacity material like basalt rock and dead sea salt to increase the amount of energy stored. Therefore, developing such a storage module will help to attain better energy storage capacity with lesser charging and discharging time. However, the thermal and mechanical characterisation of storage material is required. The outcomes in the literature so far and fewer research developments dedicated to this technology will encourage scientists to elaborate on the study by mixing high thermal conductivity materials into concrete for enhanced storage performances. The effect of shape, size and weight ration of mixing materials should be deeply addressed to obtain the excellent property improvements.
- Drinking and irrigation water facility could be improved using the locally available solar intensity level and SHS material. In India, the places such as delta regions of Narmada, Tapti, and Kaveri rivers has a high solar intensity, the sand available on

these river basins can be explored for the use of high-temperature thermal energy storage material. Therefore, proving such TES technology will help to develop the CSP plants near to the banks of these rivers for the cost-effective and high capacity thermal energy storage solution. The development of such a CSP plant can be used for a large-scale thermal desalination plant for 24/7 operation. In India, clean drinking water is one of the high priority issues that should be addressed by the Indian research community.

REFERENCES

Aeron, 2019. Sun Tracking Solutions for CSP and PV Solar Plants || Aeron [WWW Document]. URL https://www.aeronsystems.com/sun-tracking-solutions-for-csp-and-pv-solar-plants-for-improved-efficiency/ (accessed 9.9.19).

Alister Doyle, 2019. Nationally Determined Contributions (NDC) - Global Outlook Report 2019 | United Nations Framework Convention on Climate Change. New York.

Alva, G., Liu, L., Huang, X., Fang, G., 2017. Thermal energy storage materials and systems for solar energy applications. Renew. Sustain. Energy Rev. 68, 693–706. https://doi.org/10.1016/j.rser.2016.10.021

Aly, S.L., El-Sharkawy, A.I., 1990. Effect of storage medium on thermal properties of packed beds. Heat Recover. Syst. CHP 10, 509–517. https://doi.org/10.1016/0890-4332(90)90201-T

Andreu-Cabedo, P., Mondragon, R., Hernandez, L., Martinez-Cuenca, R., Cabedo, L., Julia, J.E., 2014. Increment of specific heat capacity of solar salt with SiO2nanoparticles. Nanoscale Res. Lett. 9, 1–11. https://doi.org/10.1186/1556-276X-9-582

Bai, F., Xu, C., 2011. Performance analysis of a two-stage thermal energy storage system using concrete and steam accumulator. Appl. Therm. Eng. 31, 2764–2771. https://doi.org/10.1016/j.applthermaleng.2011.04.049

Basecq, V., Michaux, G., Inard, C., Blondeau, P., 2013. Short-term storage systems of thermal energy for buildings: a review. Adv. Build. Energy Res. 7, 66–119. https://doi.org/10.1080/17512549.2013.809271

Bataineh, K., Gharaibeh, A., 2018. Optimal design for sensible thermal energy storage tank using natural solid materials for a parabolic trough power plant. Sol. Energy 171, 519–525. https://doi.org/10.1016/j.solener.2018.06.108

Beasley, D.E., Clark, J.A., Holstege, M.J., 1985. Observations on the Decay of a Thermocline in a Rock Bed With No Net Fluid Flow. J. Sol. Energy Eng. 107, 50–53. https://doi.org/10.1115/1.3267653

Bergman, T.L., Incropera, F.P., DeWitt, D.P., Lavine, A.S., 2011. Fundamentals of heat and mass transfer, 7th ed. John Wiley & Sons, Ltd.

Bindra, H., Bueno, P., Morris, J.F., Shinnar, R., 2013. Thermal analysis and exergy evaluation of packed bed thermal storage systems. Appl. Therm. Eng. 52, 255–263. https://doi.org/10.1016/j.applthermaleng.2012.12.007

Biswas, G., 2003. Introduction to Fluid Mechanics and Fluid Machines, 2nd ed. Tata McGraw-Hill Publishing Company Limited.

Bracken, N., Macknick, J., Tovar-Hastings, A., Komor, P., Gerritsen, M., Mehta, S., 2015. Concentrating Solar Power and Water Issues in the U.S. Southwest.

Brosseau, D., Kelton, J.W., Ray, D., Edgar, M., Chisman, K., Emms, B., 2005. Testing of Thermocline Filler Materials and Molten-Salt Heat Transfer Fluids for Thermal Energy Storage Systems in Parabolic Trough Power Plants. J. Sol. Energy Eng. 127, 109–116. https://doi.org/10.1115/1.1824107

Brown, F.C., Bi, Y., Chopra, S.S., Hristovski, K.D., Westerhoff, P., Theis, T.L., 2018. End-of-Life Heavy Metal Releases from Photovoltaic Panels and Quantum Dot Films: Hazardous Waste Concerns or Not? ACS Sustain. Chem. Eng. 6, 9369–9374. https://doi.org/10.1021/acssuschemeng.8b01705

Buscemi, A., Panno, D., Ciulla, G., Beccali, M., Lo Brano, V., 2018. Concrete thermal energy storage for linear Fresnel collectors: Exploiting the South Mediterranean's solar potential for agri-food processes. Energy Convers. Manag. 166, 719–734. https://doi.org/10.1016/j.enconman.2018.04.075

Cárdenas, B., León, N., 2013. High temperature latent heat thermal energy storage: Phase change materials, design considerations and performance enhancement techniques. Renew. Sustain. Energy Rev. 27, 724–737. https://doi.org/10.1016/j.rser.2013.07.028

Cascetta, M., Cau, G., Puddu, P., Serra, F., 2014. Numerical investigation of a packed bed thermal energy storage system with different heat transfer fluids. Energy Procedia 45, 598–607. https://doi.org/10.1016/j.egypro.2014.01.064

Chamsa-ard, W., Brundavanam, S., Fung, C., Fawcett, D., Poinern, G., 2017. Nanofluid Types, Their Synthesis, Properties and Incorporation in Direct Solar Thermal Collectors: A Review. Nanomaterials 7, 131. https://doi.org/10.3390/nano7060131

Clémençon, R., 2016. The Two Sides of the Paris Climate Agreement: Dismal Failure or Historic Breakthrough? J. Environ. Dev. https://doi.org/10.1177/1070496516631362

COMSOL Multiphysics, 2017. www.comsol.com.

Cordaro, J.G., Rubin, N.C., Bradshaw, R.W., 2011. Multicomponent Molten Salt Mixtures Based on Nitrate/Nitrite Anions. J. Sol. Energy Eng. 133. https://doi.org/10.1115/1.4003418

CSH India, 2001. Steam Cooking System for 6000 people by using Scheffler Dishes at BrahmaKumaris, Gurgaon. UNDP-GEF Concentrated Solar Thermal Heat (CSH) Project, MNRE, New delhi, India: Government of India (www.cshindia.in/images/List-of-Reports/English/LFR_E.pdf).

Dassault systems, 2018. www.dymola.com.

Diago, M., Iniesta, A.C., Soum-Glaude, A., Calvet, N., 2018. Characterization of desert sand to be used as a high-temperature thermal energy storage medium in particle solar receiver technology. Appl. Energy 216, 402–413. https://doi.org/10.1016/j.apenergy.2018.02.106

Dincer, I., Rosen, M., 2011. Thermal Energy Storage Systems and Applications, Second Edi. ed, A John Wiley and Sons, Ltd., Publication. Wiley-Blackwell, New York, USA.

Ding, W., Bonk, A., Bauer, T., 2018. Corrosion behavior of metallic alloys in molten chloride salts for thermal energy storage in concentrated solar power plants: A review. Front. Chem. Sci. Eng. https://doi.org/10.1007/s11705-018-1720-0

Ding, W., Gomez-Vidal, J., Bonk, A., Bauer, T., 2019. Molten chloride salts for next generation CSP plants: Electrolytical salt purification for reducing corrosive impurity level. Sol. Energy Mater. Sol. Cells 199, 8–15. https://doi.org/10.1016/j.solmat.2019.04.021

do Couto Aktay, K.S., Tamme, R., Müller-Steinhagen, H., 2008. Thermal Conductivity of High-Temperature Multicomponent Materials with Phase Change. Int. J. Thermophys. 29, 678–692. https://doi.org/10.1007/s10765-007-0315-7

Doretti, L., Martelletto, F., Mancin, S., 2019. A simplified analytical approach for concrete sensible thermal energy storages simulation. J. Energy Storage 22, 68–79. https://doi.org/10.1016/j.est.2019.01.029

Eames, P.C., Norton, B., 1998. The effect of tank geometry on thermally stratified sensible

heat storage subject to low Reynolds number flows. Int. J. Heat Mass Transf. 41, 2131–2142. https://doi.org/10.1016/S0017-9310(97)00349-9

Elliott, D., 2013. Renewables: A review of sustainable energy supply options. IOP Publishing, Great Britain: Institute of Physics. https://doi.org/10.1088/978-0-750-31040-6

Epting, J., Müller, M.H., Genske, D., Huggenberger, P., 2018. Relating groundwater heat-potential to city-scale heat-demand: A theoretical consideration for urban groundwater resource management. Appl. Energy 228, 1499–1505. https://doi.org/10.1016/j.apenergy.2018.06.154

Feldhoff, J.F., Benitez, D., Eck, M., Riffelmann, K.-J., 2010. Economic Potential of Solar Thermal Power Plants With Direct Steam Generation Compared With HTF Plants. J. Sol. Energy Eng. 132, 041001. https://doi.org/10.1115/1.4001672

Felizardo, F., Guerreiro, L., Roig-Flores, M., Alonso, M.C., Collares-Pereira, M., 2019. Compatibility tests between high temperature concrete and molten salts to be used for a thermal energy storage, in: AIP Conference Proceedings. AIP Publishing LLC, p. 200019. https://doi.org/10.1063/1.5117734

Fernández, A.G., Gomez-Vidal, J., Oró, E., Kruizenga, A., Solé, A., Cabeza, L.F., 2019. Mainstreaming commercial CSP systems: A technology review. Renew. Energy 140, 152–176. https://doi.org/10.1016/j.renene.2019.03.049

Fernandez, A.I., Martnez, M., Segarra, M., Martorell, I., Cabeza, L.F., 2010. Selection of materials with potential in sensible thermal energy storage. Sol. Energy Mater. Sol. Cells 94, 1723–1729. https://doi.org/10.1016/j.solmat.2010.05.035

Fricker, H.W., 1991. Solar Energy Materials High-temperature heat storage using natural rock 24, 249–254.

Gao, L., Zhao, J., Tang, Z., 2015. A Review on Borehole Seasonal Solar Thermal Energy Storage. Energy Procedia 70, 209–218. https://doi.org/10.1016/j.egypro.2015.02.117

Geyer, M., Bitterlich, W., Werner, K., 1987. The Dual Medium Storage Tank at the IEA/SSPS Project in Almeria (Spain); Part I: Experimental Validation of the Thermodynamic Design Model. J. Sol. Energy Eng. 109, 192. https://doi.org/10.1115/1.3268205

Gibb, D., Johnson, M., Romaní, J., Gasia, J., Cabeza, L.F., Seitz, A., 2018. Process integration of thermal energy storage systems – Evaluation methodology and case studies. Appl. Energy 230, 750–760. https://doi.org/10.1016/j.apenergy.2018.09.001

Gil, A., Medrano, M., Martorell, I., Lázaro, A., Dolado, P., Zalba, B., Cabeza, L.F., Lá zaro, A., Dolado, P., Zalba, B., Cabeza, L.F., 2010. State of the art on high temperature thermal energy storage for power generation. Part 1—Concepts, materials and modellization. Renew. Sustain. Energy Rev. 14, 31–55. https://doi.org/10.1016/j.rser.2009.07.035

Girardi, F., Giannuzzi, G.M., Mazzei, D., Salomoni, V., Majorana, C., Di Maggio, R., 2017. Recycled additions for improving the thermal conductivity of concrete in preparing energy storage systems. Constr. Build. Mater. 135, 565–579. https://doi.org/10.1016/j.conbuildmat.2016.12.179

Good, P., Zanganeh, G., Ambrosetti, G., Barbato, M.C., Pedretti, A., Steinfeld, A., 2014. Towards a Commercial Parabolic Trough CSP System Using Air as Heat Transfer Fluid. Energy Procedia 49, 381–385. https://doi.org/10.1016/j.egypro.2014.03.041

Goswami, D.Y., 2015. Principles of Solar Engineering. CRC Press/ Taylor & Francis, Boca Raton.

Grirate, H., Agalit, H., Zari, N., Elmchaouri, A., Molina, S., Couturier, R., 2016. Experimental and numerical investigation of potential filler materials for thermal oil thermocline storage. Sol. Energy 131, 260–274. https://doi.org/10.1016/j.solener.2016.02.035

Gude, V.G., 2015. Energy storage for desalination processes powered by renewable energy and waste heat sources. Appl. Energy 137, 877–898. https://doi.org/10.1016/j.apenergy.2014.06.061

Gudmundsson, O., Thorsen, J.E., Brand, M., 2018. The role of district heating in coupling of the future renewable energy sectors. Energy Procedia 149, 445–454. https://doi.org/10.1016/j.egypro.2018.08.209

Guillot, S., Faik, A., Rakhmatullin, A., Lambert, J., Veron, E., Echegut, P., Bessada, C., Calvet, N., Py, X., 2012. Corrosion effects between molten salts and thermal storage material for concentrated solar power plants. Appl. Energy 94, 174–181.

https://doi.org/10.1016/j.apenergy.2011.12.057

Guo, C., Zhu, J., Zhou, W., Chen, W., 2010. Fabrication and thermal properties of a new heat storage concrete material. J. Wuhan Univ. Technol. Sci. Ed. 25, 628–630. https://doi.org/10.1007/s11595-010-0058-3

Hänchen, M., Brückner, S., Steinfeld, A., 2011. High-temperature thermal storage using a packed bed of rocks – Heat transfer analysis and experimental validation. Appl. Therm. Eng. 31, 1798–1806. https://doi.org/10.1016/j.applthermaleng.2010.10.034

Hasnain, S.M., 1998. Review on sustainable thermal energy storage technologies, Part I: heat storage materials and techniques. Energy Convers. Manag. 39, 1127–1138. https://doi.org/10.1016/S0196-8904(98)00025-9

Hauer, A., 2013. International renewable energy agency Technology-Policy Brief E17.

Herrmann, U., Kelly, B., Price, H., 2004. Two-tank molten salt storage for parabolic trough solar power plants. Energy 29, 883–893. https://doi.org/10.1016/S0360-5442(03)00193-2

Hoivik, N., Greiner, C., Barragan, J., Iniesta, A.C., Skeie, G., Bergan, P., Blanco-Rodriguez, P., Calvet, N., 2019. Long-term performance results of concrete-based modular thermal energy storage system. J. Energy Storage 24, 100735. https://doi.org/10.1016/J.EST.2019.04.009

Ismail, K.A.R., Stuginsky Jr, R., 1999. A parametric study on possible fixed bed models for pcm and sensible heat storage. Appl. Therm. Eng. 19, 757–788. https://doi.org/10.1016/S1359-4311(98)00081-7

Jemmal, Y., Zari, N., Maaroufi, M., 2017. Experimental characterization of siliceous rocks to be used as filler materials for air-rock packed beds thermal energy storage systems in concentrated solar power plants. Sol. Energy Mater. Sol. Cells 171, 33–42. https://doi.org/10.1016/j.solmat.2017.06.026

Jemmal, Y., Zari, N., Maaroufi, M., 2016. Thermophysical and chemical analysis of gneiss rock as low cost candidate material for thermal energy storage in concentrated solar power plants. Sol. Energy Mater. Sol. Cells 157, 377–382. https://doi.org/10.1016/j.solmat.2016.06.002

Jian, Y., Bai, F., Falcoz, Q., Xu, C., Wang, Y., Wang, Z., 2015a. Thermal analysis and design of solid energy storage systems using a modified lumped capacitance method. Appl. Therm. Eng. 75, 213–223. https://doi.org/10.1016/j.applthermaleng.2014.10.010

Jian, Y., Falcoz, Q., Neveu, P., Bai, F., Wang, Y., Wang, Z., 2015b. Design and optimization of solid thermal energy storage modules for solar thermal power plant applications. Appl. Energy 139, 30–42. https://doi.org/10.1016/j.apenergy.2014.11.019

John, E., Hale, M., Selvam, P., 2013. Concrete as a thermal energy storage medium for thermocline solar energy storage systems. Sol. Energy 96, 194–204. https://doi.org/10.1016/j.solener.2013.06.033

John, E.E., Hale, W.M., Selvam, R.P., 2011. Development of a High-Performance Concrete to Store Thermal Energy for Concentrating Solar Power Plants, in: ASME 2011 5th International Conference on Energy Sustainability, Parts A, B, and C. ASMEDC, Washington, DC, USA, pp. 523–529. https://doi.org/10.1115/ES2011-54177

John, E.E., Hale, W.M., Selvam, R.P., 2010. Effect of High Temperatures and Heating Rates on High Strength Concrete for Use as Thermal Energy Storage, in: ASME 2010 4th International Conference on Energy Sustainability, Volume 2. ASMEDC, pp. 709–713. https://doi.org/10.1115/ES2010-90096

Kalaiselvam, S., Parameshwaran, R., 2014. Thermal Energy Storage Technologies for Sustainability: Systems Design, Assessment and Applications, Thermal Energy Storage Technologies for Sustainability: Systems Design, Assessment and Applications. Elsevier Inc., London. https://doi.org/10.1016/C2013-0-09744-7

Kalogirou, S.A., 2009. Solar Energy Collectors, in: Solar Energy Engineering. Elsevier, pp. 121–217. https://doi.org/10.1016/B978-0-12-374501-9.00003-0

Kalogirou, S.A., 2004. Solar thermal collectors and applications. Prog. Energy Combust. Sci. 30, 231–295. https://doi.org/10.1016/j.pecs.2004.02.001

Kant, K., Shukla, A., Sharma, A., Kumar, A., Jain, A., 2016. Thermal energy storage based solar drying systems: A review. Innov. Food Sci. Emerg. Technol. https://doi.org/10.1016/j.ifset.2016.01.007

Kearney, D., Herrmann, U., Nava, P., Kelly, B., Mahoney, R., Pacheco, J., Cable, R., Potrovitza, N., Blake, D., Price, H., 2003. Assessment of a Molten Salt Heat Transfer

Fluid in a Parabolic Trough Solar Field. J. Sol. Energy Eng. 125, 170–176. https://doi.org/10.1115/1.1565087

Kearney, D., Kelly, B., Herrmann, U., Cable, R., Pacheco, J., Mahoney, R., Price, H., Blake, D., Nava, P., Potrovitza, N., 2004. Engineering aspects of a molten salt heat transfer fluid in a trough solar field. Energy 29, 861–870. https://doi.org/10.1016/S0360-5442(03)00191-9

Khare, S., Dell'Amico, M., Knight, C., McGarry, S., 2013. Selection of materials for high temperature sensible energy storage. Sol. Energy Mater. Sol. Cells 115, 114–122. https://doi.org/10.1016/j.solmat.2013.03.009

Khoury, G.A., 2000. Effect of fire on concrete and concrete structures. Prog. Struct. Eng. Mater. 2, 429–447. https://doi.org/10.1002/pse.51

Klein, P., Roos, T.H., Sheer, T.J., 2013. Experimental investigation into a packed bed thermal storage solution for solar gas turbine systems. Energy Procedia 49, 840–849. https://doi.org/10.1016/j.egypro.2014.03.091

Kline, S.J., Mcclintock, F.A., 1953. Describing Uncertainties in Single-Sample Experiments. Mech. Eng. 75, 3–8.

Kobe, K.A., 1957. Applied mathematics in chemical engineering (Mickley, Harold S., Sherwood, Thomas K., and Reed, Charles E.). J. Chem. Educ. 34, A552. https://doi.org/10.1021/ed034pA552.1

Kousksou, T., Bruel, P., Jamil, A., El Rhafiki, T., Zeraouli, Y., 2014. Energy storage: Applications and challenges. Sol. Energy Mater. Sol. Cells 120, 59–80. https://doi.org/10.1016/j.solmat.2013.08.015

Kuravi, S., Trahan, J., Goswami, D.Y., Rahman, M.M., Stefanakos, E.K., 2013. Thermal energy storage technologies and systems for concentrating solar power plants. Prog. Energy Combust. Sci. 39, 285–319. https://doi.org/10.1016/j.pecs.2013.02.001

Laing, D., Steinmann, W.-D., Fiß, M., Tamme, R., Brand, T., Bahl, C., 2008. Solid Media Thermal Storage Development and Analysis of Modular Storage Operation Concepts for Parabolic Trough Power Plants. J. Sol. Energy Eng. 130, 011006. https://doi.org/10.1115/1.2804625

Laing, D., Steinmann, W.-D., Tamme, R., Richter, C., 2006. Solid media thermal storage for parabolic trough power plants. Sol. Energy 80, 1283–1289. https://doi.org/10.1016/j.solener.2006.06.003

Lanahan, M., Tabares-Velasco, P.C., 2017. Seasonal Thermal-Energy Storage: A Critical Review on BTES Systems, Modeling, and System Design for Higher System Efficiency. Energies 10, 743. https://doi.org/10.3390/en10060743

Li, B.X., Chen, M.X., Cheng, F., Liu, L.P., 2004. The mechanical properties of polypropylene fiber reinforced concrete. J. Wuhan Univ. Technol. Mater. Sci. Ed. 19, 68–71. https://doi.org/10.1007/bf02835065

Li, T., Wang, R., Kiplagat, J.K., Kang, Y., 2013. Performance analysis of an integrated energy storage and energy upgrade thermochemical solid–gas sorption system for seasonal storage of solar thermal energy. Energy 50, 454–467. https://doi.org/10.1016/j.energy.2012.11.043

Lin, W.Y., Li, T., Akasyah, L., Lim, J.W.M., Xu, H., Py, X., Rawat, R.S., Romagnoli, A., 2019. Comparison of sintering condition and radio frequency plasma discharge on the conversion of coal/biomass fly ash into high-temperature thermal energy storage material. Energy Convers. Manag. 192, 180–187. https://doi.org/10.1016/j.enconman.2019.03.076

Lingayat, A.B., Chandramohan, V.P., Raju, V.R.K., Meda, V., 2020. A review on indirect type solar dryers for agricultural crops – Dryer setup, its performance, energy storage and important highlights. Appl. Energy. https://doi.org/10.1016/j.apenergy.2019.114005

Liu, M., Belusko, M., Steven Tay, N.H., Bruno, F., 2014. Impact of the heat transfer fluid in a flat plate phase change thermal storage unit for concentrated solar tower plants. Sol. Energy 101, 220–231. https://doi.org/10.1016/j.solener.2013.12.030

Llorente García, I., Álvarez, J.L., Blanco, D., 2011. Performance model for parabolic trough solar thermal power plants with thermal storage: Comparison to operating plant data. Sol. Energy 85, 2443–2460. https://doi.org/10.1016/j.solener.2011.07.002

Lopez Ferber, N., Pham Minh, D., Falcoz, Q., Meffre, A., Tessier-Doyen, N., Nzihou, A., Goetz, V., 2019. Ceramics from Municipal Waste Incinerator Bottom Ash and Wasted

Clay for Sensible Heat Storage at High Temperature. Waste and Biomass Valorization 1–14. https://doi.org/10.1007/s12649-019-00617-w

Louis Tse, 2016. Thermodynamic Modeling of Thermal Energy Storage Systems Using Novel Storage Media. University of California, Los Angeles.

Lugolole, R., Mawire, A., Okello, D., Lentswe, K.A., Nyeinga, K., Shobo, A.B., 2019. Experimental analyses of sensible heat thermal energy storage systems during discharging. Sustain. Energy Technol. Assessments 35, 117–130. https://doi.org/10.1016/j.seta.2019.06.007

Mahmood, M., Traverso, A., Nicola, A., Massardo, A.F., Marsano, D., Cravero, C., 2018. Thermal energy storage for CSP hybrid gas turbine systems : Dynamic modelling and experimental validation. Appl. Energy 212, 1240–1251. https://doi.org/10.1016/j.apenergy.2017.12.130

Martins, M., Villalobos, U., Delclos, T., Armstrong, P., Bergan, P.G., Calvet, N., 2015. New Concentrating Solar Power Facility for Testing High Temperature Concrete Thermal Energy Storage. Energy Procedia 75, 2144–2149. https://doi.org/10.1016/j.egypro.2015.07.350

Mawire, A., McPherson, M., 2009. Experimental and simulated temperature distribution of an oil-pebble bed thermal energy storage system with a variable heat source. Appl. Therm. Eng. 29, 1086–1095. https://doi.org/10.1016/j.applthermaleng.2008.05.028

Mawire, A., McPherson, M., Heetkamp, R.R.J. va. den, Mlatho, S.J.P., 2009. Simulated performance of storage materials for pebble bed thermal energy storage (TES) systems. Appl. Energy 86, 1246–1252. https://doi.org/10.1016/j.apenergy.2008.09.009

Medrano, M., Gil, A., Martorell, I., Potau, X., Cabeza, L.F., 2010a. State of the art on high-temperature thermal energy storage for power generation. Part 2—Case studies. Renew. Sustain. Energy Rev. 14, 56–72. https://doi.org/10.1016/j.rser.2009.07.036

Medrano, M., Gil, A., Martorell, I., Potau, X., Cabeza, L.F., 2010b. State of the art on high-temperature thermal energy storage for power generation. Part 2—Case studies. Renew. Sustain. Energy Rev. 14, 56–72. https://doi.org/10.1016/j.rser.2009.07.036

Mehling, H., Cabeza, L.F., 2008. Heat and cold storage with PCM, Heat and Mass Transfer. Springer Berlin Heidelberg, Berlin, Heidelberg. https://doi.org/10.1007/978-3-540-

68557-9

Mesquita, L., McClenahan, D., Thornton, J., Carriere, J., Wong, B., 2017. Drake Landing Solar Community: 10 Years of Operation, in: Proceedings of SWC2017/SHC2017. International Solar Energy Society, Freiburg, Germany, pp. 1–12. https://doi.org/10.18086/swc.2017.06.09

Miliozzi, A., Chieruzzi, M., Torre, L., 2019. Experimental investigation of a cementitious heat storage medium incorporating a solar salt/diatomite composite phase change material. Appl. Energy 250, 1023–1035. https://doi.org/10.1016/j.apenergy.2019.05.090

Miró, L., Gasia, J., Cabeza, L.F., 2016. Thermal energy storage (TES) for industrial waste heat (IWH) recovery: A review. Appl. Energy 179, 284–301. https://doi.org/10.1016/j.apenergy.2016.06.147

MNRE-Government of India, 2019. Annual Report | Ministry of New and Renewable Energy [WWW Document].

Moffat, R.J., 1988. Describing the uncertainties in experimental results. Exp. Therm. Fluid Sci. 1, 3–17. https://doi.org/10.1016/0894-1777(88)90043-X

Mohan, G., Venkataraman, M., Gomez-Vidal, J., Coventry, J., 2018. Assessment of a novel ternary eutectic chloride salt for next generation high-temperature sensible heat storage. Energy Convers. Manag. 167, 156–164. https://doi.org/10.1016/j.enconman.2018.04.100

Montañés, R.M., Windahl, J., Pålsson, J., Thern, M., 2018. Dynamic Modeling of a Parabolic Trough Solar Thermal Power Plant with Thermal Storage Using Modelica. Heat Transf. Eng. 39, 277–292. https://doi.org/10.1080/01457632.2017.1295742

National Renewable Energy Laboratory, 2019. Concentrating Solar Power Projects [WWW Document]. Natl. Renew. Energy Lab. URL https://solarpaces.nrel.gov/ (accessed 8.10.19).

Nazir, H., Batool, M., Bolivar Osorio, F.J., Isaza-Ruiz, M., Xu, X., Vignarooban, K., Phelan, P., Inamuddin, Kannan, A.M., 2019. Recent developments in phase change materials for energy storage applications: A review. Int. J. Heat Mass Transf. 129, 491–523. https://doi.org/10.1016/j.ijheatmasstransfer.2018.09.126

Neises, T., Turchi, C., 2014. A Comparison of Supercritical Carbon Dioxide Power Cycle Configurations with an Emphasis on CSP Applications. Energy Procedia 49, 1187–1196. https://doi.org/10.1016/j.egypro.2014.03.128

Niyas, H., Prasad, L., Muthukumar, P., 2015. Performance investigation of high-temperature sensible heat thermal energy storage system during charging and discharging cycles. Clean Technol. Environ. Policy 17, 501–513. https://doi.org/10.1007/s10098-014-0807-7

Ö Paksoy, H., 2007. Thermal Energy Storage for Sustainable Energy Consumption: Fundamentals, Case Studies and Design (NATO Science Series II: Mathematics, Physics and Chemistry).

Okello, D., Nydal, O.J., Nyeinga, K., Banda, E.J.K., 2016. Experimental investigation on heat extraction from a rock bed heat storage system for high temperature applications. J. Energy South. Africa 27, 30. https://doi.org/10.17159/2413-3051/2016/v27i2a1339

Ozger, O.B., Girardi, F., Giannuzzi, G.M., Salomoni, V.A., Majorana, C.E., Fambri, L., Baldassino, N., Di Maggio, R., 2013. Effect of nylon fibres on mechanical and thermal properties of hardened concrete for energy storage systems. Mater. Des. 51, 989–997. https://doi.org/10.1016/j.matdes.2013.04.085

Pacheco, J.E., Showalter, S.K., Kolb, W.J., 2002. Development of a Molten-Salt Thermocline Thermal Storage System for Parabolic Trough Plants. J. Sol. Energy Eng. 124, 153. https://doi.org/10.1115/1.1464123

Pacio, J., Wetzel, T., 2013. Assessment of liquid metal technology status and research paths for their use as efficient heat transfer fluids in solar central receiver systems. Sol. Energy 93, 11–22. https://doi.org/10.1016/j.solener.2013.03.025

Paksoy, H.O., Andersson, O., Abaci, S., Evliya, H., Turgut, B., 2000. Heating and cooling of a hospital using solar energy coupled with seasonal thermal energy storage in an aquifer. Renew. Energy 19, 117–122. https://doi.org/10.1016/S0960-1481(99)00060-9

Panwar, N.L., Kaushik, S.C., Kothari, S., 2011. Role of renewable energy sources in environmental protection: A review. Renew. Sustain. Energy Rev. 15, 1513–1524. https://doi.org/10.1016/j.rser.2010.11.037

Pardo, P., Deydier, A., Anxionnaz-Minvielle, Z., Rougé, S., Cabassud, M., Cognet, P., 2014.

A review on high temperature thermochemical heat energy storage. Renew. Sustain. Energy Rev. 32, 591–610. https://doi.org/10.1016/j.rser.2013.12.014

Pelay, U., Luo, L., Fan, Y., Stitou, D., Rood, M., 2017. Thermal energy storage systems for concentrated solar power plants. Renew. Sustain. Energy Rev. 79, 82–100. https://doi.org/10.1016/j.rser.2017.03.139

Pilkington Solar International GmbH, 2000. Survey of Thermal Storage for Parabolic Trough Power Plants; Period of Performance: September 13, 1999 - June 12, 2000, Other Information: PBD: 29 Sep 2000. National Renewable Energy Laboratory (U.S.), Golden, CO (United States).

Prasad, L., Muthukumar, P., 2013. Design and optimization of lab-scale sensible heat storage prototype for solar thermal power plant application. Sol. Energy 97, 217–229. https://doi.org/10.1016/j.solener.2013.08.022

Psomopoulos, C.S., 2013. Solar Energy: Harvesting the Sun's Energy for Sustainable Future, in: Handbook of Sustainable Engineering. Springer Dordrecht, Dordrecht, pp. 1065–1107. https://doi.org/10.1007/978-1-4020-8939-8_117

Rao, C.R.C., 2018. Experimental and Numerical Investigations on Sensible Heat Storage Systems (Thesis). Indian Institute of Technology Guwahati.

Rao, C.R.C., Niyas, H., Muthukumar, P., 2018. Performance tests on lab–scale sensible heat storage prototypes. Appl. Therm. Eng. 129, 953–967. https://doi.org/10.1016/j.applthermaleng.2017.10.085

Razak, A., Irwan, Y., Leow, W., Irwanto, M., Safwati, I., Zhafarina, M., 2016. Investigation of the Effect Temperature on Photovoltaic (PV) Panel Output Performance. Int. J. Adv. Sci. Eng. Inf. Technol. 6, 682. https://doi.org/10.18517/ijaseit.6.5.938

Renewables 2019 Global Status Report, 2019. Paris: REN21 Secretariat.

Riaz, M., 1977. Analytical Solutions for Single- and Two-Phase Models of Packed-Bed Thermal Storage Systems. J. Heat Transfer 99, 489–492. https://doi.org/10.1115/1.3450725

Romero, M., Buck, R., Pacheco, J.E., 2002. An Update on Solar Central Receiver Systems, Projects, and Technologies. J. Sol. Energy Eng. 124, 98–108.

https://doi.org/10.1115/1.1467921

Schlipf, D., Schicktanz, P., Maier, H., Schneider, G., 2015. Using Sand and other Small Grained Materials as Heat Storage Medium in a Packed Bed HTTESS. Energy Procedia 69, 1029–1038. https://doi.org/10.1016/j.egypro.2015.03.202

Schumann, T.E.W., 1929. Heat transfer: A liquid flowing through a porous prism. J. Franklin Inst. 208, 405–416. https://doi.org/10.1016/S0016-0032(29)91186-8

Selvam, R.P., Castro, M., 2010. 3D FEM Model to Improve the Heat Transfer in Concrete for Thermal Energy Storage in Solar Power Generation, in: ASME 2010 4th International Conference on Energy Sustainability, Volume 2. ASME, pp. 699–707. https://doi.org/10.1115/ES2010-90078

Singh, H., Saini, R.P., Saini, J.S., 2010. A review on packed bed solar energy storage systems. Renew. Sustain. Energy Rev. 14, 1059–1069. https://doi.org/10.1016/j.rser.2009.10.022

Singh, S., Sørensen, K., 2017. Concrete thermal energy storage for steam generation: A numerical investigation. Linköping University Electronic Press, pp. 234–240. https://doi.org/10.3384/ecp17138234

Singh, S., Sørensen, K., Condra, T., Batz, S.S., Kristensen, K., 2019. Investigation on transient performance of a large-scale packed-bed thermal energy storage. Appl. Energy 239, 1114–1129. https://doi.org/10.1016/j.apenergy.2019.01.260

Sivakumar, A., Santhanam, M., 2007. A quantitative study on the plastic shrinkage cracking in high strength hybrid fibre reinforced concrete. Cem. Concr. Compos. 29, 575–581. https://doi.org/10.1016/j.cemconcomp.2007.03.005

Skinner, J.E., Brown, B.M., Selvam, R.P., 2011. Testing of High Performance Concrete as a Thermal Energy Storage Medium at High Temperatures, in: ASME 2011 5th International Conference on Energy Sustainability, Parts A, B, and C. ASMEDC, pp. 723–728. https://doi.org/10.1115/ES2011-54463

Skinner, J.E., Strasser, M.N., Brown, B.M., Panneer Selvam, R., 2014. Testing of High-Performance Concrete as a Thermal Energy Storage Medium at High Temperatures. J. Sol. Energy Eng. 136, 021004. https://doi.org/10.1115/1.4024925

Sragovich, D., 1989. Transient analysis for designing and predicting operational performance

of a high temperature sensible thermal energy storage system. Sol. Energy 43, 7–16. https://doi.org/10.1016/0038-092X(89)90095-9

Strasser, M.N., Selvam, R.P., 2014. A cost and performance comparison of packed bed and structured thermocline thermal energy storage systems. Sol. Energy 108, 390–402. https://doi.org/10.1016/j.solener.2014.07.023

Sukhatme SP, N.J., 2008. Solar Energy: Principles of Thermal Collection and Storage, 3rd ed. Tata McGraw-Hill, New Delhi.

Tamme, R., Laing, D., Steinmann, W.-D., 2004. Advanced Thermal Energy Storage Technology for Parabolic Trough. J. Sol. Energy Eng. 126, 794–800. https://doi.org/10.1115/1.1687404

Tamme, R., Laing, D., Steinmann, W.-D., 2003. Advanced Thermal Energy Storage Technology for Parabolic Trough, in: Solar Energy. ASMEDC, pp. 563–571. https://doi.org/10.1115/ISEC2003-44033

Tian, Y., Zhao, C.Y., 2013. A review of solar collectors and thermal energy storage in solar thermal applications. Appl. Energy 104, 538–553. https://doi.org/10.1016/j.apenergy.2012.11.051

U.S. Energy Information Administration, 2018. Annual Energy Outlook 2018 with projections to 2050.

Van Lew, J.T., Li, P., Chan, C.L., Karaki, W., Stephens, J., 2011. Analysis of Heat Storage and Delivery of a Thermocline Tank Having Solid Filler Material. J. Sol. Energy Eng. 133, 021003. https://doi.org/10.1115/1.4003685

Van rooyen, D., Copson, h. r, Berry, w. e, 1969. Corrosion Behavior of Nickel-Chromium-Iron Alloy 600 in Borated Pressurized Water Reactor Environments. Corrosion 25, 194–198. https://doi.org/10.5006/0010-9312-25.5.194

Villada, C., Bonk, A., Bauer, T., Bolívar, F., 2018. High-temperature stability of nitrate/nitrite molten salt mixtures under different atmospheres. Appl. Energy 226, 107–115. https://doi.org/10.1016/j.apenergy.2018.05.101

Wu, M., Li, M., Xu, C., He, Y., Tao, W., 2014. The impact of concrete structure on the thermal performance of the dual-media thermocline thermal storage tank using concrete

as the solid medium. Appl. Energy 113, 1363–1371. https://doi.org/10.1016/j.apenergy.2013.08.044

Xu, B., Han, J., Kumar, A., Li, P., Yang, Y., 2017. Thermal storage using sand saturated by thermal-conductive fluid and comparison with the use of concrete. J. Energy Storage 13, 85–95. https://doi.org/10.1016/j.est.2017.06.010

Xu, B., Li, P.W., Chan, C.L., 2012. Extending the validity of lumped capacitance method for large Biot number in thermal storage application. Sol. Energy 86, 1709–1724. https://doi.org/10.1016/j.solener.2012.03.016

Xu, C., Wang, Z., He, Y., Li, X., Bai, F., 2012. Sensitivity analysis of the numerical study on the thermal performance of a packed-bed molten salt thermocline thermal storage system. Appl. Energy 92, 65–75. https://doi.org/10.1016/j.apenergy.2011.11.002

Xu, X., Valmiki, M.M., Pradhan, S., Liu, H., Li, P., 2010. Solar Thermal Closed-Helium Brayton Cycle With High Temperature Phase-Change Thermal Storage, in: ASME 2010 4th International Conference on Energy Sustainability, Volume 2. ASMEDC, pp. 627–635. https://doi.org/10.1115/ES2010-90388

Year End Review 2018 - MNRE [WWW Document], 2018. . Press Inf. Bur. Gov. India. URL http://pib.nic.in/newsite/PrintRelease.aspx?relid=186228 (accessed 7.15.19).

Zalba, B., Marín, J.M., Cabeza, L.F., Mehling, H., 2003. Review on thermal energy storage with phase change: Materials, heat transfer analysis and applications, Applied Thermal Engineering. https://doi.org/10.1016/S1359-4311(02)00192-8

Zanganeh, G., Pedretti, A., Zavattoni, S., Barbato, M., Steinfeld, A., 2012. Packed-bed thermal storage for concentrated solar power - Pilot-scale demonstration and industrial-scale design. Sol. Energy 86, 3084–3098. https://doi.org/10.1016/j.solener.2012.07.019

Zavattoni, S.A., Barbato, M.C., Pedretti, A., Zanganeh, G., Steinfeld, A., 2014. High temperature rock-bed TES system suitable for industrial-scale CSP plant - CFD analysis under charge/discharge cyclic conditions. Energy Procedia 46, 124–133. https://doi.org/10.1016/j.egypro.2014.01.165

Zaversky, F., Rodríguez-García, M.M., García-Barberena, J., Sánchez, M., Astrain, D., 2014. Transient Behavior of an Active Indirect Two-tank Thermal Energy Storage System During Changes in Operating Mode – An Application of an Experimentally Validated

Numerical Model. Energy Procedia 49, 1078–1087. https://doi.org/10.1016/j.egypro.2014.03.117

Zografos, A.I., Martin, W.A., Sunderland, J.E., 1987. Equations of properties as a function of temperature for seven fluids. Comput. Methods Appl. Mech. Eng. 61, 177–187. https://doi.org/10.1016/0045-7825(87)90003-X

Zunft, S., Hänel, M., Krüger, M., Dreißigacker, V., Göhring, F., Wahl, E., 2011. Jülich Solar Power Tower—Experimental Evaluation of the Storage Subsystem and Performance Calculation. J. Sol. Energy Eng. 133, 031019. https://doi.org/10.1115/1.4004358

APPENDIX-A

The list major components used in the setup of the experiment and their technical specifications are explained below;

- A centrifugal blower of capacity 120 m^3/h, made up of stainless steel is used for supplying air. The blower is powered by a variable frequency driven motor (3 phase induction – 2 hp) to control its speed. Butterfly and spherical ball valves are used to control the airflow direction.
- Calibrated K- type thermocouples are fitted at various locations for continuous recording of temperature variation inside the TES using a Data Acquisition System with a resolution of ±0.1 K (Model: Agilent 34970A).
- A Testo make Pitot tube-based differential pressure meter (Model: 512) is used for monitoring the air velocity.
- An air heater of capacity 48 kW (1 kW per heater element) with nichrome elements is used for supplying air at the required temperature. The power control of the heater is automatic. Selec make temperature controller ensures power on/off control according to the required conditions of inlet air temperature. A flame-retardant glass fibre single core cable supplied by LAPP India (ÖLFLEX® HEAT 650 SC) is used for power supply to the heater elements.

The entire system is insulated with 102 mm thick ceramic wool (k = 0.12 W/m-K) blanket.

APPENDIX-B

Flowchart describing the 1-D model simulation

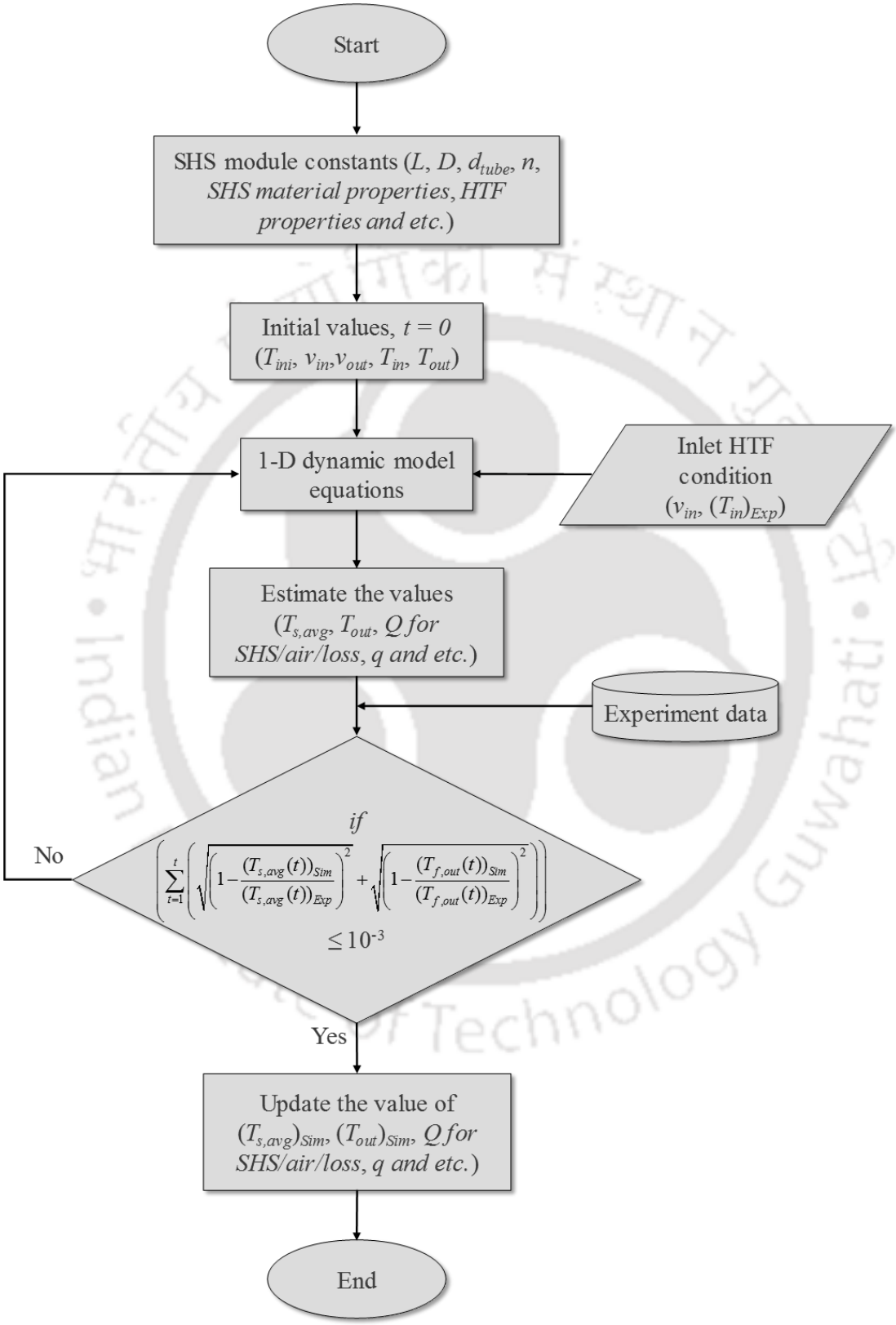

List of Publications and Conference presentations

Peer-reviewed Journals

1. **Vigneshwaran, K**., Sodhi, G.S., Muthukumar, P., Guha, A. and Senthilmurugan, S., 2019. Experimental and numerical investigations on high temperature cast steel based sensible heat storage system. *Applied Energy, 251*, p.113322. (Impact Factor – 8.426).

2. **Vigneshwaran, K**., Sodhi, G.S., Muthukumar, P. and Subbiah, S., 2019. Concrete based high temperature thermal energy storage system: Experimental and numerical studies. Energy Conversion and Management, 198, p.111905. (Impact Factor - 7.181).

3. **Vigneshwaran, K**., Sodhi, G.S., Muthukumar, P., Arvind, V.K., Balamurugan, G., Sriram, S. and Senthilmurugan, S., 2019. Experimental investigation of a Cast-Steel based Thermal Energy Storage System. *Energy Procedia, 158*, pp.4664-4670. (Cite score-1.3).

4. Sodhi, G.S., Jaiswal, A.K., **Vigneshwaran, K**., and Muthukumar, P., 2019. Investigation of charging and discharging characteristics of a horizontal conical shell and tube latent thermal energy storage device. *Energy Conversion and Management, 188*, pp.381-397. (Impact Factor - 7.181).

5. Sodhi, G.S., **Vigneshwaran, K**., Jaiswal, A.K., and Muthukumar, P., 2019. Assessment of Heat Transfer Characteristics of a Latent Heat Thermal Energy Storage System: Multi Tube Design. *Energy Procedia, 158*, pp.4677-4683. (Cite score-1.3).

6. Rao, C.R.C., **Vigneshwaran, K.,** Hakeem Niyas., and Muthukumar, P., (2019). Performance investigation of lab-scale sensible heat storage prototypes, *International Journal of Green Energy*. (Impact Factor - 1.302).

7. Sodhi, G.S., **Vigneshwaran. K.**, Muthukumar. P., 2019. Effects of geometrical parameters and thermal boundary conditions on the heat transfer characteristics of a phase change material inside a cylindrical annulus. *Journal of Solar Energy Engineering.* (Under review) (Impact Factor - 1.367).

Peer-reviewed Conferences

1. **K. Vigneshwaran**, Gurpreet Singh Sodhi, P. Muthukumar, Anurag guha, S. Senthilmurugan, "Experimental study and dynamic thermal modeling of solid sensible heat storage system", *11th International Conference on Applied Energy* (ICAE 2019) at

Mälardalen University, Västerås, Sweden, Aug 12-15 2019. (Presented work has been recommended for the special edition of Applied Energy Journal (Impact Factor – 8.426)).

2. **K. Vigneshwaran**, Gurpreet Singh Sodhi, P. Muthukumar, S. Senthilmurugan, "Concrete based Sensible Heat Storage System: Experimental Investigations", *5th International Conference on Polygeneration* (ICP 2019) at Kyushu University, Japan, May 15-17 2019.

3. **K. Vigneshwaran**, Gurpreet Singh Sodhi, P. Muthukumar, S. Senthilmurugan, "Experimental investigation of a Cast-Steel based Thermal Energy Storage System", *10th International Conference on Applied Energy* (ICAE 2018) at The Hong Kong Polytechnic University, Hong Kong, August 22- 25 2019.

4. **K. Vigneshwaran**, Gurpreet Singh Sodhi, P. Muthukumar, S. Senthilmurugan, "Performance study of cast-steel based medium temperature thermal energy storage system: experiment" *Research Conclave' 2019* at Indian Institute of Technology Guwahati, Guwahati, India, March 14-17 2019.

5. Gurpreet Singh Sodhi, **K. Vigneshwaran**, A. K. Jaiswal, P. Muthukumar, "Assessment of Heat Transfer Characteristics of a Latent Heat Thermal Energy Storage System: Multi Tube Design", *10th International Conference on Applied Energy* (ICAE 2018) at The Hong Kong Polytechnic University, Hong Kong, August 22-25 2019.

6. **K. Vigneshwaran**, P. Muthukumar, S. Senthilmurugan, "Modelling and Performance Analysis of Concrete Based Sensible Heat Storage" *Research Conclave' 18*, Indian Institute of Technology Guwahati, Guwahati, India, March 8-11 2018.

7. **K. Vigneshwaran**, Ravi Chandra Rao, P. Muthukumar, S. Senthilmurugan, "Sensible Heat Thermal Energy Storage System: Modelling and Simulation" *24th National and 2nd International ISHMT-ASTFE Heat and Mass Transfer Conference* (IHMTC-2017) at Birla Institute of Technology & Science, Pilani - Hyderabad, India, December 27-30 2017.

8. Gurpreet Singh Sodhi, **K. Vigneshwaran**, P. Muthukumar, "Thermal modeling and investigation of multi tube latent heat thermal energy storage system" *Research Conclave' 2019* at Indian Institute of Technology Guwahati, Guwahati, India, March 14-17 2019.

Thank you for reading